Safety and energetic efficiency in wearable robots. Innovative actuated devices

Politecnico di Bari

Department of Mechanics, Mathematics and Management
MECHANICAL AND MANAGEMENT ENGINEERING
Ph.D. Program
ING-IND/13–APPLIED MECHANICS

Final Dissertation

Safety and energetic efficiency in wearable robots

Innovative actuated devices

---

by

Roberta Alò :

Referees:

Prof. Dr. J.L. Pons

Prof. Dr. L. Gastaldi

Supervisors:

Prof. Dr. G. Mantriota

Prof. Dr. Bottiglione

Prof. Dr. H. van der Kooij

Coordinator of Ph.D Program:

Prof. Dr. G. Demelio

XXIX cycle, 2014-2016

to my family

alla mia famiglia

Vedi, in questi silenzi in cui le cose
s'abbandonano e sembrano vicine
a tradire il loro ultimo segreto,
talora ci si aspetta
di scoprire uno sbaglio di Natura,
il punto morto del mondo, l'anello che non tiene,
il filo da disbrogliare che finalmente ci metta
nel mezzo di una verità.
Lo sguardo fruga d'intorno,
la mente indaga accorda disunisce
nel profumo che dilaga
quando il giorno piú languisce.
Sono i silenzi in cui si vede
in ogni ombra umana che si allontana
qualche disturbata Divinità.

Ma l'illusione manca e ci riporta il tempo
nelle città rumorose dove l'azzurro si mostra
soltanto a pezzi, in alto, tra le cimase.
La pioggia stanca la terra, di poi; s'affolta
il tedio dell'inverno sulle case,
la luce si fa avara - amara l'anima.
Quando un giorno da un malchiuso portone
tra gli alberi di una corte
ci si mostrano i gialli dei limoni;
e il gelo dei cuore si sfa,
e in petto ci scrosciano le loro canzoni
le trombe d'oro della solarità.

(from "I limoni", Eugenio Montale)

Contents

Abstract

Wearable robots are person-oriented robots worn by human operators and aimed at assisting users' movements. They provide human limbs with physical support and functional supplement by enhancing the strength of wearer's joint in order to give people with mobility impairments the chance to regain the ability to walk over the ground, upstairs and downstairs, or to augment the performance of able-bodied wearers.

Research in the field of wearable robots started in late 1960s in USA and Yugoslavia for military and medical purposes respectively and even though a lot of progresses have been done especially in the last two decades, a lot of challenges are still associated with them and several research contributions aim to overcome current limitations. Portability is one of the main requirement of wearable robots. It is conceived as the capability to be worn and carried around by users who need to be supported in a large variety of operational scenarios and for an extended length of time. Comfortable and ergonomic mechanical structures, as well as efficient and convenient actuation systems ensure portability of this robotic devices.

Current actuation technologies challenge the development of portable and effective wearable robots. Actuation of these devices must fulfil often opposing requirements which are hard to conciliate at the same time. They must be powerful enough for providing the high peak of torque and power demanded in a gait cycle of locomotion tasks, they should have a low energy consumption in order to increase the operating range of the device and finally they must be as small and lightweight as possible in order to decrease the metabolic expenditure and facilitate portability.

Efficient actuatosr capable of exploiting the passive dynamic of human walking by storing and releasing energy according to the phases of the gait cycle, can reduce the energy requirement of the motor leading to the development of long lasting and lightweight systems.

More than the joint power augmentation, also the balance challenges the development of portable wearable robots. Most of wearable robots have been not primarily designed to assist balance and users have to count on conventional assistive technologies, such as canes or crutches, to prevent the risk of falling. However, these external assistive devices are hold in the hands and this is not convenient for people with limited strength in upper limbs. Furthermore, they can interfere with balance in some situations and they reduce the effectiveness of wearable robots in comparison to wheel chairs. Multi degree of freedom actuated joints would improve gait stability, despite the increase of the weight and of the control complexity.

Robotic assistive technologies, such as moment exchange actuators, have the potential of providing balance assistance to the wearer in his daily life actions and consistently with human balance control. They detect the subject's loss of balance and exert corrective actions to avoid or delay the risk of falling. Balance assistive devices can either be included in powered wearable robots or be worn separately by subjects suffering balance disorders to control and improve their balance.

This thesis gives a contribution to the development of portable wearable robots in terms of energetic efficiency and safety. The current actuation technologies for joint power augmentation and balance assistance have been investigated with the aim of finding novel solutions that could improve the portability of wearable robots for human locomotion assistance and human strength augmentation. The investigation resulted in the development of two concepts of actuated devices focused on enhancing joint strength and on balance compensation respectively.

1 Introduction

1.1 Overview

The number of people with mobility impairment is rapidly increasing. The extent and consequences related to movement disorders make this a relevant health global issue deserving attention both from a social and ethical point of view. One of the main causes of movement disorders is the aging of population. Over-60 global population percentage was 11.5% in 2012 and is expected to double in 2050 [1]. Indeed, the low birth rate and the high life expectancy make the aging tendency unlikely to stop. The weakened muscle strength in elderly people involves frailty which is often reflected by reduced physical activities, such as walking less frequently, which in the worst scenarios contributes to accelerate the deterioration of the neuromuskuloskeletal system and to arise degenerative age related pathologies like stroke. Unfortunately, dysfunctions in lower limbs do not affect elderly people only, but it is related also to cerebral paralysis and orthopedic injuries. Furthermore, even though nearly 75% of the strokes occurs in people older than 65, it hits also people under 30 because of accidents and diseases, imposing a long term and high financial burden on family and society. Mobility impairments also affect lower extremity amputees, that are often dissatisfied by the passive nature of prostheses which constrain their mobility and cause a larger metabolic energy consumption than non amputee[1]. More than mobility restrictions, paralysis causes secondary medical consequences like osteoporosis, muscle dystrophy, obesity, coronal hearth disease, diabetes, insulin resistance, which clearly contribute to worse the quality of life of these people. Rehabilitation training is therefore highly important for these patients in order to recover and regain mobility. A valid daily life assistance especially concerning mobility and autonomy, is provided by wearable robotic devices which utilize the state of the art of technologies to help disabled people to regain the ability to stand and walk, contributing to increasing the expectation of life for people with impaired

mobility. [2]

These robotic devices can be also used to augment the physical abilities of able-bodied humans to enhance their performance in industrial and military work. Legged robots are demanded to transport heavy objects because their easy adaptability to a wide range of terrains, even to those inaccessible to wheeled vehicle, and because they can decrease the likelihood of injuries in stressing working task and improve the efficiency of work [1].

Research in the field of wearable robots started in late 1960s in USA and Yugoslavia for military and medical purposes respectively and even though a lot of progresses have been done especially in the last two decades, a lot of challenges are still associated with them [3, 4]. An overview on different categories of wearable robots is hereafter provided, with the aim of highlighting the current state of the art of these technologies and the aspects needed to be developed and further improved .

1.2 Wearable robots

Wearable robots are person-oriented robots worn by human operators and aimed at assisting users' movements. They provide human limbs with physical support and functional supplement by enhancing the strength of wearer's joint in order to give people with mobility impairments the chance to regain the ability to walk over the ground, upstairs and downstairs, or to augment the performance of able-bodied wearers.

Wearable robots may act alongside the user's limb, such as in the case of exoskeletons and orthoses, or they may replace a missing limb lost after an amputation, such as in the case of prostheses. Even though they are all expected to perform human limb functions, important conceptual differences exist between them. The design of these devices faces diverse issues and follows different principles. The main point is that while the former are external rigid structures tracing the outer shape of the human limb, the latter can be seen as extensions of human body which replicate entirely the biological limb even in its shape, size and weight [5].

Exoskeletons and orthoses are assemblies of links almost parallel to human bones with the function of supporting body weight and of reinforcing joints. It is important that robotic and biological joints are well aligned in order to ensure a proper transfer

of motion from the robot to the human limb. This is not an easy matter due to the complexity of rotational axis of skeletal joints, which for instance are not fixed. Prostheses must support body weight as well, but they are demanded to replicate accurately the pattern of human walking without any fixed constraint on the degree of freedom (d.o.f.) to actuate.

Despite differences related to their specificity, wearable robots share a deep interaction with the human body. They can all be seen as a set of complex combination of different technologies integrated with each other and interacting with the human actor to perform the demanded function. Wearable robots integrate human intelligence and robot power to enhance the strength of wearer's joint and give the chance to people with mobility disorders to regain the ability to walk over the ground, upstairs and downstairs.

The intrinsic dual interaction of wearable robots with humans is performed both by a cognitive and a physical point of view. Cognitive (cHRI) and physical human robot interactions (pHRI) are commonly distinguished [5]. cHRI deals with the flow of information exchanged between the two actors involved, which aims to make the wearer aware of the possibilities of the robot and which allows him to control the robot. Information exchanged is the result of processing, manipulating and organizing of data acquired by a set of sensors to measure bioelectrical and biomechanical variables (e.g. electromiography, electroneuronography). pHRI supports the flow of power between the robot and the wearer and is based on the set of actuators and rigid structures which generates forces to be transmitted to human body to overcome physical limits. pHRI and cHRI are not independent, rather they interact and influence each other in both directions. For instance, it could happen either that physical interaction is modified by the cognitive interaction or that it triggers a perceptual cognitive process. Human-robot interface (HRi) supports both cHRI and pHRI through control of the flow of information and power in order to ensure their operations are linked informationally, mechanically or electronically.

Although the principle of the interaction between the robot and the human is basically common to all the wearable robots, there are aspects strictly related to the specific function that these devices are demanded to fulfill. For instance the extent of the interaction depends on the final aim of the robot. According to the function that they perform in cooperation with the human actor, wearable robots can be classified as it follows:

- *wearable robots for rehabilitation*: to help people with mobility disorders in the rehabilitation of musculoskeletal strength, motion control and gait;
- *wearable robots for human assistance*: to enable paralyzed patient to regain the ability to stand up, sit down, walk just as an able bodied person;
- *wearable robots for human strength augmentation*: to augment human strength of able bodied humans in order to facilitate the execution of certain tasks.

Furthermore, wearable robots can be distinguished according to the part of the body they are substituting or empowering. Full body, lower limbs and upper limbs exoskeletons exist. This is another relevant aspect which involves different aspects to be faced in the design. For instance lower limbs wearable robots are simpler to design, but harder to control. In this thesis, the attention is focused on wearable robots for lower limbs. The way in which actuation technologies could face actual relevant problems related to the assistance of human locomotion through wearable robots has been examined.

1.3 Design requirements and research challenges

Even though in the last two decades a lot of progresses have been done in the field of wearable robots, a lot of challenges are still associated with them and several research contributions aim to overcome current limitations. The development of wearable robots pursues specifications and design requirements which are related factually to the function they are supposed to address (e.g., rehabilitation, human assistance, strength augmentation), and which result in differences in the mechanical design, actuation and control.

Wearable robots for rehabilitation of lower limbs are not usually intended to be portable stand-alone systems. Rather, the majority of the robots belonging to this category are bulky devices including a treadmill, a weight support and rigid external structures worn by the patient in their rehabilitative training session. Furthermore, since they are focused on motion recovery, rehabilitative wearable robots are often limited in the scope of operational modes in which they are capable of providing assistance. Indeed their main requirement is to perform standard and repetitive movements with the capability of adapting them to the motion and to the grade of recovery of the patient.

Portability is instead one of the main requirement of wearable robots for human locomotion assistance and strength augmentation. It is conceived as the capability to be worn and carried around by users who need to be supported in a large variety of operational scenarios and for an extended length of time. This results in specific control methods and design requirements of both mechanical structures and actuation.

In order to make the usage of portable wearable robots convenient and long-lasting, their mechanical interface has to be designed with the aim of preventing user's discomfort and fatigue, which could limit the length of time that a device can be worn. Therefore strong consideration is addressed in the design of the frames, which should be customized to individual contours and anatomy, as well as to the materials used in the view of making them comfortable, lightweight and small.

Actuation is another crucial aspect related to the development of functional and autonomous portable wearable robots. Actuation of these devices must fulfill often opposing requirements which are hard to be addressed at the same time by current technologies. They must be powerful enough for providing the high peak of torque and power demanded in a gait cycle of locomotion tasks, they should have a low energy consumption in order to increase the operating range of the device and finally they must be as small and lightweight as possible in order to decrease the metabolic expenditure and facilitate portability. As a consequence of the difficult conciliation of weight and performance requirements of the actuation, most currently developed wearable robots for lower limbs are heavy and they can provide limited torques and power, restricting the effectiveness of these devices, especially in case of patient assistance. Therefore, lightweight actuator and efficient transmission are very important issues that researchers in this field have to face. A lot of research effort is focused on the design of innovative and efficient actuators capable of exploiting the passive dynamic of human walking by storing and releasing energy according to phases of the gait cycle, to reduce the energy requirement of the motor. Typically, these actuators are bioinspired solutions including a compliant element in parallel or in series to the motor [6, 7, 8, 9, 10, 11, 12, 13, 14] to replicate the natural behavior of human tendons which store and release energy. In particular, the Series Elastic Actuator (SEA) permits to reduce the motor peak power and the energy requirement[13, 15]. However, benefits of SEAs depend on the stiffness of the elastic element, whose optimal value changes according to the torque-angle characteristics of gait cycle[16]. This limit of SEAs recently motivated the development of

compliant actuators with adjustable, load-dependent stiffness of the elastic element [17, 18, 19]. Despite their advantages, these actuators often result to be inadequate because of their weight, efficiency and torque [20]. For instance, a SEA decreases the motor power requirement by reducing the motor speed more than a stiff actuator, but it also transfers the same force or torque to the motor, affecting its size, its weight, and also its efficiency [21].

Joint power augmentation is not the only requirement that actuators of portable wearable robots are demanded to fulfill. Another challenging issue to face in order to pursue the principle of portability, deals with the balance of these devices. This aspect is more relevant in assistive than in strength enhancing robots because of the mobility and balance impairments of the wearer. Balance can be improved by reinforcing hip and ankle strategy or assisting foot placement[22, 23]. Actuators of hip abduction/adduction plays a significant role in walking and standing balance. Even though wearable robots are usually actuated in the sagittal plane and the lack of actuated d.o.f. in the frontal plane limits the capability of these robots to contribute to maintain balance. However, most of wearable robots have been not primarily designed to assist balance and users have to count on conventional assistive technologies, such as canes or crutches, to prevent the risk of falling. However, these external assistive devices, which have to be hold in hand/having to be hold in hand, are not convenient for people with limited strength in upper limbs. Furthermore, they can interfere with balance in some situations and they actually reduce effectiveness of wearable robots in comparison to their major competitors, the wheel chairs.

An increasing research topic deals with the development of wearable and portable robotic solutions aimed both at detecting the subject's loss of balance and at providing corrective actions to avoid or delay the risk of falling. These technology-based applications mainly are reactionless actuators, as gyroscopes or inertial flywheels, which exert corrective actions on the human body by transferring the angular momentum between the wearer and the actuator[24, 25, 26, 27]. They are supposed to provide balance assistance to the wearer in his daily life actions and consistently with human balance control. Indeed, it is important that these devices provide assistance only when it is needed in order to make the rehabilitation more effective and to best promote neural recovery [28]. These balance assistive devices can either be included in powered wearable robots or be worn separately by subjects suffering balance disorders to control and improve their balance. Indeed, they are mostly con-

ceived as minimalistic solutions which can be easily integrated to the upper body through a backpack.

Another limitation of the development of wearable robots deals with the lack of direct information exchange between human wearer's nervous system and wearable robot. Sensors currently used in this application cannot obtain accurately and quickly wearer's intention, with the effect of limiting the assistance coming from these devices to only some function such as walking on a level ground, climbing stairs, standing up and sitting down. This aspect will not be further investigated because it goes over the intent of this thesis.

1.4 Contributions

This thesis gives a contribution to the development of portable wearable robots in terms of energetic efficiency and safety. The currently actuation technologies for joint power augmentation and balance assistance have been investigated with the aim of finding novel solutions that could improve the portability of wearable robots for human locomotion assistance and human strength augmentation. The investigation resulted in the development of two concepts of actuated devices focused on enhancing joint strength and on balance compensation respectively.

In order to be usable, wearable robots should meet severe weight restrictions, which are incompatible with the required actuator's size. Reducing the energy and power consumption of the source of power is a valuable way for reducing the weight and size of the actuator and for permitting a long-lasting usage of the device, with consequent advantages in terms of portability. Energy recovery is a commonly accepted solution to pursue this goal, but it does not always entail effective motor downsizing, which can be achieved if both the motor power and torque requirements are reduced. It is indeed well known that the size of an actuator is related to the value of its rated torque. SEAs, which include springs as energy storage devices, reduce the peaks of electric power and the energy consumption, but they transfer the same torque at the motor shaft.

The concept of an innovative actuator with energy recovery capabilities which also aims at downsizing the electric motor is presented in this thesis. Actuator's name is Flywheel-Infinitely Variable Transmission (F-IVT) actuator and its application in powering knee joints of wearable robots has been considered. It includes a brushless

DC motor, a flywheel, an Infinitely Variable Transmission (IVT) and a fixed ratio drive (FR) gear. The main ideas behind the concept of the F-IVT come from the intrinsic energetic efficiency of legged locomotion. First of all, the passive dynamic of human walking gives the chance to recover energy and thus to reduce the energy consumption of the actuator. The instant power of leg joints oscillates between positive and negative power, and thus energy can be stored in an energy storage device under the passive phases of walking, and released otherwise. Furthermore, all the kinetic and kinematic characteristics of leg joints change in a periodic fashion in a gait cycle and the peaks power values are highly larger than the average values in this application. These latest peculiarities of walking gait cycles can be exploited in order to fulfill the total joint energy requirement with a constant low input power provided by the motor and with an additional changeable power provided by the energy storage device. In the F-IVT the flywheel is the energy storage device and also the main source of power of the actuator, whose kinetic energy changes cyclically according to knee energy needs of storing or releasing energy. Instead the motor works at nearly fixed operating point and delivers an almost constant amount of power, whose value is closer to the average demand of power in a cycle than to the peaks. The F-IVT replicates the same operating principle of an automotive mechanical Kinetic Energy Recovery System (KERS), in which energy is moved from the tyres to the flywheel where it is stored when the vehicle breaks, and released when it accelerates.

Besides acting as an energy storage device, the flywheel reduces the irregularity of the motor working point, which is almost fixed over the whole gait cycle. The IVT, a continuously variable transmission whose speed ratio can seamlessly change between positive and a negative limit values, is crucial to keep the motor speed nearly constant while the desired knee speed is always matched, as well as to control the flow of energy between the joint and the flywheel.

Among the benefits of the F-IVT, the most important is the stabilization of the working point of the motor, which is required to provide an almost constant power, by far lower than the peak of the power requested by the knee. Also the torque requested by the motor is greatly reduced with a consequently remarkable motor downsizing possibility. Furthermore, if the motor working point is almost fixed, a smart design can lead the motor to work always with high efficiency. Two different architectures of the F-IVT actuator have been considered: the rotative F-IVT and the linear F-IVT. They differ from each other for the final ratio drive included: it

is an harmonic drive in the former and a ball screw in the latter.

Energy recovery is a smart strategy for reducing power and energy consumption of actuators of lower limb joints. Specific advantages are expected at the knee joint in level ground walking because its energy expenditure in a gait cycle is negative. This means that knee passive phases, in which muscles absorb energy from the joint, prevail on its active phases, in which they deliver power to the joint. Therefore, the energetics of human walking could conceptually be exploited to fulfill the total knee power requirement, without resorting to any additional power injection from motors. This idea gave rise to the self-powered F-IVT actuator in which the flywheel is the only source of power which stores and delivers energy from/to the knee joint by changing the speed ratio of an Infinitely Variable Transmission according to the phase of the gait cycle.

A simulation tool for evaluating the energetic efficiency of the flywheel based actuators has been built and the predicted performances of the actuators have been compared with the ones of other efficient actuators for lower limbs joints to assess if the F-IVT could be a potential actuator for wearable robots or not.

The second contribution of this thesis deals with bipedal balancing, a relevant problem of bipedal robotic systems acting in cooperation with human body. Human balance is the result of complex and synergic strategies of the neuromuskuloskeletal systems, which are difficult to replicate in robots. It would require complex control strategies to be implemented in a system with multiple active degrees of freedom, each actively controlled by actuators which affect the size and the weight of the robot. The easiest way to face the bipedal balance issue without complicating the control and mechanics of the robot, is to rely on external aids, like crutches or walker, which basically help user's balance by increasing his base of support. This happens for instance in [29]. However, holding in the hands these external aids constrains user's freedom of movement and, in case of mobility impairments, this fact could bring the wearer to prefer to move around on a wheelchair.

A wearable moment exchange device including a reaction wheel has been developed with the aim of assisting people in keeping balance in the frontal plane. It has been named flywheel inertia actuator to highlight its main component, the flywheel. Its action replicates the same balancing function of the arms for human body and of the pole for a funambulist. Both arms and pole rotate to generate a reaction torque of the same size but opposite direction with respect to the balance disruptive force

acting on the human body. Similarly, in the balance device a brushless electric motor accelerates the flywheel in order to have a corrective torque that helps the subject to regain balance.

The main advantage of the flywheel inertial actuator is to impart a free moment to a body without the need of contacting it with a frame. Indeed it is included into a backpack to connect the device to the user's upper body. It is easy to be worn and it is also a valuable assistive technology to be used independently from exoskeletons and orthoses. People with balance impairments who do not wear active orthoses, could use it in their rehabilitation sessions or to receive everyday life assistance. In order to promote the natural recovery of the patient, the control of the flywheel inertia actuator has been developed so that it acts consistently with human intent and provides assistance only when it is needed.

This thesis discusses the safety and efficiency of wearable robots and it is structures as follows.

Section 2 introduces biomechanical concepts of human locomotion and balance to define the design requirements of wearable robots. Furthermore section 2 provides an overview of the state of the art on actuation technologies aimed at enhancing joint strength and at assisting human balance.

Section 3 explains the working principle of the flywheel based actuators for knee power augmentation. Three different architectures of this kind of actuation are presented: the *rotating F-IVT*, the *linear F-IVT* and the *self-powered F-IVT*. Their design concept is discussed and a simulation tool for estimating their performance is provided. In the end, section 3 includes the sizing procedure for efficiency optimization of the flywheel based actuators.

Section 4 describes the flywheel inertial actuator developed for balance assistance. The concept of the actuator, its design and control are deeply discussed. Additionally, the protocol of experiments planned to test the device is explained.

Section 5 collects the results of this research study. Performance of the flywheel based actuators have been estimated and compared with those of other efficient actuation technologies for wearable robots. The flywheel inertia actuator has been tested on human subjects and the results of the experimental activity are discussed in this section.

Section 6 critically overviews the contributions of this thesis. The results are compared with the performance of existing technologies for joint empowering and balance

assistance. Current limitations of the research study and future research opportunities are also discussed.

2 State of the Art

2.1 Overview

Wearable robots are technological devices worn by human operators with the final aim of assisting the wearer in his movements and actions by enhancing the strength of his joints. They can restore functions of individuals with legs or arms pathologies or help healthy people to perform with less effort some difficult tasks such as carrying heavy loads or covering long distances.

Wearable robots are basically wearable mechanical structures equipped with well-integrated electronics that interact with the human body both on a physical and on a cognitive level. In this respect, physical human robot interaction (pHRI) and cognitive human robot interactions (cHRI) are usually distinguished [5]. The former refers to the set of actuators and rigid structures that generates forces and powers to be transmitted to human body to overcome physical limits. Instead the latter aims to make the wearer aware of the possibilities of the robot and permits him to control it. cHRI involves the flow of information exchanged between the two actors involved, that is the result of processing, manipulating and organizing of data acquired by a set of sensors to measure bioelectrical and biomechanical variables (e.g. electromiography, electroneurography). pHRI and cHRI are both supported by Human-robot interface (HRI), which ensures that their operations are linked informationally, mechanically or electronically.

Classification of wearable robots can follow different principles dealing with several aspects such as the part of the body they enhance, the level and way of interaction with the human body, their function. In order to provide a comprehensive overview of these technologies, the most relevant aspects of wearable robots are exposed with their related typical classifications.

- *Full-body, upper-limbs and lower-limbs wearable robots*

Wearable robots can assist both upper and lower limbs movements, together, as it happens in full body wearable robots, or separately, as in upper and lower limbs robots. The former are usually attached to the arms, trunk and legs of the wearer, whose both upper and lower limbs joints are strengthen (Fig. 2.1a). Instead the latter support either the movement of upper (Fig. 2.1f) or lower (Fig. 2.1b, 2.1e, 2.1c, 2.1e) human extremities. In figure 2.1 some examples of full body, upper limbs and lower limbs wearable robots are provided. Upper and lower limbs wearable robots face different design challenges. For instance lower limbs wearable robots have simpler mechanical structures than upper limbs robot because of the fewer number of degree of freedoms, but they need more powerful actuators.

- *Parallel or series interaction with the human body*

Wearable robots are mechatronic devices operating in series or in parallel to human limbs with the aim of restoring or augmenting the physical performance of the wearer. Depending on how the device interacts with the human limb, two categories of wearable robots are distinguished:

- *powered prosthesis*: operate in series to human limbs to replace missing parts of a limb that they are required to replicate in its shape, size, weight and ultimately in its function (Fig. 2.1c2.1f);

- *powered orthoses and exoskeleton*: are rigid structures working alongside human limbs of wearers suffering reduced locomotion ability [30, 31](Fig. 2.1e,2.1d), and of an able-bodied wearer [4, 32](Fig. 2.1b2.1a) respectively.

- *Function of wearable robots*

According to the function that they perform in cooperation with the human actor, wearable robots can be classified as it follows:

- *wearable robots for rehabilitation*: help people with mobility disorders in the rehabilitation of musculoskeletal strength, motor control and gait (Fig. 2.1d);

- *wearable robots for human assistance*: enable a paralyzed patient to regain the ability to stand up, sit down, walk just as an able bodied person (Fig. 2.1c2.1e2.1f);

- *wearable robots for human strength augmentation*: augment human strength of able bodied humans in order to facilitate the execution of certain tasks (Fig. 2.1a2.1b2.1e).

One of the main threads of this thesis deals with the portability of wearable robots for lower limbs, that is an issue mainly concerning devices for human assistance and

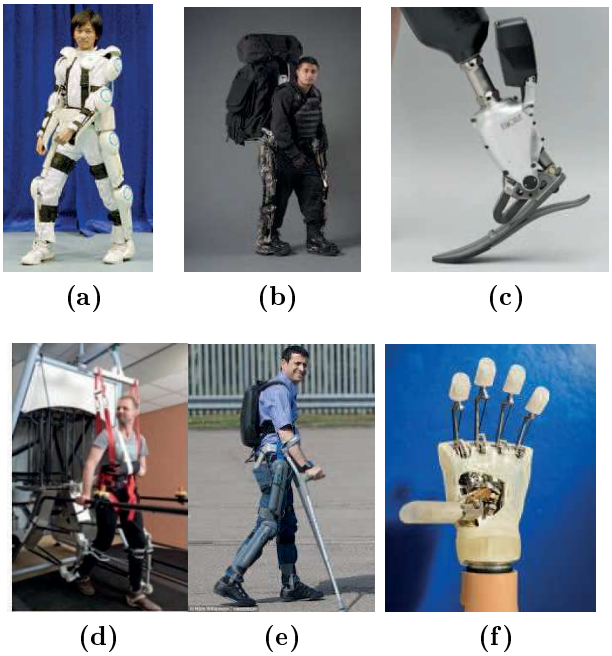

Figure 2.1: Some examples of full body (a), upper limbs (f) and lower limbs wearable robots *(b, c, d, e). a)* HAL, developed by Japan's Tsukuba University and the robotics company Cyberdyne, is the first full body powered exoskeleton. *b)* Berkeley Lower Extremity Exoskeleton (BLEEX) is the first functional energetically autonomous load carrying human exoskeleton. *c)* First powered ankle-foot prosthesis developed by the Biomechatronics research group at the MIT Media Lab. *d)* Gait rehabilitation robot LOPES developed at the University of Twente. *e)* ReWalk is a wearable robotic exoskeleton that provides powered hip and knee motion to enable individuals with spinal cord injury (SCI) to stand upright, walk, turn, and climb and descend stairs. *f)* My-HAND is the innovative prosthesis developed at the Biorobot Institute Sant'anna Pisa. It moves according to user's intention and it can reproduce the fundamental natural hand grasps (eg., precision grasp, lateral grasp and power grasp).

strength augmentation. Indeed, portability is not a design requirement of robots for rehabilitation which are usually fixed to bulky structures including treadmills and weight supports, and mostly receive power from the electricity grid. In order to be portable, wearable robots need to be equipped with powerful actuators capable of delivering the high torques/forces demanded in walking, as well as they need to be comfortable for the wearer in order to ensure a long-lasting usage of the robot. The portability of lower limbs wearable robots has been examined with a focus on the energetic efficiency and on the safety of these devices.

Another relevant aspect for ensuring the portability of wearable robots is their balance. Even if the balance of these robots is crucial for the safety of the wearer, current robots do often not ensure it, rather they rely on external support structures like crutches or walkers . Most of wearable robots have indeed been designed for joint power augmentation and not for balance.

These aspects have been deeply investigated in order to highlight which are the design matters of portable lower limbs wearable robots and to evaluate some possible technological solutions that could increase their energetic efficiency and safety. These contents are discussed below and in the following chapter of the thesis. Furthermore, because of the close interaction of these devices with the human actor, concepts of biomechanics of human walking relevant for this application are also presented.

2.2 Biomechanics of human walking

Wearable robots for lower limbs are mainly required to assist the wearer during walking by delivering the needed amount of power to perform the task, and by supporting physically and safely the wearer. Their design cannot exclude the biomechanics of human walking in order to mimic functional movements executed by biological mechanisms, and to take advantage from some of its peculiar aspects in the view of an effective design of the device. Therefore, an overview of some concepts of the biomechanics of human walking, that are useful to understand the design requirements of these robots as well as to draw inspiration for their design, follows below.

2.2.1 Anatomical planes

The biological structures and the direction of movements of the human body are described with reference to anatomical planes, which are hypothetical planes used to transect the human body (Fig. 2.2).

- *Coronal Plane or Frontal Plane*: vertical plane that separates the body into anterior and posterior parts.
- *Sagittal Plane or Lateral Plane*: vertical plane that divides the body into equal right and left halves.
- *Horizontal Plane or Transverse Plane*: horizontal plane that divides the body or any of its parts into upper and lower parts. This plane runs perpendicular to the coronal and sagittal planes and in an upright human is parallel, or horizontal, to the ground.

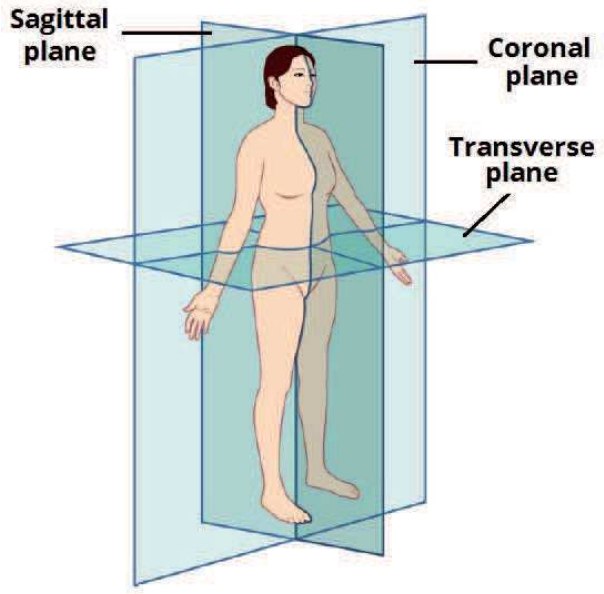

Figure 2.2: Reference anatomical planes used for describing locations and movements of structures of the human body.

2.2.2 Gait cycle

Human walking is a cyclic movement in which each leg alternates its role of supporting human weight and of advancing toward a new position. The gait cycle describes the walking cycle for one leg and conventionally starts (0%) and ends (100%) at

two successive heel strikes of the same foot. It is made up of two main phases: the stance phase and the swing phase. In the stance phase the foot is on the ground, acting as a support for the human body, whereas in the swing phase, which begins around at 60% of the cycle, the foot is off the ground and moves forward to a new supporting point (Fig 2.4). Each main phase of the gait cycle further consists of sub-phases (initial contact, loading response, mid-stance, terminal stance, preswing, initial swing, mid-swing, terminal swing) identified by different contact conditions between the foot and the ground (Fig 2.4) [3].

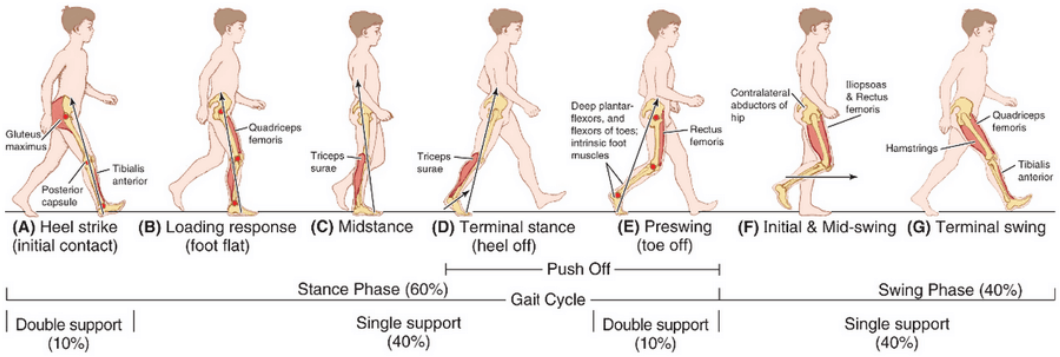

Figure 2.3: Gait cycle of human walking begins and ends at the heel strike of the same foot. Contact events distinguish the different phases and sub-phases of the the gait cycle. Their location is given as approximate percentages of the gait cycle. Adapted from [33].

Clinical gait analysis (CGA) data are kinematic and kinetic quantities which describe the motion of a leg joint in a gait cycle of walking. Being human legs multi degree of freedom systems, these quantities are always defined relatively to anatomical reference planes. The sagittal plane is the dominant plane of motion during human locomotion.

Figure 2.4 shows the CGA data of leg joints of an healthy individual walking at the speed of 1.1 m/s. Even if CGA data may differ somewhat across subject and condition, the qualitative nature of this data does not change. It can be noticed that each joint performs a cyclic motion in a gait cycle and that speeds, torques and powers oscillate between positive and negative values. CGA are useful for defining the kinematic and kinetic layout of the design wearable robots. They are usually heavily analyzed to define the the range of motion of leg joints of wearable robots, as well as to compute the joint torque and power requirement needed for the actuation design.

Investigation of CGA data also allows to detect relevant peculiarities of human walking that could be replicated in the robotic devices in order to take advantage of some efficient biological mechanisms. Each leg joint performs positive and negative work in a gait cycle, giving the possibility to recover energy. This possibility is relevant at the knee joint, whose total energy demand is negative in level ground walking. This means that knee joint is usually dissipating power during the gait cycle and therefore its dynamics could be controlled by power dissipative devices. However, the power at the individual joints changes dramatically if the walking speed changes or if walking on a positive incline or ascending stairs. Therefore, it is desirable to include also knee joint actuators in wearable robots to ensure that the power needed to perform a large range of locomotion regimes can be delivered.

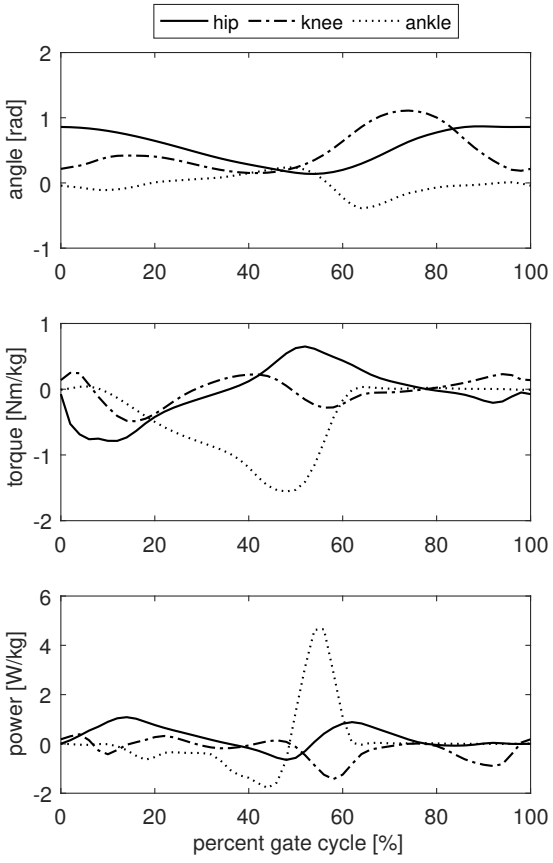

Figure 2.4: Representative angles, moments, and power of the leg flexion/extension joints over the gait cycle. Data are average curves from seven walking trials adapted from [3].

2.2.3 Human balance

Human balance is the results of fine inter-played mechanisms and joint strategies controlled by the central nervous system, which uses the information provided by the sensory systems to generate muscle corrective actions [34]. A list of the main strategies used by humans to maintain balance during standing and during locomotion follows below.

- *Ankle strategy*: involves only ankle movement to maintain the center of mass (COM) within the base of support (BoS) and to move consequently the Zero Moment Point (ZMP), which is the point where the line of action of the ground reaction force intersects with the ground. The ankle strategy is used to actively maintain balance for small amounts of sway, when the perturbation is small and the support surface is firm. It is one of the prevailing balance strategy in stance.
- *Hip Strategy*: moves the upper body in the opposite direction with respect to the lower body to maintain the CoM over the BoS. Hip strategy reacts to large and fast perturbations and is usually employed when one is standing on narrow or compliant surfaces. Both the ankle and the hip strategies maintain stability within the stability limits.
- *Foot placement*: helps to maintain stability by adjusting foot placement. The stepping strategy realigns the BoS relative to the CoM, when one takes a step to keep from falling. It is the strategy predominantly used during locomotion.
- *Arms*: rotate around the shoulder joint to change the angular momentum of the body. Arm rotations play an effective role in balance recovery.

Human balance control strategies cannot be overridden in the design of walking assist devices, that should provide only assist as needed to promote a cooperative robotic support and to facilitate the user's adaptation to the robotic device[25].

2.3 Actuators in Wearable Robotics

Wearable robots transfer power to human limbs by mean of actuators located near the controlled leg joint. These actuators usually include motors and transmission devices assembled in different schemes. The stiff coupling of the motor to the leg

joint through a transmission device characterizes most of the commercially available systems [35] and, among them, it is the one which involves the greatest demand of electrical power and the highest value of the torque to be provided by the motor [6]. As a consequence of that, heavy and large sized actuators are often been chosen preventing the development of portable wearable robots with low energy consumption and large operating range.

The actuation system is a significant aspect in the design of such devices because it affects their effectiveness. In order to be usable, wearable robots should meet severe weight requirements, which are incompatible with the required actuator size. Thus, researchers in this area agree on the importance of improving the efficiency of the actuation system, to reduce the energy consumption and the peak power of the motor [3, 16]. This requires that the motor operates efficiently and that the whole actuation system is designed in such a way that it exploits the human locomotion dynamics [9, 36]. In fact, human walking can be very efficient: the power request of each joint is sometimes positive and sometimes negative, thus giving the chance to recover a part of the energy [37].

Much research effort is indeed focused on the design of innovative and efficient actuators capable of exploiting the passive dynamic of human walking by storing and releasing energy according to the phases of the gait cycle reducing the energy requirement of the motor and thus enlarging the operating range of the device, keeping it as lightweight as possible.

Electric machines are usually chosen to power exoskeletons [12, 38] because of their high efficiency [39, 12]. Even if electric drives are usually reversible, energy recovery is not usually considered [40, 41], because of the relatively low efficiency of the mechanical to electrical energy conversion and of the battery charge/discharge process[9, 42]. Moreover, because the gait cycle frequency is some thousands cycles per hour, the batteries would be easily stressed to failure. One of the most commonly used methods to save energy is the application of springs [43, 44]. A well-known solution in literature is the Series-Elastic Actuator (SEA), where an elastic element is introduced between the motor and the load[45, 46, 47, 31, 48]. The spring stores energy and delivers peak power values greater than the limit power of the motor [49, 13, 50], as well as it offers greater shock tolerance, lower reflected inertia, more accurate and stable force control [15]. Variations of the above solutions include the introduction of parallel elasticity [40] or clutches [11]. However the introduction of

series or parallel elasticity, with or without clutches, does not give any advantage in the optimization of the efficiency of the motor, that still works in a wide range of speed and torque. Furthermore, a SEA decreases the motor power requirement by reducing the motor speed more than a stiff actuator, but it also transfers the same force or torque to the motor, affecting its size, its weight, and also its efficiency [21, 20]. This evidence has recently motivated the development of compliant actuators with adjustable, load-dependent stiffness of the elastic element [19, 18, 17], which more than making SEAs convenient for a larger range of walking regimes, allows the motor to work at the most efficient conditions.

Some of the latest actuation technologies for wearable robots are reviewed below.

2.3.1 Series Elastic Actuator

Series Elastic Actuators (SEAs) have been extensively employed in wearable devices for lower limbs. In SEAs a spring is put in series between the motor and the artificial powered joint (Fig. 2.5) to mechanically store energy. The spring increases the actuation efficiency by storing energy during negative power portions of the gait cycle and then releasing the stored energy during subsequent portions of the cycle, reducing motor work requirements and/or adjusting the speed regime of the motor [16].

Beyond the energy storage capabilities, the elastic element gives other advantages to the actuation system such as greater shock tolerance, lower reflected inertia, more accurate and stable force control, limited high-frequency actuator impedance[6, 15, 13].

Figure 2.5: Block diagram of SEAs, in which a spring is in series to the motor and the gear train.

Since the force/displacement characteristic of the spring is linear (Eqs. 2.12.2), the SEA is very efficient in powering the knee joint because it can be designed to take advantage of the linear torque-angle (or spring-like) relationship of the knee in the early-stance flexion-extension phase of level ground walking (Fig. 2.32.4). In particular if the stiffness of the spring (K) is chosen equal to the slope of the torque-angle curve, the spring alone would render the spring-like relationship, resulting in a

great reduction of the motor mechanical energy requirement. Series-elastic actuators (SEAs) have been used in both ankle and knee prostheses to effectively reduce the energy consumption of the devices [16, 12, 47, 36].

The electric power and energy requirement of a SEA to power knee joint can be calculated through a function of the angle (ϑ_M) and torque (C_M) requirement of the SEA motor:

$$\vartheta_M = \left(\frac{C_K}{K} + \vartheta_K\right) \frac{1}{\tau_{GT}} \tag{2.1}$$

$$C_M = \left(\frac{C_K \tau_{GT}}{\eta_{GT}}\right) \tag{2.2}$$

In equations 2.12.2 $C_K$and ϑ_K are the knee torque and angles, K is the stiffness of the spring, , τ_{GT} and η_{GT} are respectively the speed ratio and the efficiency of the gear train.

2.3.2 Parallel Elastic Actuator

Parallel elastic actuators (PEAs) combine DC motors with parallel springs that are engaged and disengaged by clutches (Fig. 2.6). Parallel elasticity can largely reduce power and torque requirements for actuators in legged systems [51, 52]. The peak torque requirement of ankle and hip actuators is expected to be reduced respectively of the 48% and 66% when using parallel springs around these joints in exoskeletons [52]. PEA of [10], that mimics the torque and motion patterns of knee extensors muscles in human rebounding, reduces the energy consumption of the actuator by about 80% and the peak torque requirement for the DC motor by about 66%. PEAs are also included in the Virtual Scenario Haptic Rendering Device of TU Munich[53], in the knee joint of the robot Saika-4[54], in the powered ankle-foot prosthesis of MIT[55].

A disadvantage of parallel elastic actuators (PEAs) is that they could limit movement dexterity. Indeed, a spring in parallel to a motor reduces the energy consumption and torque requirements for motions with torque patterns that fit the parallel

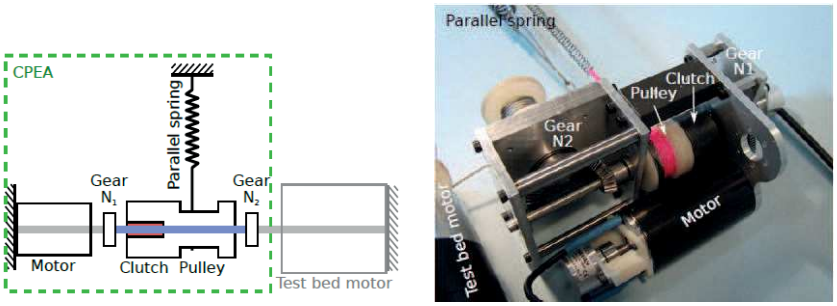

(a) (b)

Figure 2.6: PEAs Schematic picture (a) and prototype (b) of the PEA presented in [40]. When the clutch is disengaged, the shaft (blue) connecting the two gear stages can rotate independent of the pulley. Only when the clutch is engaged, the pulley rotates together with the shaft, thus extending the spring.

spring, but in other motions or gait phases it can hinder the movement. To resolve these limitations the hardware design of PEAs is usually challenged by the need to engage and disengage the parallel elasticity depending on the gait phase. To this aim, simple trigger-based control has been developed for the Clutchable Parallel Elastic Actuator (CPEA) of [40].

2.3.3 Clutchable-Series Elastic Actuator

The Clutchable-Series Elastic Actuator (C-SEA) (Fig. 2.7) was developed to overtake one limit of SEAs that is related to the inefficiency of the motor in the stance phase [11]. In fact, even if SEAs greatly reduces the motor mechanical energy requirement in the stance phase when the spring alone powers the knee joint, the electric motor works at very slow speeds and thus very inefficiently. The C-SEA improved the design of SEAs by including a clutch on the motor shaft that is conveniently activated or deactivated according to the cycle phase. In particular, during the spring-like phase of the gait cycle the clutch is activated and the spring renders the complete torque-angle relationship while the motor is required to supply only reactionary torque; during the other phases of the cycle, the clutch is deactivated and the C-SEA works as a SEA.

Equations similar to SEAs' govern the operation of the C-SEA (Eqs. 2.12.2). The

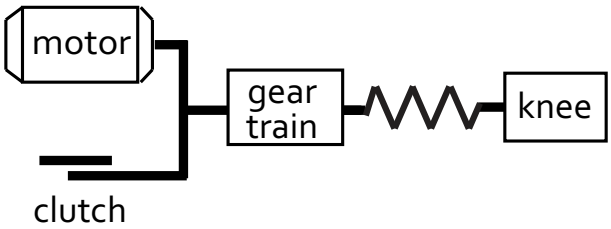

Figure 2.7: Model of the clutchable series-elastic actuator. A clutch connected to the motor allows two mechanical states of the actuator. When the clutch is engaged the motor provides only a reactionary torque and the spring renders the knee angle and torque. When the clutch is disengaged, it operates as a SEA.

complete set of equations given in [11]follows:

$$\vartheta_M = \left\{ \left(\frac{C_K}{K} + \vartheta_K\right) \frac{1}{\tau_{GT}} \quad clutch\ on \right. \tag{2.3}$$

$$C_M = \left\{ \left(\frac{C_K \tau_{GT}}{\eta_{GT}}\right) \quad clutch\ on \right. \tag{2.4}$$

When the clutch is not active, a constant clutch current (i_C) and voltage (v_C) are provided by the motor.

Rouse [11]proved that the stiffness of the spring of the C-SEA does not affects the electrical power profiles, but determines very different knee kinematics. Indeed, when the stiffness affect the knee angle displacement, the clutch absorbs a nearly constant electrical power. Therefore the optiml stiffness is selected by minimizing the kinematic similarity defined as:

$$\Psi = \int \left(\vartheta_{CSEA} - \vartheta_K\right)^2 dt$$

where ϑ_{CSEA} is the output displacement of the C-SEA and ϑ_K is the output displacement of the knee joint.

2.3.4 Continuously variable series elastic actuator.

The Continuously-variable series-elastic actuator (CV-SEA) has been presented in [9] as an efficient actuator for legged locomotion. It includes a continuously variable transmission (CVT) between a motor and a series elastic element (Fig. 2.8). More than reducing the motor energy and power requirements by storing and releasing mechanical energy in a spring as in traditional SEAs, the CVT in CV-SEA finely tunes motor speed profiles for optimal electrical efficiencies during motor work production and also reduces the torque seen at the motor, with resultant advantages in terms of motor undersizing. The motor efficiency further improves if an IVT, that make the motor work at almost fixed operating point, is used instead than a CVT (IV-SEA).

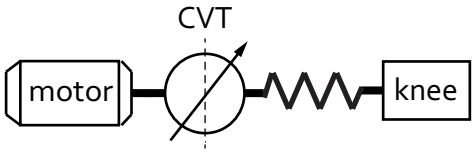

Figure 2.8: Schematic of the Continuously Variable Series Elastic Actuator. It consists of three elements in series: an electromagnetic motor, a CVT and an elastic element. The series elastic element can reduce motor work and power, increase actuator efficiency and limit motor/transmission shock, while the CVT can further optimize the speed profile of the motor for greater actuator efficiency. [9]

Differently from Variable Stiffness Actuator including a continuously variable transmissions between the load and an elastic element, the stiffness of the elastic element seen by the load remains constant. CV-SEA places a variable transmission between the motor and elastic element to control the dynamics of the motor.

The energy efficiency of the CV-SEA was compared to three other architectures: a direct drive with no elastic element, a SEA, and an IV-SEA. The estimation of the energy requirement of each actuator suggests that the CV-SEA can consistently reduce the energy associated with actuating human knee during level ground walking. Although the advantages in terms of motor efficency and motor torque reduction, the IV-SEA performs worse than CV-SEA because of the inefficiency of the IVT at high transmission ratio.

2.3.5 Variable stiffness actuator

The concept of Variable Stiffness Actuator (VSA) bears to overcome an intrinsic limitation of the SEA, that is that the mechanical stiffness of the compliant element can be optimized only for a single task and/or user, since it is fixed. Applying the concept of VSA to lower limb wearable robots would therefore allow to adapt the actuator stiffness not only to the user, but also to the detected gait and cadence using an appropriate adaptive controller.

The adaptive stiffness can be obtained on the basis of different principles. In any case, VSAs always require two motors: one to control the equilibrium position and the second to control stiffness. The different actuators from literature can be classified into three major groups:

- *Spring Preload*: the stiffness is adjusted by changing the pretension or preload on the spring. The preload of a a single spring [56, 57] or of more springs is changed by two motors working antagonistically [58, 59] or independently [60].
- *Changing transmission between load and spring*: the stiffness is altered by changing the transmission ratio between the output link and the elastic elements. This class can be further divided into the following subclasses:

  - Lever length: the stiffness is adapted by controlling the configuration of a lever mechanism [61, 62, 63, 64, 65].

  - Nonlinear mechanical link: The stiffness is adapted by controlling the properties of a nonlinear mechanical link [66, 67].

  - Continuously variable transmission: The stiffness is adapted by controlling the transmission ratio of a continuously variable transmission [68, 69].
- *Physical properties of the spring*: The physical structure of the spring itself is altered [70].

2.4 Balance Assistive Devices

Balance assistive devices are wearable and portable technologies that helps the wearer to keep his balance, thus avoiding or delaying the risk of falling. Fall prevention is recognized as an important health issue within UK, Europe, North America

and Australia [71]. The aging of global population in the latest decades has contributed to make it a relevant research topic aimed at developing technology-based fall prevention systems that could reduce the health, social and economical impact of falling. Indeed, the risk of falling increases with age often because physical, functional and cognitive impairments. Unfortunately, fall prevention does not concern only aged population, but it is also a relevant issue for young people affected by balance disorders.

Exoskeletons could be a valid option for providing assistance to subjects with balance impairment even if they have some limitations that do not make them the best option for supporting posture stability. Especially for what concerns aged people, exoskeletons are usually too heavy and uncomfortable, and they are often not easy to be worn without the help of another person. Furthermore, most of the commercially available exoskeletons have no function to stabilize the posture of the wearer [27], rather they are mainly designed for joint power augmentation. Therefore, balance assistive devices focused on ensuring wearer's stability have been developed. These devices are basically actuation technologies that exert a corrective action on the wearer subject after having detecting his loss of balance. Compared to exoskeletons, these technologies, that are usually integrated to the human body through a backpack, are easier to wear and they do not impede walking.

These devices could provide assistance to people with balance impairments, who does not need wearing exoskeletons, as well as they could be included in exoskeletons to control postural stability. Indeed, bipedal balancing of current exoskeletons is often ensured by conventional assistive technologies such as crutches aimed at increasing the wearer's base of support. Nevertheless, even if they are the most spread balance support devices, they involve significant musculoskeletal and metabolic effort from the patient and constrain his arms function [72]. Multi degree of freedom actuated joints would improve gait stability, but the total weight of the robots would increase too much. Indeed, exoskeletons are usually actuated only in the sagittal plane, limiting the capability of these robots to contribute to maintain lateral stability and to provide active lateral weight shift.

Furthermore, balance assistive devices could be worn separately from the exoskeletons becoming effective portable robotic solutions for rehabilitation of patients suffering of balance disorders.

Balance assistive devices are supposed to provide stability assistance to the wearer

in his daily life actions and consistently with human balance control. Indeed, it is important that these devices provide assistance only when it is needed in order to make the rehabilitation more effective and to best promote neural recovery [28].

These technology-based applications are mainly reactionless actuators, as gyroscopes or inertial flywheels, which exert corrective actions on the human body by transferring the angular momentum between the wearer and the actuator [25, 26, 27, 24]. Both reaction wheels and controlled moment gyroscopes consist of a rotating flywheel connected to a rotor and they transfer free moments to the body without structures on the joints. Despite these similarities, their operation is totally different: reaction wheels generates moment by changing the spin rate of the flywheel, instead controlled moment gyroscopes generates moment by rotating outer gimbals. The inertial effect of the flywheel, which has recently found a high-level application in the Cubli balancing robot [73], has been used to counteract perturbations in the frontal plane in the balance assistance devices proposed in [24]. The concept of CMGs, largely investigated in aerospace, has been elaborated and applied to human balancing by [25], who have proposed a wearable backpack device which include multiple lightweight CMGs capable of providing balance assistance in any fall direction. A variant of this latest device has been elaborated upon by [27] and [26] constructed a simplified prototype. A thorough description of the existing concepts of actuated devices for bipedal balancing follows here.

2.4.1 Giroscopic effect for human balance/ control moment gyroscopes and variable speed control moment gyroscopes

Control moment gyroscopes (CMGs) are actuated devices that takes advantage of the gyroscopic effect of a spinning wheel to stabilize the motion of unstable systems like bicycles, monorail car or two-wheeled automobile [74], mobile robots [75, 76], spacecrafts [77].

In a CMG, a flywheel is coupled to a gimbal that is free to rotate around an axis that is perpendicular to the flywheel spin axis (Fig. 2.9a). When the gimbal rotates and the flywheel is spinning around its axis, a torque is generated around the cross product direction of the flywheel and spin axes. The magnitude of the torque is proportional to the product of the flywheel and gimbal angular velocities. Therefore,

high torques can be generated easily and be controlled rapidly through the velocities of spin axes.

CMGs are considered among those walking assist devices that keep posture of user's trunk and enable the user to walk safely (Fig. 2.9b). These devices usually includes $N \geq 2$ CMGs to control posture of subjects around roll and pitch axes, which are the prevailing falling directions in humans. The number of CMGs included into the device leads to different configurations of the system which involve different posture control low methods [27] . Regardless of the method adopted, state feedback control defines the target postural control torque to be generated by CMGs, in which gimbals change their angular velocity and the flywheel spins at constant speed.

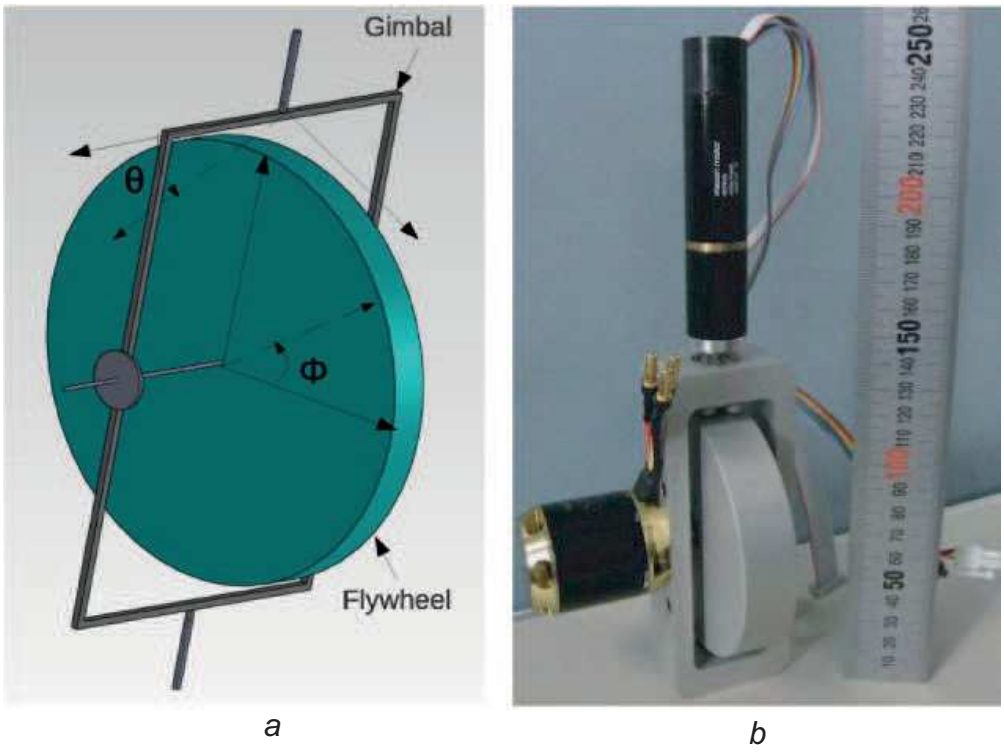

Figure 2.9: Diagram and experimental prototype of the control moment gyroscope presented in [27]. The flywheel is mounted on a gimbal that rotates around its longitudinal spin axis. When the gimbal rotates, the orientation of the flywheel spin rotates and a torque is generated around a third axis orthogonal to flywheel and the gimbal spin axes.

it is supposed to be attached to human body by orthopedic corset in order to have the backpack tightly attached to human trunk and pelvis. Each VSCMG has 2 actutors controlling the gimbal speed and the rotation speed of the reaction wheel.

Gyroscopic effect of CMGs is used in combination with the inertial effect of the flywheel accelerated around its spin axis in variable speed control moment gyroscopes (VSCMGs) [78, 79]. A VSCMG that is able to counteract human falls in any direction has been presented in [25]. This is supposed to be included into a backpack tightly attached to human trunk and pelvis ans it includes $N \geq 2$ VSCMGs with gimbals aligned with the longitudinal axis of the human (Fig.2.10). Each VSCMG has 2 actuators controlling the gimbal speed and the rotation speed of the reaction wheel. The inertial effect of the flywheel is useful to instantaneously compensate for errors in the transverse plane. As in CMGs, the coordination of gimbal accelerations is important to prevent moments about the longitudinal axis caused by inertia of VSCMGs about the gimbal axis. Furthermore, in VSCMGs gimbals must be stopped once the spin axis of the reaction wheel is aligned with the required torque vector to avoid oscillation around this configuration where no desirable moments can be produced by CMG effect.

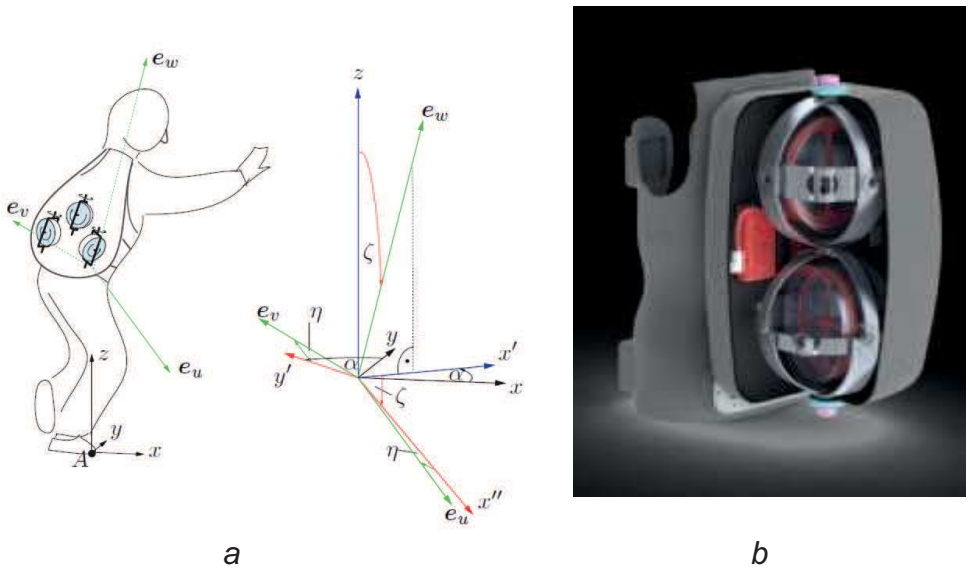

Figure 2.10: Balance assistive device presented in [25]. Three variable speed control moment gyroscopes are included into a backpack worn by a human subject to counteract perturbations in any directions.

A controller acting consistently with the human control has been designed for this application. An open loop assistance control generates a feed-forward moment profile when the loss of balance is detected and until the human body is in the desired final configuration, that coincides with the vertical standing position at zero velocity. An alternative goal could be to slow down the fall and give the patient more time to

regain balance by himself. The reference torque to be tracked by the controller in the transverse plane is calculated through the equation of motion for the VSCMG assembly and for the human, modeled as an inverted pendulum pivoting around point A (Fig.2.10). A minimizing a cost function that penalizes torque control error, actuator torques and actuator power, solves the obained indeterminate equation system.

The balance action of a system including 3 VSCMGs of about 3 kg each, has been predicted through simulations which proved that it is able to correctly track the desired moment profile when it starts from configurations different from the upright position, until a maximum angular shift of 10° from the vertical. Even if the system is not able to generate a torque that compensates for larger angles, a beneficial effect is anyway expected. Indeed, an alternative goal of the balance device could slow down the fall and give the patient more time to regain balance by himself.

2.4.2 Inertial effect for human balance

The movement of the upper body relative to the lower body plays a big role to regain balance. When someone is about to lose his balance one of the strategies adopted to counteract the perturbing action is the rotation of his arms or his trunk in the same direction of the balance disruptive force. As long as they accelerate, the arms and the trunk generate an inertial torque on the human body that helps the subject to regain balance. The same effect is exploited by funambulists walking on wires while holding a long pole to keep balance. Several studies have been carried on to examine the balancing effect of a spinning flywheel on inverted pendulums [80, 81]. The torque generated when a rotating inertia is speed up, can be used to balance systems in the plane that is orthogonal to the flywheel spin axis. Based on this principle, spinning flywheel are accelerated to apply a corrective action on the human body to counterbalance perturbing actions in the frontal plane [24]. The human balance-keeping feedback control is replicated by the balance device presented in [24], that, once the lose of balance is detected, generates a counter torque based on the measurement of body deflections. Furthermore it supports human balance in harmony with the human's own posture control mechanisms such as postural reflexes, that are supposed to work correctly in the "natural recovery area", which is limited by threshold values of sway speed and angles (Fig. 2.11).

The balance device of [24], whose specs are listed in table2.1, has been tested in

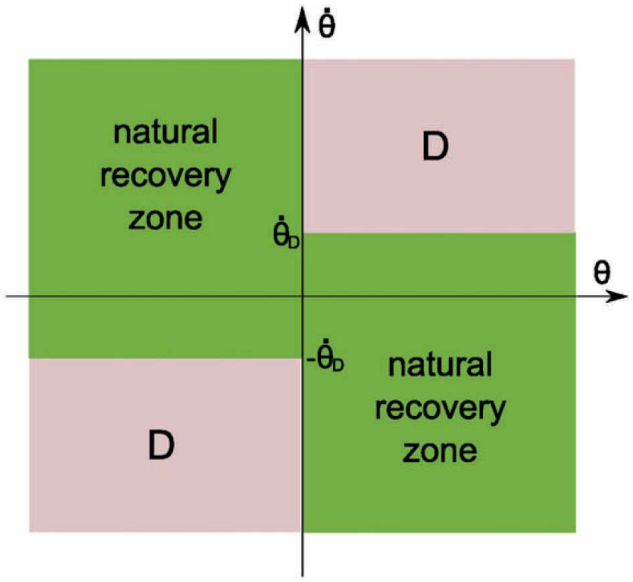

Figure 2.11: Diagram illustrating the working operating area of the device (D). The balance device of [24] is supposed to work consistently with human's own posture control mechanisms, that are supposed to work correctly in the Natural Recovery Area. The operating area of the device is limited by threshold value on the sway speed when both the sway angle and speed have the same orientation. The digram is adapted from [24].

standing and walking (Fig. 2.12) and an it has been proved to enhance the human balance performance action by providing a maximum balance torque of about 7 Nm. During tests the effect of feedforward and feedback control lows have been compared, proving that a more efficient control low that matches human innate postural reflexes must be designed to improve the balance keeping action of the balance device.

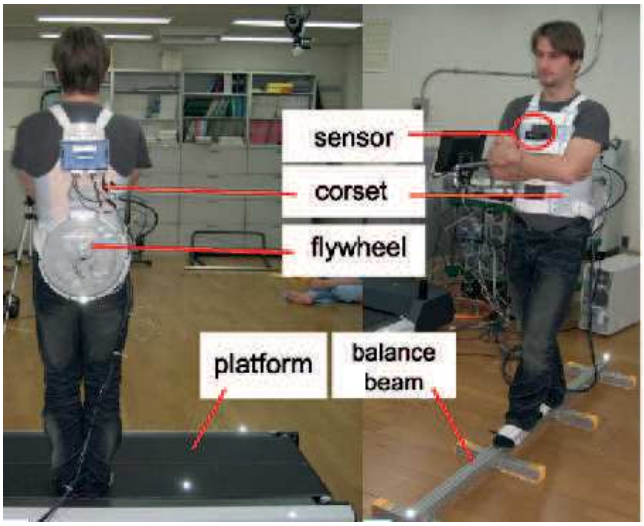

Figure 2.12: Balance assistive device presented in [24]tested in human stance and walking. It provides a corrective torque to the human body accelerating the flywheel once the subject loses his balance.

Parameter name	Value
Flywheel weight	2.2 kg
Flywheel diameter	300 mm
Flywheel moment of inertia	0.028 $kg\,m^2$
Motor stall torque	4.5 Nm
Motor nominal torque	0.5 Nm
Motor maximal prmissible speed	5000 rpm
Pulley ratio	4:1

Table 2.1: Technical features of the balance device presented in [24]

3 Flywheel-Infinitely Variable Transmission Actuators

3.1 Overview

One of the greatest limits to the development of powered orthoses, exoskeletons and prostheses, deals with their portability that is often limited by current actuation technologies which impede the development of devices with both reasonable weight and acceptable operating range [5]. This is a relevant issue especially in wearable robots for lower limbs because of the high power demand of locomotion tasks. Actuators must supply high peaks of power and torque in order to replicate the walking patterns. Nevertheless, the size of an actuator is basically affected by its torque and power requirements (e.g., the higher they are, the bigger and heavier is the motor), and thus the actuation design of these robots usually results in a compromise between powerful systems and small and lightweight devices. The stiff coupling of the motor to the leg joint through a transmission gear, which characterizes most of the commercially available systems, is the actuation scheme that is mainly affected by this issue because the motor is selected with reference to the leg joint requirements.

Energy recovery is a smart strategy to face this problem and reduce the net energy consumption of actuators of these legged robots. Leg joints require positive and negative power in walking gait cycles, giving the chance to recover energy. Energy recovery during normal operation could extend the portability of wearable devices by enlarging their operating range and by reducing the power demanded to the motor. Different actuators with energy recovery capabilities have been developed with this aim. However, beyond the motor power, also the motor torque requirement should be reduced in order to achieve an effective motor downsizing and thus solving the nodal question of actuation requisites. Indeed, the size and the weight of a motor increase with the nominal torque.

These fulfillments are addressed by the Flywheel-Infinitely Variable Transmission (F-IVT) actuator, a new concept of actuator in which the main source of power is a high speed rotating mass (flywheel) acting as a kinetic energy storage device. The flywheel energy storage has been recently reconsidered in the automobile field under the denomination of mechanical KERS (Kinetic Energy Recovery System). It is one possible short-term solution to achieve an improvement of the fuel economy performance of automobiles. In mechanical KERS, the energy is moved from the load (vehicle) to the flywheel under negative work phases and from the flywheel to the load otherwise [82] . When the vehicle brakes, its kinetic energy, instead than being dissipated in thermal losses, is delivered from the tires to the flywheel where it is stored (Fig.3.1). Under this phase, the speed ratio of the variator decreases in order to permit the recovery energy path. Conversely, when the vehicle accelerates energy is moved from the flywheel to the tires by increasing the speed ratio of the variator. Under this latest condition additional power is provided by the thermal engine. It is worth to notice that in a powertrain with a mechanical KERS, as well as in the F-IVT, the energy recovery does not involve any energy conversion, with advantage in terms of efficiency.

Inspired by KERS, the F-IVT is supposed to lead to potential benefits when employed in powering knee bionic joints. The key and non-conventional elements of this alternative design of actuator are the flywheel and a micro Infinitely Variable Transmission (IVT). This particular powertrain configuration permits to exploit efficiently the dynamics of human locomotion which offers the possibility to recover energy: energy is stored in the flywheel under the passive phases of the gait cycle and it is delivered to the knee joint under the active phases (Fig. 3.2). The IVT plays a significant role in the actuator: by changing its speed ratio (τ_{IVT}) in a range defined by a positive (τ_{IVT}^{max}) and a negative boundary values (τ_{IVT}^{min}), it controls the flow of energy between the flywheel and the joint, and always adapts the nearly constant flywheel speed to the desired joint speed.

The concept of the F-IVT has been elaborated upon in two different variants of the actuator. The first one, that will be referred to simply as F-IVT from now on, includes a motor in the power train which acts as an additional source of energy and delivers an almost constant amount of power to mostly compensate for power losses in the power train. The second variant is a self-powered actuator whose only source of power comes from the energy absorbed by the knee and stored in the flywheel. Differently from the first option, the latest is expected to power knee joint only in

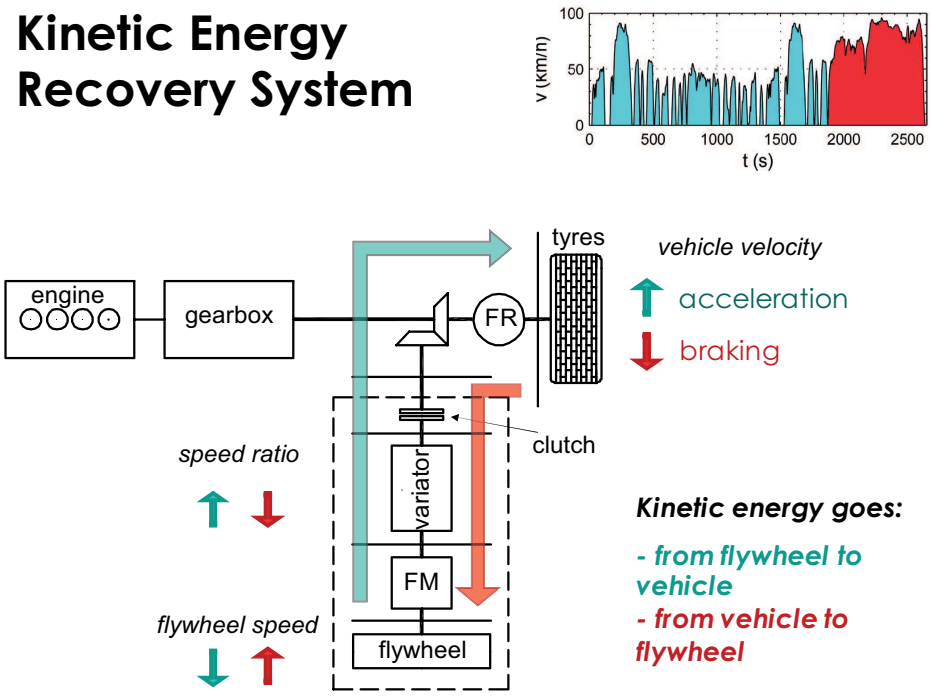

Figure 3.1: The mechanical KERS consists of a flywheel connected to the engine by a variable ratio transmission. The energy produced by the vehicle during braking is stored and converted by a system of pulleys and gears that works on the block gear-converter-flywheel. The arrows show the direction of power flows in a power train including a mechanical KERS: energy flows from the tires to the flywheel when the vehicle brakes, and from the flywheel to the tyres when it accelerates. Adapted from [82].

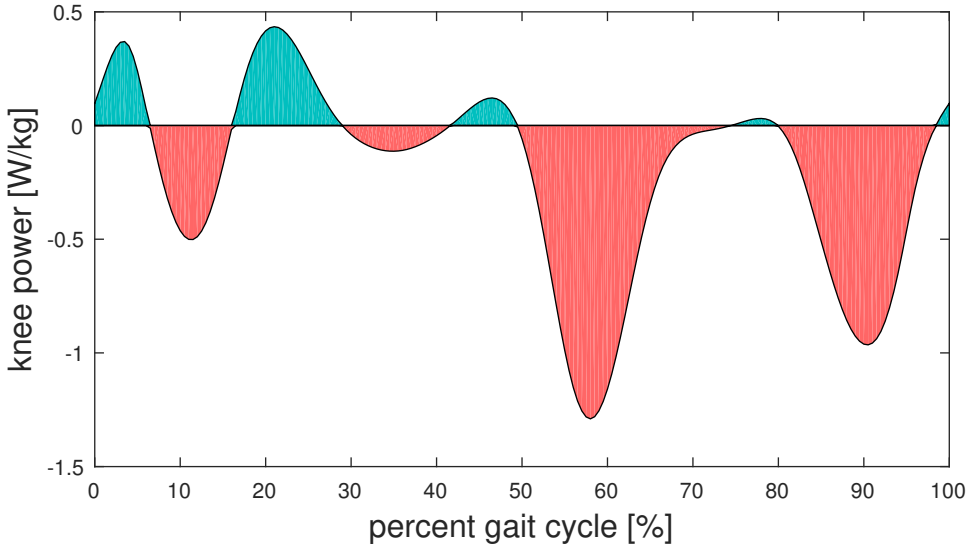

Figure 3.2: Instant power requirement of the knee joint in level ground walking at natural speed. The active and passive phases of the gait cycle are distinguished: in the active phases the power is positive and the knee demands power, in the negative ones the power is negative the knee dissipates power.

locomotion conditions whit negative energy expenditure in a cycle. Therefore, power demanding activities, as stairs climbing, have not been considered in the evaluation of the self-powered F-IVT.

3.2 Flywheel - Infinitely Variable Transmission

The F-IVT is an actuator with energy recovery capabilities for knee joints of wearable robots. It includes a brushless DC motor, a flywheel, a micro Infinitely Variable Transmission (IVT) and a fixed ratio drive gear (FR) (Fig. 3.3). The working principle and the resulting advantages of the F-IVT mainly depend on the combined action of the flywheel and the IVT, which are are the key elements of the actuator. The flywheel, a high speed rotating mass, is coupled directly to the motor and they spin at the same almost constant velocity. It acts as a mechanical energy storage device and reduces the motor motion irregularity in order to make it work efficiently. The IVT is a continuously variable transmission whose speed ratio, which is defined as the ratio between its output and the input shaft velocities, changes continuously in a range limited by a maximum positive and a minimum negative boundary values. The continuous change of τ_{IVT} adapts the nearly constant motor

speed to the variable angular velocity of the knee. An IVT and not a CVT is needed in this application because the knee speed spans among positive and negative value. The IVT performs a crucial role in the actuator also because its speed ratio controls the direction of the power flow between the flywheel and the knee: energy is stored in the flywheel when the knee power demand is negative (reverse motion) and it is released otherwise (forward motion), as it is schematically depicted in figure 3.3.

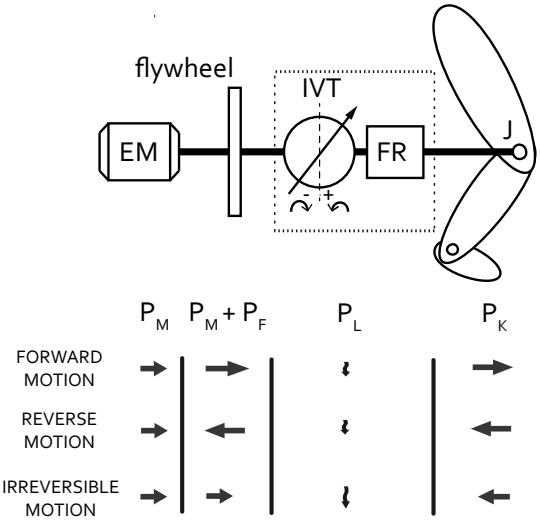

colora questa figura: bande colorate per ogni sezione

Figure 3.3: Fluxes of power in the F-IVT under forward, reverse and irreversible motion conditions. The arrows indicate the power flows direction in each of them:P_M motor power, P_F rate of change of the kinetic energy of the flywheel, P_L power losses in the transmission devices, P_K knee power.

The main idea behind the concept of the F-IVT actuator comes from the evidence that legged locomotion can be very efficient. Indeed the instant power requirement of leg joints oscillates between positive and negative values in a gait cycle (Fig. 3.2), meaning that joints sometimes need power for propulsion (positive power) and sometimes need to be braked (negative power). Furthermore joint power, as well as all the kinetic and kinematic characteristics of the joints, changes in a periodic fashion in a gait cycle. For these reasons the average power per gait is much smaller than the peak power (positive and negative) requested, being even negative in the case of the knee joint in normal walking. These peculiarities of human walking suggest that, beyond the possibility to recover energy during gait cycles, the total knee power requirement can be satisfied by delivering the energy recovered and by a constant input power, delivered for instance by the motor.

This is the operating principle actually performed by the F-IVT actuator. Indeed, more than exploiting the passive dynamic of human walking by recovering energy, the working principle of the F-IVT makes the energy storage device the main source of power of the actuator. The flywheel in the F-IVT filters the variable knee power request and the motor only feeds the system with the average power need to work. The motor delivers almost a constant amount of power to mostly compensate for power losses in the power train. Therefore, being the motor speed nearly constant, the motor applies an almost constant torque to the flywheel, thus working on a fixed operating point at optimal energetic efficiency.

The stabilization of the working point of the motor is one of the most relevant benefits of the F-IVT which could bring to remarkable motor downsizing. Indeed, since average power and torque are much smaller than their peak values, the motor can be greatly undersized. Furthermore, if the motor working point is almost fixed, a smart design can lead to make the motor work always with high efficiency.

Two different design of have been elaborated: the *rotating F-IVT* and the *linear F-IVT* (Fig. 3.4). They differ from each other in the final transmission stage that is a harmonic drive (HD) gear in the *rotating F-IVT* and it is a ball screw (BD) plus a mechanism in the linear F-IVT. The different actuation scheme of the *rotating* and the *linear F-IVT* also involves relevant differences about the embodiment of the overall assembly: the *rotating F-IVT* is fixed concentrically to the knee joint, while the mechanism joins the *linear F-IVT* to the knee joint and adapts the BS output linear motion to the rotating one of the knee. A schematic picture of the mechanism is given in figure 3.4c. The output shaft of the BS is connected to the link l_2 of the mechanism, whose length changes as the linear displacement of the BS. The actuator is rigidly joined to the femur trough links l_1 and l_3 , and it is fixed to the tibia by the rigid body identified by the link l_3 and by the constant angle ψ. It is expected that the very high efficiency of BS in the linear F-IVT, and the possibility to optimize the geometry of the mechanism in order to achieve a more efficient usage of the IVT should lead to a much better energy saving performance in comparison with the *rotating F-IVT*. Indeed, it is expected that the lower power losses in the BS than in the HD would improve the power profile at the output shaft of the IVT of the *linear F-IVT* that, if the average efficiency of the IVT in both the actuation schemes is nearly the same, would result in a greater amount of energy to be stored and a more efficient usage of the energy delivered by the flywheel.

The different actuation scheme of the *rotating* and *linear F-IVT* also involves relevant differences about the embodiment of the overall assembly. Even though the connection of the actuator to the human joint is expected to be more complex in the *linear* than in the *rotating F-IVT*, the side encumbrance of the former is lower. Indeed, while the *rotating F-IVT* is nearly aligned with the joint axis resulting in a side positioning of the actuator, the linear F-IVT is mainly located in the back of the leg. The *linear F-IVT* is also expected to conform better than the *rotating* one to the variable rotational axis of the knee joint.

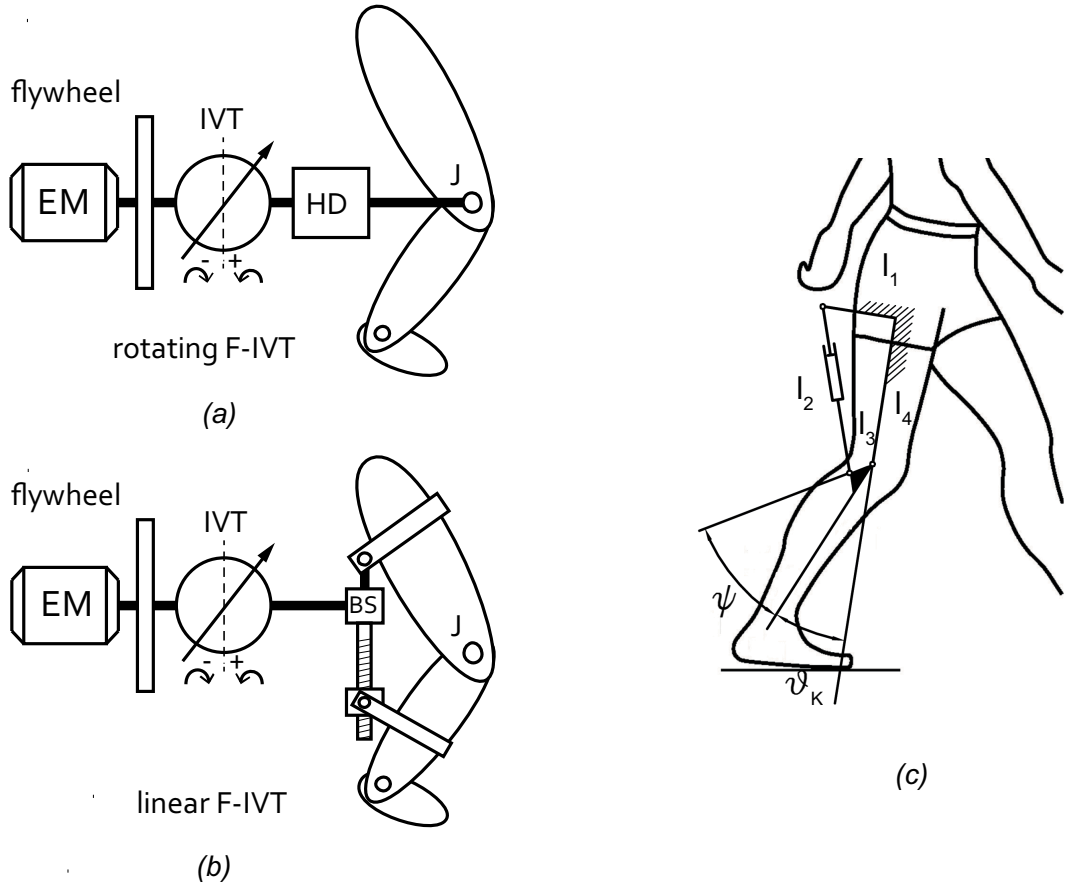

Figure 3.4: Schemes of the two different designs of the F-IVT actuator: *a)* the *rotating F-IVT* is made up of a Brushless DC motor, of a flywheel, of an IVT and of a HD gear; *b)* the *linear F-IVT* includes a Brushless DC motor, a flywheel, an IVT, a BS (ball screw) and a mechanism. In the picture *c)* details on the geometry of the mechanism of the *linear F-IVT*, which joins the actuator to the human limb, are given.

3.2.1 Infinitely Variable Transmissions

The alternate motion of the knee joint requires a mechanical transmission that is able to change seamlessly the speed ratio from positive to negative values (IVT). Different typologies of IVT have been proposed in literature [83, 84, 85, 86, 87, 88] each of them based on a different working principle. The most popular configuration of IVT is the shunted CVT architecture, which is the one considered in the F-IVT performance simulations. In truth, there are different typologies if IVTs that would probably be more suitable for exoskeletons because of their simpler construction [86], even though their performance are still under investigation. The shunted CVT architecture of IVT is made of the following component devices: a micro-toroidal CVT, a micro planetary gear train (PG) and a fixed speed ratio drive (FR). In order to evaluate and compare the efficiency of different joint drives, accurate models of the power loss in the drive components, and in particular in the transmission, are necessary[89]. The micro-toroidal CVT was assumed to incorporate a torque-sensitive mechanism, which permits to supply a clamping force on the CVT proportional to the transmitted torque, with a resulting efficiency very close to the optimal one obtained through an optimal control of the clamping force [90]. CVT, shunted CVT and IVT transmissions have been extensively studied theoretically and experimentally in the past[91, 90, 92, 93, 94, 95, 96], thus efficiency models of these transmissions both in direct and reverse operation are available in the literature[89, 97][89, 97]. Furthermore, novel unconventional applications have already been proposed [98]. In the proposed system the IVT permits the motor to work almost at fixed operating point, close to the most efficient condition, by adapting the speed ratio to the end-user requirements. This latest aspect is a great advantage in the mechanical systems where the IVT is introduced because it permits to cut off motor's consumptions and size [98, 99, 100]. These achievements are very important for exoskeletons, since they lead to the improvement of the operating range and the wearability.

Efficiency Model

Among the different typologies of IVT proposed in literature [83, 84, 85, 86, 87, 88], the most popular one is the shunted CVT architecture (Fig. 3.5) which includes the following component devices: a micro-toroidal CVT (Continuously Variable Transmission), a PG (micro planetary gear train) and a FR (fixed speed ratio drive). An

IVT with shunted CVT architecture was considered in the F-IVT actuator, because mathematical models of its efficiency are well established in the literature [89].

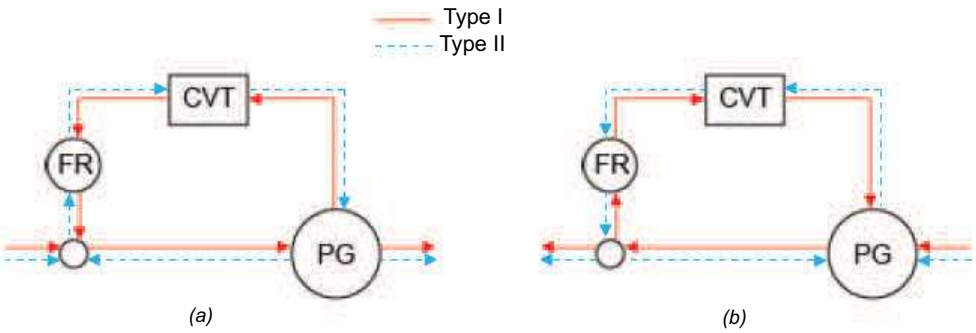

Figure 3.5: Schematic picture of the shunted CVT architecture of IVT, where power circulation of type I or of type II can take place. Figures above depict the two types of power circulation in direct *(a)* and in reverse *(b)* operating modes.

An IVT is needed in the actuation system of lower limb joints because it is able to continuously change its speed ratio between positive and negative values, permitting the motor speed to be kept constant or nearly constant, while the joint always works at the desired speed value. The IVT speed ratio is given as a function of the transmission ratios of all the components of the IVT:

$$\tau_{IVT} = \frac{1 + \tau_{CVT}\tau_{FR}\chi}{1 + \chi} \tag{3.1}$$

Where τ_{FR} is the speed ratio of the FR and χ is the basic transmission ratio of the PG. Very often the lower and upper bounds of τ_{CVT} are fixed, being an intrinsic geometric feature of the device. The IVT under consideration includes a micro-toroidal CVT whose ratio range varies between 0.4 and 2.5. The speed ratio range of the IVT has also to be fixed to match the requirements of the load. Once the lower and upper bounds of τ_{IVT} and τ_{CVT} are chosen, both τ_{FR} and χ can be calculated through Eq. 3.1. The IVT enlarges the transmission ratio range of the CVT, but this increase involves a power circulation in the IVT device, which can be reverse or forward according to the relationship between τ_{IVT} and τ_{CVT}. The reverse power circulation, which is named power flow of Type I, is characterized by a monotonic decrease of τ_{IVT} when τ_{CVT} increases, conversely the forward power circulation, named power flow of Type II, by a monotonic increase of τ_{IVT} when τ_{CVT} increases.

The IVT with a Type I power flow for positive value of the τ_{IVT} and with a Type II power flow for the negative ones, was chosen as the most adequate for our purposes. The efficiency of the IVT (η_{IVT}) was modeled as in [89], considering the different operating modes of the transmissions, i.e. the direct, the reverse mode and the conditions under which the IVT is not back-drivable. η_{IVT} is affected by the type of power circulation both in direct and reverse operating mode. The efficiency of the IVT is estimated through the following equations in forward (from flywheel to the knee) or reverse (from the knee to the flywheel) operations:

$$\text{forward mode } \eta_{IVT} = \begin{cases} \frac{1+\tau_{CVT}\tau_{FR}\chi}{1+\tau_{CVT}\tau_{FR}\chi\eta_{CVT}\eta_{FR}}, & \text{Type I}(\tau_{IVT} \geq 0) \\ \\ \frac{\eta_{CVT}\eta_{FR}(1+\tau_{CVT}\tau_{FR}\chi)}{\eta_{CVT}\eta_{FR}+\tau_{CVT}\tau_{FR}\chi}, & \text{Type II}(\tau_{IVT} < 0) \end{cases} \tag{3.2}$$

$$\text{reverse mode } \eta_{IVT} = \begin{cases} \frac{\eta_{CVT}\eta_{FR}+\tau_{CVT}\tau_{FR}\chi}{\eta_{CVT}\eta_{FR}(1+\tau_{CVT}\tau_{FR}\chi)}, & \text{Type I}(\tau_{IVT} \geq 0) \\ \\ \frac{1+\tau_{CVT}\tau_{FR}\chi\eta_{CVT}\eta_{FR}}{1+\tau_{CVT}\tau_{FR}\chi}, & \text{Type II}(\tau_{IVT} < 0) \end{cases} \tag{3.3}$$

where η_{CVT} and η_{FR} are respectively the efficiency of CVT and FR, for which the following values are assumed: $\eta_{CVT} = 0.93$, $\eta_{FR} = 0.98$. η_{CVT} is assumed to be constant because a micro-toroidal CVT equipped with a torque sensitive device was considered. The torque sensitive cam, a simple and inexpensive device, permits to supply a clamping force on the CVT proportional to the transmitted torque, with a resulting efficiency very close to the optimal that would be obtained through an optimal control of the clamping force [91]. Such system permits to reach almost the highest value of efficiency for any requested load [101, 102] also minimizing the effect of the speed ratio of the CVT on the value of its efficiency as demonstrated in [103]. As a consequence of these achievements, we considered that the micro-toroidal CVT with torque sensitively regulated clamping force included in the F-IVT has the efficiency almost independent on the speed ratio and the load in our simulations. In the F-IVT, an IVT with a Type I power flow for positive value of the τ_{IVT} and with a Type II power flow for the negative ones is considered.

Figure 3.6 shows the efficiency curves of the IVT included in the linear F-IVT. It

can be noticed that η_{IVT} is very low for small values of τ_{IVT}, close to the neutral gear condition ($\tau_{IVT} = 0$) [98], and increases with the absolute value of τ_{IVT} up to reach its maximum value at the boundaries of the IVT ratio range (τ_{IVT}^{min}, τ_{IVT}^{max}). Thus, the ratio range can be chosen according to the speed range of the knee joint to improve the global efficiency of the IVT. It is also important to notice that the efficiency in forward operation is larger than in reverse operation in particular at small $|\tau|$, and that if η_{IVT} is null τ_{IVT}, the back drive ability of the transmission is not permitted.

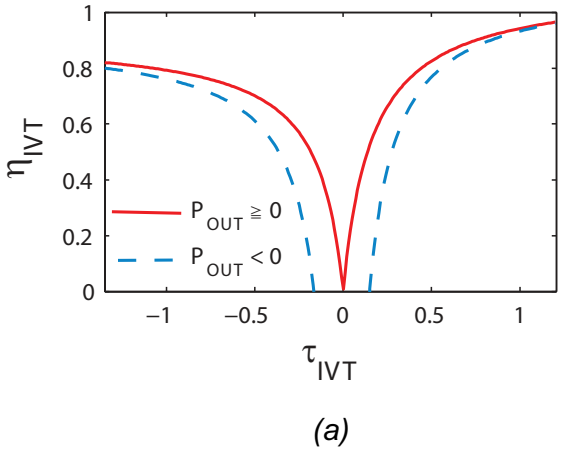

Figure 3.6: IVT efficiency map in forward and reverse operation mode according to [89]. η_{IVT} is mainly a function of τ_{IVT} and it reaches its highest values for τ_{IVT} close to the boundaries of the IVT ratio ($\tau_{IVT}^{min} = -0.85, \tau_{IVT}^{max} = 1$).

3.2.2 Harmonic Dive Gears

Efficiency Model

The HD unit is directly connected to the knee joint. Harmonic Drives are usually chosen in biomechatronics application because of the large torque capacity, high gear ratios and small size [39]. HD efficiency depends mainly on the speed of the input shaft and on the torque of the output shaft [104] as well as their size, the temperature and the lubrication. In figure 3.7the efficiency of the HD unit is given as a function of the absolute values of the output torque (C_{OUT}) and speed in direct ($P_{OUT} \geq 0$) and reverse ($P_{OUT} < 0$) operation respectively. HD drives permit the power flow inversion only under certain conditions of output torque and input speed, being irreversible otherwise. All these aspects have been considered in the model of

the HD unit efficiency, following the guideline given by one manufacturer (Harmonic Drive AG).

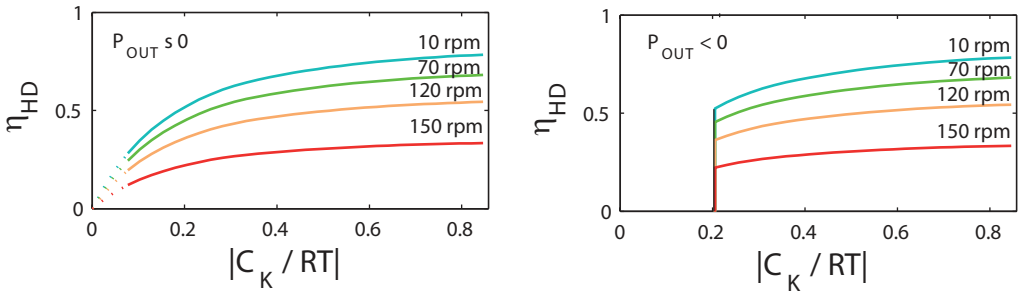

Figure 3.7: Efficiency maps of the HD gear. The maps distinguish the performance of the transmission devices in forward ($P_{OUT} \geq 0$), reverse ($P_{OUT} < 0$) and irreversible motion conditions. η_{HD} is given as a function both of the output motor speed and of the torque at the output shaft normalized to the rated torque (RT) of the HD gear selected.

3.2.3 Actuator Model

A simulation tool for estimating the performance of the actuator in terms of energetic efficiency has been developed.Three performance indexes have been mainly considered: the energy consumption (per gait), the peak of electric power and the peak of motor torque. These are significant quantities for the development of lightweight and portable wearable robots because they affect the size and the weight of the actuator, as well as the operating range of the device. The energetic and power requirements of all the actuators have been calculated through a back-dynamic approach, that is to say starting from the load characteristics (knee angle and torque vs time) given as input data to the model (Fig. 2.4).

In particular, level ground walking in a range of speeds and stairs climbing at different inclination have been considered as locomotion conditions. Herewith an explanation of the mathematical model of the actuator follows.

The following equation is the power balance equation of the F-IVT, in which the motor power (P_M) and the rate of change of the kinetic energy of the flywheel (P_F) overcome power losses into the transmission devices (P_L) to satisfy at each time the

power request of the knee joint (P_K):

$$P_K = P_M + P_F + P_L \tag{3.4}$$

Each term of equation 3.4 is explained below. In the F-IVT the motor must provide an almost constant power, while the flywheel provides the variations of the requested power at the knee joint. As a consequence of the working principle of the F-IVT,P_M is given by the product of a nearly constant angular speed ω_M and a constant torque (C_M). The continuously variation of τ_{IVT} between positive and negative values ensures that the constant motor speed (ω_M) and the changeable knee angular velocity (ω_K) are always matched. The kinematic relationship between ω_M and ω_K is expressed by:

$$\omega_M = \frac{\omega_K}{\tau_{IVT}\tau_{FR}} \tag{3.5}$$

where τ_{FR} is the fixed speed ratio of the final transmission stage of the F-IVT. τ_{FR} is equal to the transmission gear ratio of a harmonic drive (τ_{HD}) in the *rotating F-IVT,* and it is given by the product of the constant speed ratio of the ball screw ($\tau_{BS} = \frac{lead}{2\pi}$) and the instant value of the speed ratio of the mechanism (τ_{MECH}) , which comes from its kinematic analysis:

$$\tau_{MECH} = \frac{\omega_K}{\dot{l}_2} \tag{3.6}$$

with $\dot{l}_2$ the time derivative of the length of the link l_2 of the mechanism.

With the motor speed being nearly constant , in order to achieve an almost constant power delivery, the motor is supposed to be controlled with constant torque given by:

$$C_M = \frac{1}{T\bar{\omega}_M}\int_0^T (P_F - P_L)dt \tag{3.7}$$

where T is the period of the gait cycle, $\bar{\omega}_M$ is the mean value of the motor angular

speed and $(P_F - P_L)$ is the total amount of powerto be provided by the motor and flywheel block.

The power delivered by the flywheel (P_F of Eq. 3.4) is the rate of change of its kinetic energy that a function of the flywheel inertia (J_F), of the angular motor speed ($omega_M$) and acceleration ($\dot{\omega}_M$):

$$P_F = -J_F \dot{\omega}_M \omega_M \tag{3.8}$$

Equation 3.8 shows clearly that the flywheel inertia (J_F), the angular motor speed (ω_M) and acceleration ($\dot{\omega}_M$) are the factors that affect the storage capacity of the flywheel. Neglecting $\dot{\omega}_M$that has few relevance in this application, a bigger and/or heavier flywheel or mass rotating very fast may lead to a maximization of the flywheel storage capacity. However, actuators for lower limbs have to face

In order to have a realistic evaluation of the performance of the actuator, the power lost (P_L) in all the mechanical drives of the F-IVT has been considered in the total power balance of the system (Eq. 3.4). P_L can be calculated by adopting detailed efficiency models of all the mechanical drives included into the actuators. These models estimates the power losses considering the real operating condition of the devices as the actual values of speeds and torques and the direction of the power flow (i.e. forward or reverse operating mode). The adopted efficiency models also consider the non reversible motion condition, which implies that P_M, P_F and P_K are all delivered to the transmission and dissipated as heat losses (Fig. 3.3). This situation can involve the IVT, the FR or both simultaneously, depending on the actual values of speed and torque. In particular, the model given in [89] has been adopted for predicting the efficiency of the IVT (η_{IVT}) and the guidelines of the data sheets of HD and BS gears have been followed for estimating the efficiency of the adopted fixed ratio drive (η_{HD}, η_{BS}). In the *linear F-IVT* power losses in the mechanism are neglected. The BS always delivers power with almost constant and high efficiency both in the forward and reverse mode.

Power losses in the F-IVT can be estimated with following equation where the

forward and reverse operating modes are distinguished:

$$P_L = \begin{cases} -(1-\eta^f_{IVT}\eta^f_{BS})(P_M + P_F), \text{forward mode} \\ \\ -(1-\eta^r_{IVT}\eta^r_{BS})P_K, \text{reverse mode} \end{cases} \tag{3.9}$$

In equation 3.9 $\eta^f_{IVT}, \eta^r_{IVT}, \eta^f_{FR}, \eta^r_{FR}$ are the efficiency of the IVT and of the FR in forward (f) and reverse (r) power flows.

The previous equations are collected into an iterative procedure aimed at predicting the working points of the motor ($\omega_M(t)$,$C_M(t)$). The iterative calculation is necessary to find the actual value of $\omega_M(t)$ in the gait cycle, which is not known a priori. Starting from a guess constant motor speed value (ω^0_M), we compute first the corresponding values of $C_M(t)$ (Eq. 3.7) and than those of $\dot{\omega}_M(t)$ (Eqs. 3.4, 3.9, 3.8), from which ω^1_M can be obtained through a numerical method (Newton-Raphson method). At integration step j, an error is defined as $Err_j = \frac{1}{T}\int_0^T (\omega^{j+1}_F - \omega^j_F)^2 dt$. The iteration stops when $Err_j \leq Err_{max}$ where Err_{max} is the error tolerance, and requiring also that the constraints on the IVT ratio are fulfilled ($\tau^{min}_{IVT} \leq \tau_{IVT} \leq \tau^{max}_{IVT}$).

After the mechanical motor requirements are defined, the electric power demanded to the motor can be predicted through the equations governing the behavior of a DC motor:

$$i_M = \frac{C_M}{k_t} + \frac{J_M\dot{\omega}_M}{k_t} + \frac{\nu\omega_M}{k_t} + \frac{sign(\omega_M)C_{fr}}{k_t} \tag{3.10}$$

$$V_M = Ri_M + k_{emf}\omega_M \tag{3.11}$$

where i_M and V_M are respectively the electric motor current and voltage, k_t the motor torque constant, ν the damping friction coefficient, C_{fr} the Coulomb friction torque, R the motor resistance , k_{emf} the back EMF constant, J_M the motor inertia.

The electric motor power (P_{EL}) was defined as:

$$P_{EL} = \begin{cases} V_M i_M, P_M \geq 0 \\ V_M i_M \eta_{gen}, P_M < 0 \end{cases} \tag{3.12}$$

where η_{gen} is the efficiency of converting mechanical power into electrical power. According to [105], in the reverse operation it may happen that the electric motor is not able to generate electricity. In those cases, $P_{EL} = 0$. At last, the electric energy demanded at the motor electrodes is calculated as the time integral of the electric power:

$$E_{EL} = \int_0^T P_{EL} dt \tag{3.13}$$

3.2.4 Sizing Procedure

A wearable assistive device for lower limbs is expected to assist the wearer in its daily activity. Thus the F-IVT is sized to ensure some of the most common human walking regimes, which have been identified with level ground walking at different speeds (0.5, 1.1, 1.6, 2.1 m/s) [16] and stairs climbing at different inclinations (24, 36, 42°) [106]. To design an efficient F-IVT, both the most powerful and the most frequent working conditions must be considered. In particular, the former ensures that the actuator is powerful and robust enough to provide and to resist the maximum forces and torques demanded. Whereas the latter (level ground walking at 1.1 m/s) is necessary to optimally design the F-IVT in such a way it can work very efficiently over most of its operation. Level ground walking at natural speed (1.1 m/s) has been assumed to be the most common locomotion condition, while gait cycle analysis data suggest that stairs climbing at the maximum inclination is the most power demanding condition.

The optimal design of the F-IVT leads to the choice of the motor, the fixed ratio gear, the ratio range of the IVT and the related value of the motor working speed. Indeed, as it will be clarified later, the optimization of the IVT consists in the

calculation of its optimal speed ratio range, which also has a direct influence on the actual working point of the motor.

The first step of the sizing procedure is aimed at selecting a suitable motor from the catalogue of one (or more) manufacturers. The key parameter is the mean value of the power requested to the motor at the most powerful condition, the value of which has to be approximately equal to the motor nominal power. Indeed, based on the working principle of the F-IVT, the electric motor is required to provide nearly the mean value of the power demanded by the load in a cycle, while the flywheel compensates the fluctuations of the requested power.

At this step we assume that the flywheel inertia is infinite, thus the motor runs at constant speed. Under this assumption, the constant power delivered by the motor is thus calculated:

$$\bar{P}_M = \frac{1}{T}\left(\sum_i \int_{T_{f,i}} \frac{P_K dt}{\bar{\eta}^f_{IVT}\bar{\eta}^f_{FR}} + \sum_j \int_{T_{r,j}} \sum \int_{T_{r,i}} \bar{\eta}^r_{IVT}\bar{\eta}^r_{FR} P_K dt\right) \tag{3.14}$$

where $\bar{P}_M$ is the average power requested to the motor, $T_{f,i}$ and $T_{r,j}$ are the time intervals of direct and reverse operation respectively, $T = T_{f,i}+T_{r,j}$ is the duration of the gait cycle, $\bar{\eta}^{f,r}_{IVT}$ and $\bar{\eta}^{f,r}_{FR}$ are the instant efficiency values of transmission drives in forward and reverse operating mode.

According to the IVT efficiency model [89], $\eta^{f,r}_{IVT}$ depends on the direction of the power flow, on the actual value of the speed ratio relatively to the speed ratio range. However, at this stage of the sizing procedure the IVT has not yet been selected, rather it will be one of the output of the optimized sizing procedure of the device. Therefore, being impossible to estimate power losses by applying the efficiency model of [89]at this step, efficiency guess values have been assumed for the IVT in forward ($\bar{\eta}^f_{IVT} = 0.6$) and in reverse ($\bar{\eta}^r_{IVT} = 0.5$) motion conditions to calculate $\bar{P}_M$.

The efficiency of the fixed ratio drive ($\bar{\eta}^{f,r}_{FR}$) corresponds to the efficiency of the HD in the *rotating F-IVT* and to the efficiency of the BS and its joint in the *linear F-IVT*.

Based on the efficiency model of the HD, $\bar{\eta}^{f,r}_{HD}$can be estimated as a function of the load condition once the gear has been selected. According to the guidelines suggested by one manufacturer (Harmonic Drive AG), a HD gear can be selected on the basis

of the maximum torque and speed applied, therefore the HD can be chosen at this stage of the sizing procedure and the power losses easily calculated by adopting the model described in section 3.2.2. Because in this application the speed limit of the HD is by far respected (the knee speed is always lower than the maximum speed allowed), the HD gear has been chosen constraining the greatest value of the output torque in all the gait cycles examined (i.e. stairs climbing at the maximum inclination), to be less than or equal to the Repeatable Peak Torque (RPT) value of the HD gear ($max\,|C_K| \leq RPT$). The selection of the HD gear focuses at the smallest size and the greatest efficiency, mainly depending on the speed of the input shaft and on the torque of the output shaft, by means of a coefficient that is a function of the Rated Torque (RT) value of the device. Among all the admissible options of HD gears (i.e. the ones that satisfy $max\,|C_K| \leq RPT$), the smallest one with the smallest RT value is chosen.

In the *linear F-IVT* the efficiency of the FR is given by the power losses in the BS and in the joint that connects the ball screw to the knee. The efficiency of BS mostly depends on the geometry of the BS and, as it is well supported by datasheets, its value is very large and almost constant in a wide range of working conditions. Therefore, the following efficiency guess values have been assumed in forward ($\bar{\eta}^f_{BS} = 0.95$) and in reverse ($\bar{\eta}^r_{BS} = 0.94$) motion conditions. Power losses in the joints of BS have instead been neglected.

Calculation of $\bar{P}_M$ (Eq. 3.14) is repeated for each of the working conditions examined. Stairs climbing at the 42° is the most power demanding walking condition, which leads to the choice of a 120W Brushless Maxon Motor in the *rotating F-IVT* and of a 60 W Brushless Maxon Motor in the *linear F-IVT* (Table 3.1). Once a suitable motor for the application has been selected, all motor parameters (Eqs. 3.103.11) are known and step 1 is complete.

The efficiency map of the motor is a necessary ingredient for the last step of the actuator design whose goal is the optimization of the actuator with reference to its prevailing operation. The second step of the sizing procedure selects the IVT ratio range and the relative working points of the motor by minimizing the energy consumption of the actuator under the most frequent locomotion condition (level ground walking at 1.1 m/s). The energy consumption of the actuator can be minimized if both the IVT and the motor work efficiently. Therefore, an iterative routine whose output is the average working point of the motor and the boundary values

of the IVT ratio range $\tau_{IVT}^{min/max}$have been implemented. $\tau_{IVT}^{min/max}$ are defined as the minimum and the maximum value of the IVT speed ratio profile respectively. The optimization routine simulates the operation of the F-IVT under the assumption of an infinite flywheel inertia (i.e. constant motor speed) coupled to an IVT and solves the constrained optimization problem (Table 3.2) by minimizing the electric energy at the motor electrodes (objective function). The iterative routine solves the set of equation provided in section 3.2.3.

The optimization procedure of the *linear F-IVT* differs from that of the *rotating F-IVT* in some aspects related to the different FR gears included. In the *linear F-IVT*, the ratio range of the IVT and the location of the BS joints have a straightforward influence on the working points of the motor and thus on the actual energy required. The location of the BS joints plays a key role in the optimization of the *linear F-IVT*. In fact, given the angle kinematics at the knee, the location of the BS joints defines the actual instant value of the IVT ratio needed to provide the matching between the motor and the knee speeds. Since the efficiency of IVT strongly depends on the speed ratio τ_{IVT}, it follows that the location of the BS joints is important to define the actual efficiency of the whole actuator. In the light of these considerations, the optimal design of the *linear F-IVT* is done through an optimization routine aimed at finding the optimal location of the BS joints and motor working speed, to minimize the electric energy demanded. In order to speed-up the calculations, we considered the IVT+BS as "equivalent IVT" (IVT*) , the speed ratio of which is the product between the speed ratios of the IVT and of the BS, and it is bounded between a minimum and a maximum value. The objective function is the energy demanded by the motor, which must be minimized by finding the optimal set of the optimization variables l_1, l_3, l_4 and ψ(location of BS joints) $\omega_{M_{1.1}}$ (motor speed in level ground walking at 1.1 m/s). For given set of the optimization variables, the constraint indicated in Table 3.2 must also be satisfied.

The parameters of each component of the *rotating* and of the *linear F-IVT* are given in Table 3.1. Once the actuator have been sized, the operation of the F-IVT can be simulated through the model given in Section 3.2.3, whose iterative routine starts with a guess constant motor speed value ω_M^0 equal to the motor speed that minimize the energy consumption of the actuator under the assumption of an infinite flywheel inertia. Thus ω_M^0 is equal to $\omega_{M_{1.1}}$ in level ground walking at 1.1 m/s and to other optimal values of ω_M found following the same optimization principle at all the other locomotion conditions.

		Rotating F-ITV	Linear F-IVT
Brushless DC Motor	model	EC-max 40 p.n. 283871	EC-max 30 p.n. 272764
	$P_{Nom}[W]$	120	60
	$C_{fr}[mNm]$	5.2	0.03
	$J_M[g\,cm^2]$	101	21.9
	$M_M\,[g]$	720	300
	$k_{emf}\,[\frac{V}{rad/s}]$	0.0628	0.0359
	$k_t[\frac{mNm}{A}]$	62.8	35.9
	$R\,[\Omega]$	2.02	2.48
	$\nu\,[\frac{Nm}{rad/s}]$	$8.66\,10^{-6}$	$4.3\,10^{-6}$
Flywheel	$J_V[g\,cm^2]$	$5\,10^3$	$5\,10^3$
IVT	τ_{IVT}	[-1.35, 1.21]	[-1.04, 1.17]
Gear Train	τ_{FR}	1/50	$3.18\,10^{-4}\,\frac{m/s}{rad/s}$
	η_{FR}	by model	0.97
Mechanism	$l_1\,[cm]$	-	15
	$l_3\,[cm]$	-	30
	$l_4\,[cm]$	-	5
	$\psi\,[^\circ]$	-	36

Table 3.1: Model parameters of the rotating and linear F-IVT. The motor damping parameters and the coulomb friction torque are not provided by data-sheet, but they were estimated following the guide lines given by Maxon.

Optimization Problem	
Objective Function	$min(E_{EL})$ in level ground walking at speed 1.1 m/s
Optimization Variables	l_1, l_3, l_4, ψ, $\omega_{M_{1.1}}$
Constraints on the Mechanism Geometry	$l_{i_{min}} \leq l_i \leq l_{i_{max}}$ $0 \leq l_3 \sin(\psi + \vartheta_K) \leq 20\,cm$ $0 \leq \varphi_i \leq 2\pi$ $0 \leq \psi \leq \psi_{max}$
Constraints on the IVT*	$\tau^*_{IVT_{min}} \leq \tau^*_{IVT} \leq \tau^*_{IVT_{max}}$
Constraints on the Motor	$0 \leq \omega_M \leq \omega_{M_{max}}$ $0 \leq max(C_M) \leq C_{M_{max}}(\omega_M)$ in all investigated working conditions
$l_{1_{max}} = 15cm$; $l_{2_{max}} = 30cm$; $l_{4_{max}} = 30cm$; $l_{1_{min}} = 0cm$;	
$l_{3_{min}} = 5cm$; $l_{4_{min}} = 5cm$; $l_{2_{min}} = 5cm$; $\psi = \pi - max(\vartheta_K) - 10°$;	
$\tau^*_{IVT_{max}} = \tau_{IVT_{max}} \tau_{BS_{max}} = 2.1\,8\,10^{-4}\,\frac{(m/s)}{(rad/s)}$;	
$\tau^*_{IVT_{min}} = \tau_{IVT_{min}} \tau_{BS_{min}} = 1.1\,1.6\,10^{-4}\,\frac{(m/s)}{(rad/s)}$	

Table 3.2: Optimization routine aimed at finding the optimal size of the linear F-IVT which is the one that minimizes its energy consumption

3.3 Self-powered Flywheel-Infinitely Variable Transmission

The self-powered Flywheel-Infinitely Variable Transmission (self-powered F-IVT) is an actuator for knee joint of wearable robots that exploits the efficient energetics of human walking to fulfill the total joint power requirement, without resorting to any additional power injection from motors. Beyond a flywheel acting as an energy storage device, no source of power is indeed included into the actuator. By starting from the evidence that knee energy expenditure in a gait cycle of level ground walking is negative, meaning that its passive phases, in which muscles absorb energy from the knee, prevail on its active phases, in which they deliver power to the joint

(Fig. 2.4), the self-powered actuator uses only the energy recoverable from walking gait cycles to power the knee joint. The self-powered F-IVT is expected to recover energy from the knee joint under the passive phases of human walking, to store it in a flywheel and to deliver it to the knee joint when required, by controlling the IVT speed ratio.

The actuation scheme of the *self-powered F-IVT* (Fig. 3.8) is similar to that of the *linear F-IVT* (Fig. 3.4) with the difference that it does not include the motor. Figure 3.8 provides a schematic representation of the novel self-powered F-IVT actuator, whose main components are a flywheel, an Infinitely Variable Transmission (IVT) and a Ball Screw (BS) transmission. The output linear motion of the BS is adapted to the rotative motion of the knee joint through the same linkage structure of the *linear F-IVT* (3.8b). The output shaft of the BS is connected to the link l_2 of the mechanism, the length of which is regulated by the linear displacement of the BS. The actuator is rigidly joined to the femur trough links l_1 and l_3, and it is fixed to the tibia by the rigid body identified by the link l_3 and by the constant angle ψ. Lenghts l_1, l_3, l_4 and angle ψ affect the actual speed ratio between the knee joint and the input shaft of the BS transmission, so they must be determined according to some design criterion, as it will be shown in the following sections.

As it also happens in the *rotating F-IVT* and in the *linear F-IVT*, the IVT plays a significant role in the actuator. It changes its speed ratio (τ_{IVT}) in a range defined by a positive and a negative boundary values, it controls the flow of energy between the flywheel and the joint, and always adapts flywheel (nearly constant) speed to the desired joint speed.

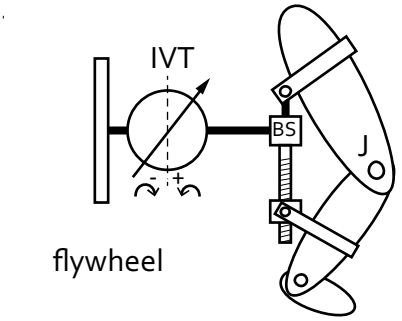

Figure 3.8: Schematic representation of the self-powered F-IVT actuator. It includes a flywheel, an Infinitely Variable Transmission (IVT), a Ball Screw (BS) and a mechanism (Mech.) to convert the linear motion at the output shaft of BS in the rotating one of the knee joint.

The main peculiarity of the *self-powered F-IVT* is that it does not include any external source of energy to deliver power to the knee joint, rather it uses the energy recoverable during the gait cycle to satisfy the total knee energy demand. As a consequence of that, the performance of the *self-powered F-IVT* in terms of power and force deliverable are strictly dependent on the actual working condition of the device: higher is the amount of energy recoverable in a gait cycle, higher is the probability that the actuator could provide the quantity of power needed. Of course, as the energy conservation principle teaches, only if the amount of energy absorbed by the joint is greater than the energy demanded, the actuator can be considered as a valid actuation option for satisfying the total knee energy demand, otherwise an external power injection would be needed. Because of that, the *self-powered F-IVT* actuator has been assessed just in level ground walking in a range of speeds.

3.3.1 Actuator Model

A mathematical model of the self-powered F-IVT has been developed to evaluate if the actuator can provide the needed knee power in level ground walking in a range of speeds without including an external source of power. In particular, the purpose is to evaluate how much energy the actuator can deliver given a certain amount of energy recoverable under the passive phases of human walking. Indeed, although the walking biomechanics data of the knee joints (power in particular) suggest that energy in a cycle is always negative, meaning that it would be always possible, in principle, to recover enough energy in the passive phases to fully power the joint in the active phases, the actual energy that can be recovered and reused depends on the efficiency of the actuator. The energetic autonomy level is a meaningful parameter to assess the energetic efficiency of a self-powered actuator. It can defined as the amount of energy provided by the actuator relatively to the energy recoverable during the gait cycle. The K index has been introduced to quantify the energetic autonomy level of the actuator:

$$K = -\frac{\int_{T_r} \eta_{BS}^r \eta_{IVT}^r P_K^r dt}{\int_{T_f} \frac{1}{\eta_{BS}^f \eta_{IVT}^f} P_K^f dt} \tag{3.15}$$

where $\eta_{BS}^{f,r}$, $\eta_{IVT}^{f,r}$ are respectively the efficiency of BS and of IVT in forward (f) and reverse (r) operation mode, which have been modeled as describes in sections 3.2.13.2.2. In the equation 3.15, K is given by the ratio between the energy actually stored in the flywheel during the passive phases of the gait cycle (T_r) and the energy delivered by the flywheel to fulfill the knee power requirement in the forward phases of the gait cycle (T_f). It is worth noting that, in the ideal case of negligible power losses (all efficiency parameters equal to one) $K > 1$ for the reasons explained above. Power loss has the effect to reduce the numerator and to increase the denominator, thus reducing the value of K with respect to the ideal case. $K < 1$ means that the device is not able by itself to activate the joint over the whole walking cycle, since it can give only a fraction K of the energy required each cycle without discharging progressively the flywheel until it stops. However, even in this case, it could be used as an auxiliary device to compensate for locomotion impairments. The equation (3.15), where K is defined on global quantities (energies) can be used to define a instantaneous effective power P_{out} as it follow:

$$P_{out} = \begin{cases} KP_K^f, & \text{forward mode } (P_K \geq 0) \\ P_K^r, & \text{reverse mode } (P_K < 0) \end{cases} \tag{3.16}$$

Equation 3.15 has been derived from the energy balance equation of the system in a cycle, that can be written by distinguishing the contribution of each term in forward and reverse modes:

$$E_F + E_{out} + E_L = E_{out}^f + E_{out}^r + E_L^f + E_L^r \tag{3.17}$$

Each term of equation 3.17 is defined as it follows:

E_{out}^f energy provided by the actuator in forward operating mode:

$$E_{out}^f = \int_{T_f} P_{out}^f dt = \int_{T_f} KP_K^f dt \tag{3.18}$$

E_{out}^r energy provided by the actuator in reverse operating mode:

$$E_{out}^r = \int_{T_r} P_{out}^r dt = \int_{T_r} P_K^r dt \tag{3.19}$$

E_L^f energy lost in the transmission devices in forward operating mode:

$$E_L^f = \int_{T_f} P_L^f dt = -\int_{T_f} K \frac{1-\eta_{IVT}^f \eta_{BS}^f}{\eta_{IVT}^f \eta_{BS}^f} P_K^f dt \tag{3.20}$$

E_L^r energy lost in the transmission devices in reverse operating mode:

$$E_L^r = \int_{T_r} P_L^r dt = \int_{T_r} (1-\eta_{IVT}^r \eta_{BS}^r) P_K^r dt \tag{3.21}$$

P_L power dissipated in the transmission devices in forward (P_L^f) and in reverse (P_L^r) operating modes:

$$P_L = \begin{cases} P_L^f = -\frac{1-\eta_{IVT}^f \eta_{BS}^f}{\eta_{IVT}^f \eta_{BS}^f} P_{out}^f, \text{forward mode} \\ P_L^r = (1-\eta_{IVT}^r \eta_{BS}^r) P_{out}^r, \text{reverse mode} \end{cases} \tag{3.22}$$

E_F energy provided by the flywheel in a cycle:

$$E_F = \int_{T_f+T_r} P_F dt \tag{3.23}$$

where P_F is the rate of change of the kinetic energy of the flywheel (Eq. 3.8).

E_F must be zero if the energy stored is exactly equal to the energy delivered each cycle (periodic motion). Notice that P_F can also be directly related to the power request by the knee through the following formula:

$$P_F = \begin{cases} P_K^f = \frac{P_{out}^f}{\eta_{IVT}^f \eta_{BS}^f}, \text{forward mode} \\ P_K^r = \eta_{IVT}^r \eta_{BS}^r P_{out}^r, \text{reverse mode} \end{cases} \tag{3.24}$$

When simulating real operating conditions, K is unknown a priori and it must be determined. We followed an iterative procedure aimed at finding the actual working points of the system. Starting from guess values of the$K$ index (K^0) and of the flywheel speed (ω_F^0), that only at first step is considered constant, we compute first P_{out}, that depends only on the knee power P_K (given as input) and the value ofK^0

(Eq.3.16). τ_{IVT} can be calculated easily since the input (flywheel) speed is known, and the output speed is given as input. Also η_{IVT} is calculated since, according to eqs. (3.2, 3.3) and the aforementioned hypotheses, it is only a function of the τ_{IVT}. Then, we compute the corresponding values of P_F from eq. (3.24) and so of $\dot{\omega}_F$ (Eqs. 3.8), from which ω_F^1 can be obtained through a numerical method. Since at the end of the first step the angular speed ω_F^1 (function of t) and the calculated coefficient K differ from the guess values ω_F^0 and K^0, an error is defined as $Err_1 = \frac{1}{T}\int_0^T(\omega_F^1 - \omega_F^0)^2 dt$. Thus, the routine is re-started until the error, defined in general as $Err_i = \frac{1}{T}\int_0^T(\omega_F^{j+1} - \omega_F^j)^2 dt]$, is below a threshold. At each step, it is also requred that that τ_{IVT} never exceeds its limits ($\tau_{IVT}^{min} \leq \tau_{IVT} \leq \tau_{IVT}^{max}$).

The starting guess value of ω_F is calculated with the following formula:

$$\omega_F^0 = \max\left(\min\left(\frac{\omega_K}{\tau_{MECH}\tau_{IVT}^{min}\tau_{BS}}\right), \max\left(\frac{\omega_K}{\tau_{MECH}\tau_{IVT}^{max}\tau_{BS}}\right)\right) \tag{3.25}$$

where τ_{BS} is the speed ratio of the ball screw, and τ_{MECH} is the kinematic law between the angular knee velocity (ω_K) and the output linear speed of BS (v_{BS}).

The calculations carried out in this thesis have been done under the assumption that the flywheel has a certain angular speed at the beginning of the gait cycle. In real life operation, before the usage the flywheel is still and it must be speed up to a certain speed value. In this thesis this aspect has been neglected; however it would be very easy to speed up the flywheel by some cycles of free movements of the legs or by a very small auxiliary motor which would be activated only to "charge" the flywheel up to its nominal level of accumulated kinetic energy.

3.3.2 Sizing procedure

The *self-powered F-IVT* has been designed with reference to a 75 kg healthy subject and for powering knee joint of wearable robots in level ground walking in a range of speeds (0.5, 1.1, 1.6, 2.1 m/s) (Fig. 2.4a). Table 3.3 lists the size of each device included into the *self-powered F-IVT* actuator. While the highest load demand has constrained the selection of the BS from data-sheet, a specific operating condition of the device has been selected in order to optimize the design of the actuator,

specifically relating to the IVT efficiency. This aspect mainly affects the design of the BS joint to the knee (i.e. the mechanism) and the selection of the IVT ratio range. The *self-powered F-IVT* actuator has been sized following the same approach used for the *linear F-IVT* actuator by considering a different objective function. Because the motor is not included in the *self-powered F-IVT* actuator, the average efficiency of the IVT has been maximized in this case.

Self-Powered F-IVT		
Flywheel	J_F[kgm²]	$5 \cdot 10^{-4}$kg $\cdot$ m^2
IVT	$[\tau_{IVT}^{min}, \tau_{IVT}^{max}]$	[-0.85,1]
BS	τ_{BS}[m/rad]	$3.2 \cdot 10^{-4}$
	$\eta_{BS}^{f}, \eta_{BS}^{r}$	$0.96, 0.95$
Mechanism	l_1[cm]	15
	l_3[cm]	30
	l_4[cm]	5
	ψ[°]	36

Table 3.3: Size of the devices included into the self-powered F-IVT actuator.

4 Flywheel Inertial Actuator

4.1 Overview

Fall prevention is an important health issue, which has a great impact on demand for health and social care services [71]. Therefore, fall prevention interventions have been recognized as good instruments to compensate for balance loss disturbances and thus to reduce falling related problems. Despite rehabilitation is a good practice to improve and reinforce balance weakness, sometimes the patient feels himself more stable and safer if he uses external supports. This motivates research efforts of developing wearable and portable robotic solutions which detect subject's loss of balance and provide corrective actions to avoid or delay the risk of falling.

An inertial flywheel reactionless actuator has been developed with the aim of compensating human balance dysfunctions. It counterbalances balance disturbance actions in the frontal plane through the inertial torque generated by accelerating and decelerating a flywheel around the falling direction. The working principle of the actuator emulates the contribution of arms in changing the angular momentum of the trunk to restore balance. Both the mechanical construction and the control signal generation have been designed in cooperation with the department of Biomechanical engineering of the University of Twente. The control of the device has been designed in order to make it work in parallel with humans. The device is started when the falling condition is detected and stopped once the steady posture is attained again. When the balancing intervention of the device is required, the flywheel is speeded up in the direction that makes its inertial torque opposite to the gravitational perturbing action. The flywheel is then slowly stopped to minimize any additional disturbance effect.

The final goal of this research activity is to evaluate how the balance performance of a subject changes by wearing the supportive device. Stance of healthy subjects has been perturbed to assess the contribution of the device in assisting human balance.

To this aim, the effectiveness of the device has been be evaluated by comparing the balance keeping performance of subjects when they wear and when they do not wear the inertial flywheel actuator.

4.2 Mechanical Design

Developing wearable human assistive technologies, such as balance keeping devices, is a challenging task. These devices are worn by human operators and are expected to interact with the human body over most of their operation. Therefore their design principles encompass both their functionality and also users' comfort and safety. The former, ensures that the device efficiently operates as it is expected to do. The latter guarantee a safe integration of the device with the human body, making sure that its shape, weight and size are comfortable and do not hurt the human wearer.

The flywheel balance is a wearable solution that supports people's balance recovery in the frontal plane through a moment exchange with a rotating inertia, the flywheel. It includes a motor, a planetary gear drive, a flywheel, a battery, electronic devices, support and covering structures. All the components are assembled together and fixed to a back plate attached to a universal corset worn by the subject close to his pelvis. A schematic overview of the mechanical design architecture is shown in figure 4.1.

The design of the balance device has been driven by the principle of minimizing the size and weight while guaranteeing certain performance. The effectiveness of the balance device is mostly related to the magnitude of the torque it can apply on the human body. The higher is its value, the stronger is the support that the user could receive. However, as the torque value increases, the size and the weight of the actuator do the same. The size of an electric motor mainly depends on the value of the rated torque, and the inertia and the acceleration of the flywheel define the value of the inertial torque. Therefore, by considering that the flywheel is one of the most critical components of the device in terms of weight and size, its maximum outer diameter has been constrained in order to limit the weight of the complete device. Starting from the maximum size of the flywheel (i.e. outer diameter of 30-35 cm) and also limiting the weight of the entire system to less than 10 kg in order to not perturb the gait of healthy subjects [107], the best combination of motor,

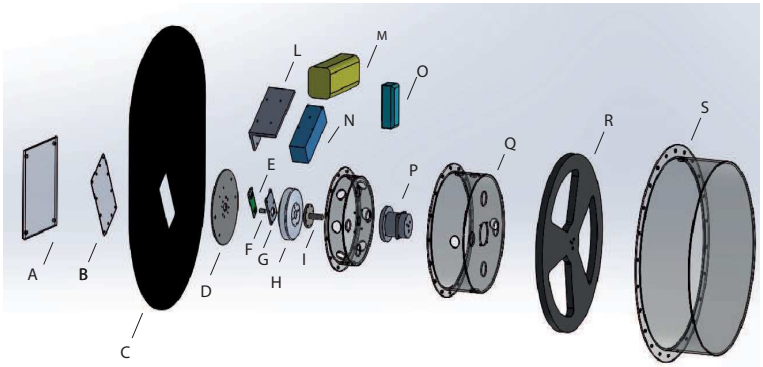

(A) POM plate	(L) Steel heat sink for the motor drive
(B) plastic cover	(M) CE certified motor drive (iPOS80x0 BX-CAT Technosoft)
(C) backplate in PMMA	(N) CE certified motor battery (LiPo Pack ZIPPY Compact 5000mAh 8S 25C.)
(D) Motor flange in PMMA	(O) CE certified logic battery (LiPo Pack 2500mAh 4s 30C)
(E) PCB	(P) PMMA Input PG support
(F) CE certified Rotary encoder (iC-MHM 14-bit absolute angle hall encoder)	(Q) Planetary gear (HD HPGP 11 A, Harmonic Drive AG)
(G) PCB support in aluminium	(R) PMMA Output PG support
(H) CE certified Outrunner brushless motor (Tiger-U8 pro)	(S) Aluminium Spoke Flywheel (D =33 cm, 1.6 kg, 0,029 $kg\ m2$)
(I) Steel Motor shaft	(T) PMMA External cover of the device

PMMA (Polymethylmethacrylaat), POM (Polyoxymethylene)

Figure 4.1: Schematic representation of the flywheel balance device.

transmission gear and flywheel has been selected.

The mechanical design of the balance assistive device also ensures its safeness. One of the potential risks that could be associated to the operation of the actuator in the worst scenario, is the explosion of the flywheel and the consequent potential breaking of the containment. To avoid this, the flywheel has been designed in order to have radial and tangential stresses lower than the safety limits [108], and the containment structure has been designed to resist flywheel explosion. In particular, the housing of the flywheel has been sized as suggested in [109], where the minimum thickness of the wall is calculated considering the energy that must be absorbed by the containment in case of failure of the flywheel.

The design procedure resulted in the balance device depicted in figure 4.2, whose final dimensions are approximately 390 x 132 x 520 mm (L x W x H) and its weight is about 6 kg (Fig. 4.3).

Figure 4.2: Flywheel inertial actuator for balance assistance. It weighs around 6 kg and its outer size is nearly 390 x 132 x 520 mm (L x W x H).

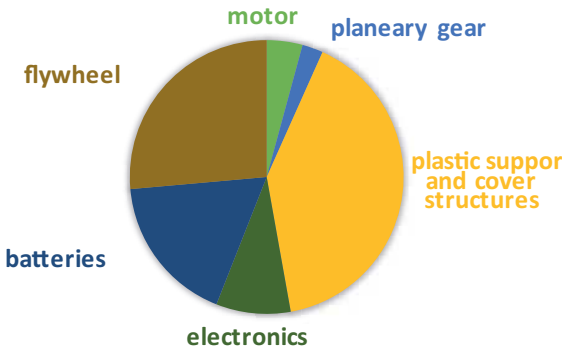

Figure 4.3: Percentage contribution of each component of the flywheel inertial actuator to the entire mass of the system.

The device is foremost a combination of commercially available products (corset, motor, battery, sensors, planetary gear, electronics) and custom parts that we designed based on personal insight and experience, and manufactured by external suppliers. The non-commercially available parts, which are labeled according to figure 4.1, are the following:(A) POM plate; (B) plastic cover, (C) backplate in PMMA, (D) Motor flange in PMMA, (E) PCB, (F) CE certified Rotary encoder (iC-MHM 14-bit absolute angle hall encoder), (G) PCB support in aluminium, (H) CE certified Outrunner brushless motor (Tiger-U8 pro), (I) Steel Motor shaft, (L) Steel heat sink for the motor drive, (M) CE certified motor drive (iPOS80x0 BX-CAT Technosoft), (N) CE certified motor battery (LiPo Pack ZIPPY Compact 5000mAh 8S 25C.), (O) CE certified logic battery (LiPo Pack 2500mAh 4s 30C), (P) PMMA Input PG support, (Q) Planetary gear (HD HPGP 11 A, Harmonic Drive AG)(R) PMMA Output PG support, (S) Aluminium Spoke Flywheel (D =33 cm, 1.6 kg, 0,029 $kg\ m2$) ,(T) PMMA External cover of the device. A detailed description of the components arranged in the flywheel inertial actuator is given below.

Universal corset: a padded plastic corset is used to connect the device to the subject. In general, the padding or any other part of the brace will not come in direct contact with the subject's skin, as it is worn over the clothes. There are threaded holes readily present in plates, packaged inside the plastic of the brace (back side). A small plate in POM (A) has been added to the slides prese<xnt in the back of the brace as well. The bolts used for this attachment have flat heads, such that they do not press in the back of the subject. No metal part of the corset is in direct contact with the wearer subject.

POM Backplate: it is used as a fixed support for the actuator and its devices. It

also connects the device to the corset.

Out-runner brushless DC motor: the Tiger-U8 pro motor (Table 4.1) has been included into the flywheel inertial actuator. It is attached to the backplate through the motor flange (i.e. a PMMA plate). Four M3 SFHCS1 screws connect the motor to the motor flange, and 3 M3x0.5 Tap screws connect the motor flange to the backplate.

K_V	170 rpm/V
MAX WATTS/TIME	1300/180 s
MAX AMPS/TIME	35 A/180s
WEIGHT	239 gr
DIMENSIONS:	86.8x25.5mm
RECOMMENDED BATTERY CONFIGURATION	6-12 S

Table 4.1: Technical characteristic of out-runner brushless dc motor Tiger-U8 pro included into the balance assistive device.

Motor shaft: a steel motor shaft is screwed to the rotor of the motor from one side (8 M3 screws), and fixed to the input side of the planetary gear from the other side (2 M3 screws).

Rotary Encoder: the absolute angle hall encoder iC-MHM 14-bit is fixed to the rotor of the motor. It is coupled to the magnet support and pressured in the motor hole. It is coupled to a PCB located on the PCB support attached to the motor flange.

Planetary Gear: the transmission gear included into the device is a planetary

gear drive from Harmonic Drive AG (Table 4.2). Its input and output flanges are fixed to the backplate by mean of two PMMA supports specifically designed.

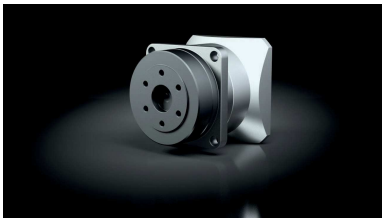

Ratio	5
Momentary peak torque	20 Nm
Maximum input speed	10000 rpm
Weight	140 gr

Table 4.2: Features of the planetary gear drive HPG-11A from Harmonic Drive AG.

Input PG support: the PMMA input Planetary Gear support is connected to the input flange of the PG with 4 M3 screws and to the backplate with 12 M5 x 0.8 screws. There are cooling holes on the surface of the support.

Output PG support: the PMMA output PG support is connected to the output flange of the PG with 4 M3 screws and to the backplate with 24 M5 x 0.8 screws. There are cooling holes on the surface of the support.

Flywheel: a six spokes flywheel in aluminium is included into the actuator. Its diameter is nearly 330 mm and it weighs around 1.6 kg. the greatest part of its mass is concentrated on the external ring in order to maximize its inertia, whose value is about $0.029 kg\,m^2$. It is connected to the output side of the PG with 3 M4x6 screws. It has been designed in order to have radial and tangential stresses lower than the safety limits [108].

Containment: a PMMA containment covers the actuator. It is connected to the backplate with 12 M5 x 0.8 screws. It has been designed in order to contain the flywheel in case of its breaking up as in [109].

Power Supply: a LiPo Pack (ZIPPY Compact 5800mAh 8s 25C, EU Warehouse) has been included. It is fixed to the backplate with strips.

Capacity(mAh) 5800 Config (s) 8 Discharge (c) 25 Weight (g) 1020 Max Charge Rate (C) 5 Length-A(mm) 167 Height-B(mm) 46 Width-C(mm) 64 Table 1 Specs of the LiPo battery included into the inertial flywheel actuator.

	Power Supply	Logic Battery
Capacity	5000 mAh	2500 mAh
Voltage	8 Cell / 29.6V	4 Cell / 14.8 V
Discharge	25C Constant / 35C	30 C Constant / 50C
Burst Weight	937g	213g
Dimensions	160x46x59mm	108x27x34mm

Table 4.3: Technical data of the power supply (LiPo Pack ZIPPY Compact) and of the logic battery (LiPo Battery RC-Plus Sportsline) included into the balance assistive device.

Logic battery: a LiPo Battery (30C-50C 2S 7.4V 2500mAh) has been included. It is fixed to the backplate with strips. It has the following specs:

Motor drive: iPOS80x0 BX-CAT Has been included (Table 4.4). It is fixed to the backplate thanks to a metal strip that acts as heat sink.

iPOS8020 BX-CAT Intelligent Drive (1600 W)	
Output current	20 A continuous, 40 A peak
Motor Supply	12-80 V
Logic Supply	12-36 V

Table 4.4: Technical data of iPOS8020 BX-CAT motor drive from Technosoft.

XSENS IMU: Inertial Measurement Units are used to track human body movements. It is a self-contained system that measures linear and angular motion usually

with a triad of gyroscopes and triad of accelerometers. XSENS IMU are supposed to be strap down to the human body.

Emergency Button: emergency stop device to be hold by the wearer to interrupt motor operation in case of danger or discomfort.

4.3 Control System Architecture

The inertial flywheel actuator device exploits the rotational action/reaction principle of the flywheel to help the user in keeping balance in the frontal plane. The control of the device has been designed consistently with the human balance control mechanism in order to make it act only when assistance is needed. This means that the device will support the subject to keep balance only when he is not able to do it by himself. This would make the rehabilitation more effective and it would best promote neural recovery.

A feedback control algorithm, that replicates the balance recovery in humans, activates and deactivates the device. It detects the subject's loss of balance and generates a counter torque based on the measurement of body deflections. When the balancing intervention of the device is required, the flywheel is speeded up in the direction that makes its inertial torque opposite to the gravitational perturbing action. The flywheel is then slowly stopped to minimize any additional disturbance effect.

Subject loss of balance can be detected through the deflection of the human body from the upright vertical posture, which identifies the reference balance position of a standing human body ($\vartheta_0 = 0°$). The vertical component of the C.O.M. velocity defines the movement of the body relatively to the upright posture: an upward velocity component means that the body is moving close to ϑ_0, instead a downward component means that it is going away from ϑ_0 and that, maybe, is falling down. In the first case, the subject is recovering the balance by himself and the balance device is not needed to provide any corrective action. Instead, in the second case, it could be asked to assist human balance recovery. However, the velocity of the C.O.M. cannot actuate the device alone. Indeed humans experience natural sway in walking and even in standing, with individual variations in terms of magnitude. The action of the device would not be worthwhile nor even beneficial when the user is performing ordinary movements and his balance is actually not perturbed. Therefore, threshold

values on the sway angle (ϑ_{th}) and speed ($\dot{\vartheta}_{th}$) have been considered together with the direction of the C.O.M. velocity, to detect the loss of balance of a subject. These conditions define the operating region of the controller of the balance device.

Figure (4.4) depicts the control scheme of the flywheel inertial actuator. Inertial measurements units (IMU) collect data on the trunk sway (ϑ,$\dot{\vartheta}$) and send them to the falling detect block. This latter, calculates the C.O.M. velocity and compares data received from the IMU with sway threshold values. If a loss of balance is detected, the controller generates the reference torque signal that the motor must provide to support user's balance. Two different controllers have been considered. The first, *Controller 1* generates a reference target torque (C_{ref}) proportional to the errors on$\vartheta$and$\dot{\vartheta}$calculated with reference on $\vartheta_{th}$and$\dot{\vartheta}_{th}$ (Eq. 4.1), the second, *Controller 2*, generates a reference target torque (C_{ref}) proportional to the errors on$\dot{\vartheta}$(Eq. 4.2).

$$C_{ref} = \begin{cases} k_{\vartheta}(\vartheta - \vartheta_{th}) + k_{\dot{\vartheta}}(\dot{\vartheta} - \dot{\vartheta}_{th}) & (|\vartheta| \geq \vartheta_{th}) \mid (\left|\dot{\vartheta}\right| \geq \dot{\vartheta}_{th}) \\ 0 & else \end{cases} \tag{4.1}$$

$$C_{ref} = \begin{cases} k_{\dot{\vartheta}}(\dot{\vartheta} - \dot{\vartheta}_{th}) & (\left|\dot{\vartheta}\right| \geq \dot{\vartheta}_{th}) \\ 0 & else \end{cases} \tag{4.2}$$

where k_{ϑ} and $k_{\dot{\vartheta}}$ are the controller gains onϑ and$\dot{\vartheta}$($k_{\vartheta} = -20\,{}^{Nm}/_{rad}$, $k_{\dot{\vartheta}} = -70\,{}^{Nm}/_{rad/s}$ for both controllers). The control torque is then compared with software motor constraints in order to ensure that the motor could safely operate as the controller expect.

4.4 Motion control

The motion control of the actuator is handled by a motor drive, that executes the motor low-level control on the basis of control signals received from a standard PC

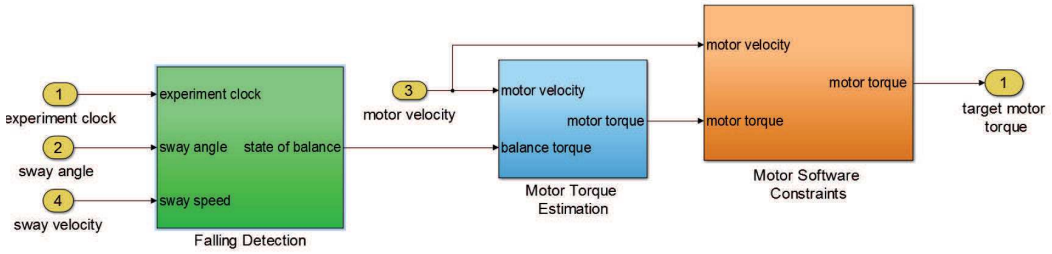

Figure 4.4: Customize simulink control model of the flywheel inertial actuator. The sway angle and velocity measured by the IMU are received by the falling detect block which compare these values with the operating area of the device. If the device is demanded to provide a corrective torque (i.e., the subject is losing his balance), a reference torque is generated and sent to the block of the motor. A non-null reference torque can be provided only if the experiment clock is started. The value reference target torque is also constrained by the software motor limitations to ensure a safe operation of the motor.

(the master device) running a real time operating system.The drive is connected both to the actuator of the balance device and with the master PC (Fig. 4.5).

The three phases of the motor, both the power and logic batteries, the emergency button, the motor absolute angle hall encoder and the IMU sensors are physically connected to the motor drive. The motor cannot be controlled without the motor drive, that is responsible for regulating the motor output while enforcing boundaries on velocity and torque to protect the drive from breaking and to ensure a safe operation of the motor. Furthermore, it receives the information about the motor position, speed and torque and send it to the master PC, that generates the control signals on the basis of these data. The Ethercat protocol governs the master/slave network connection.

Further details on the hardware components involved in the master/slave communication of the flywheel inertial actuator follows below.

- *Motor drive*

  The motor low-level control is handled by the firmware of the motor drive which is automatically booted when the motor drive is turned on. A fully digital drive with embedded motion controller from Technosoft (iPOS8020 BX-CAT) is used to control the DC brushless motor of the flywheel inertial actuator. Thanks to the embedded motion controller, the iPOS80x0 BX-CAT drive combines controller, drive and PLC functionality in a single compact unit capable of executing complex motions without requiring intervention of

Figure 4.5: Scheme of the master/slave connection of the hardware components included into the flywheel inertial actuator. The arrows indicate the network connection among master/slave devices.

an external motion controller. The drive is based on the latest DSP technology and it controls the motor with EtherCAT interface and built-in motion controller with high-level Technosoft Motion Language (TML).

TML is a high-level language that permits to program complex motion profiles for the intelligent drive/motor to execute independently. Using the high-level TML several operations can be executed directly at drive level, as setting various motion modes (profiles, PVT, PT, electronic gearing or camming, etc.), changing the motion modes and/or the motion parameters, executing homing sequences, etc. By implementing motion sequences directly at drive level, intelligence between the master and the drive in complex multi-axis applications can be distributed, reducing both the development time and the overall communication requirements.

Among the supported Motor-Sensor Configurations, in this application we used the one in which the position, speed or torque control of the brushless DC rotary motor is done by using digital Hall sensors and an incremental quadrature encoder on its shaft.

The drive's setup, tuning and motion programming has been done with Easy-Motion Studio. In this phase the drive has been set to operate in EtherCAT communication mode that permits the drive to be controlled via the appropriate masters.

Technical data of the iPOS80x0 BX-CAT are provided in Table 4.4.

- *EtherCAT network protocol*

  The iPOS80x0 BX-CAT drive uses EtherCAT with CoE as Network Communication Protocols. It is an Ethernet-based protocol developed by Beckhoff, which sets new standards for real-time performance and topology flexibility. The EtherCAT option allows the user to operate the drive, monitor the status, and change parameters from an EtherCAT master device.

  EtherCAT cards are used for analog data acquisition and signal generation. These cards are used to collect data about body kinematics, motor speed and ground reaction forces.

- *Master PC*

  The EtherCAT master device is a standard PC running Real-Time Linux that executes custom code for control signal generation and data collection from the

EtherCAT card. All control signals generated by the Real-Time Linux are sent to the motor drive and are subjected to all limiters and constraints enforced by the drive. A custom control code generated with MATLAB/Simulink is compiled and run by Etherlab, an open source toolkit for rapid real time code generation under Linux.

Two different applications, Testmanager and Data Logging Service (DLS), are used for managing the motor control process and storing simulation data respectively. An overview of the control interface of the flywheel inertia actuator follows.

– TestManager

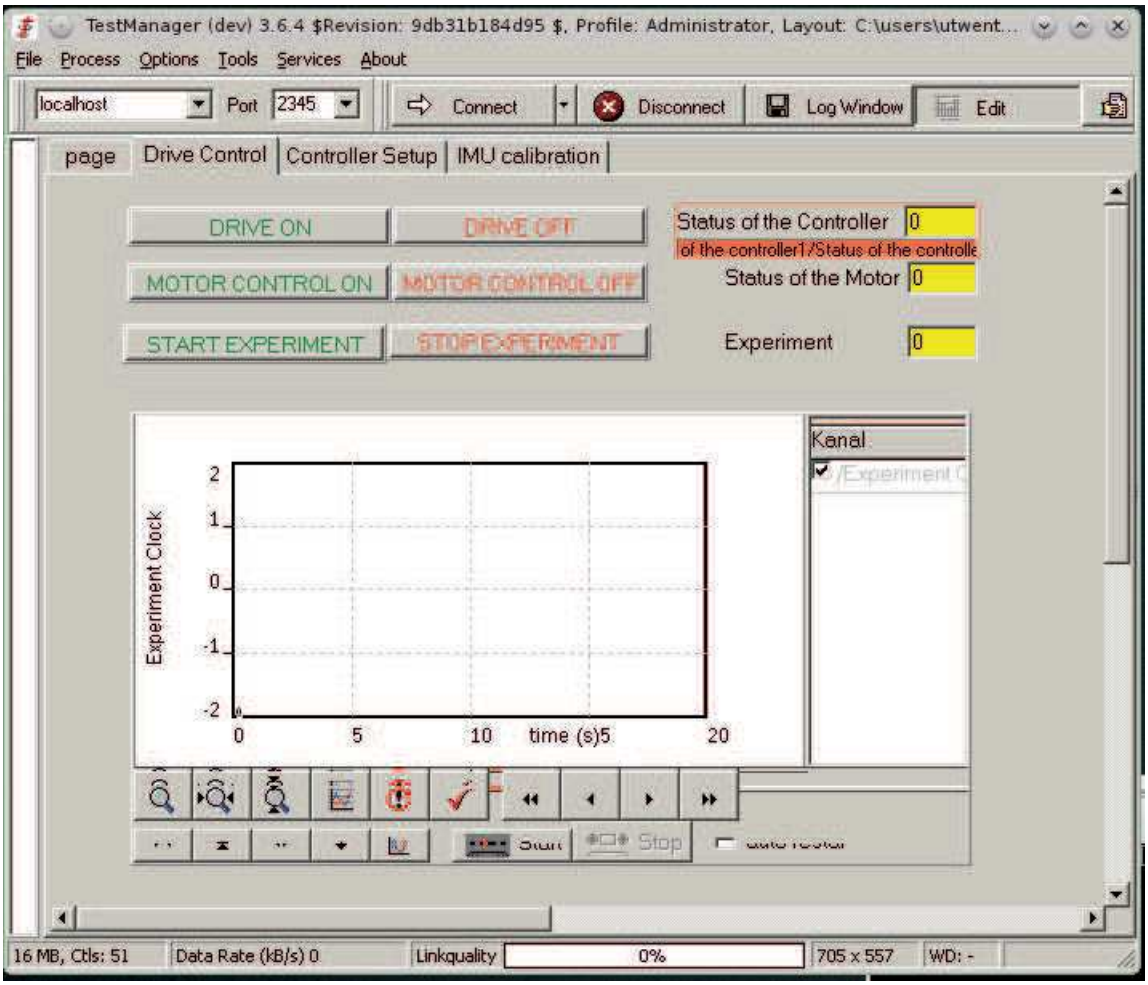

Figure 4.6: Graphical interface of the Test Manager application that allows to manually manages the Etherlab control process.

TestManager is an application that manages the Etherlab control process. It

is connected to the control process via TCP/IP port 2345. An XML-based protocol is used for the communication. Parameters and signals of the control process are registered within the application. These values can be dynamically linked to operation and visualization instruments. For that, the Testmanager gets a flexible and user-friendly operator's application. In Testmanager the user can manually switch on/off the drive, start/stop the motor and start/stop the experiment clock by clicking on the correspondent button (Fig. 4.6). The function of each button shown in figure 4.6 is explained here:

- *drive off*: it switches off the drive;

- *motor control on*: it starts the motor drive. Drive operation can be enabled only if the drive is switched on (i.e. button "DRIVE ON" clicked).

- *motor control off*: it stops the motor drive

- *start experiment*: it starts the experiment clock. A non-zero reference signal can only be generated if the clock is running.

- *start experiment*: it stops the experiment clock.

– Data Logging Service (DLS)

The Data Logging Service (DLS) is a data logging system for EtherLab, that is capable of collecting, compressing and storing high-frequency realtime data. It allows unlimited and performant access to the stored data.

– Simulink Model

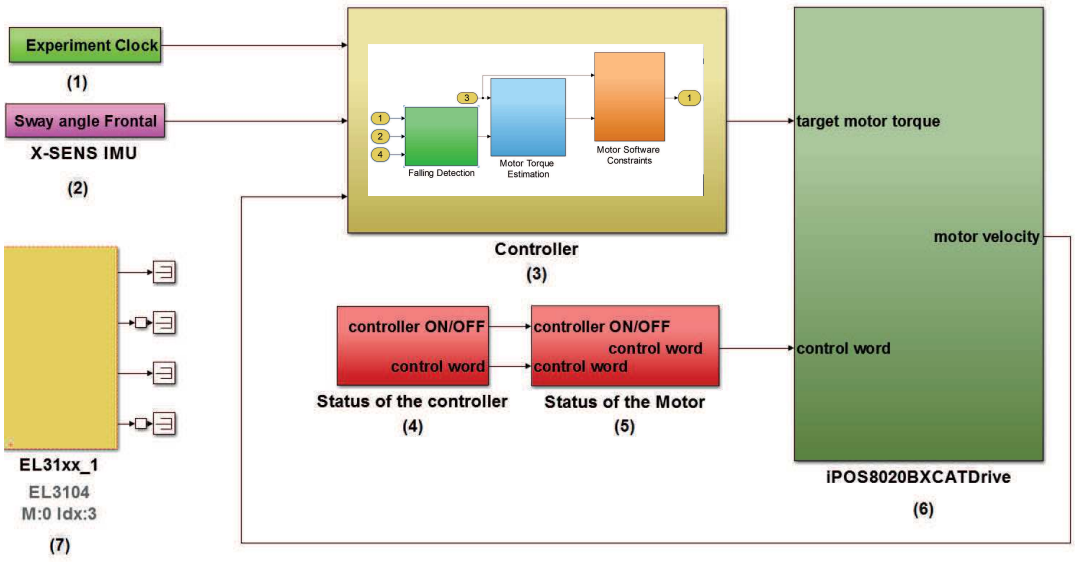

Figure 4.7: Simulink control code of the Flywheel Inertial actuator.

Figure 4.7depicts the Simulink control code that we developed to actuate the balance assistive device. The function of each block included in the custom control model is explained below.

(1) Experiment Clock: it sets the start of the control routine. It requires a manual start done through TestManager (button "Start Experiment" of Fig. 4.6). The balance assistance device cannot be actuated if the Experiment Clock is not activated.

(2) Data collection from X-SENS IMU: it collects data on the trunk sway in the frontal plane that are measured through IMU sensors. EtherCAT cards are used for analog data acquisition and signal generation.

(3) Controller: it generates the target torque signal to be sent to the motor drive. The controller output torque is zero by default and thus the flywheel does not spin. If the Experiment Clock has been started, a non-null reference torque can be generated if the loss of balance of the subject is detected. The block includes the falling detection block and motor target torque generation. The former, includes a falling detection algorithm that, based on the trunk sway (angle and velocity), establishes if the assistive action of the balance device is needed or not. The latter, generates a reference motor torque that the motor should provide. The value of the target torque is constrained by motor software limitations that prevent the system to work above the current

and voltage limits. To this aim the block receives data on the actual motor working point from the motor drive, and ensures that the motor is always demanded to work in its safe operating area.

Furthermore, the controller block also processes the signal received by the Experiment Clock. A non-null reference torque can be generated only if the Experiment Clock is activated.

(4) Status of the Controller: the controller must be manually initialized and switched on through the linux terminal window and TestManager respectively (button "Motor control on" of Fig. 4.6)

(5) Motor Drive: the operation of the drive must be enabled manually by clicking on the button "Motor on" in TestManager (Fig. 4.6).

(6) Motor Drive: it controls the motor motion accordingly to the input control signals that it receives. These signals are the control word, that defines the state of the controller and the target motor operation. Since, in this application we decide to do a torque control of the actuator by making the drive work in "cyclic synchronous torque mode", the motor target torque signal is received by the drive. The quantities measured by the encoder can be saved and read through DLS data manager and TestManager.

(6) Analog I/O data: it receives analog data useful for synchronization of different controlled measurement units used in the experimental setup, as the trigger signal that synchronizes the visualyze system, the treadmill and the pelvis perturbator.

4.5 Technical Testing

Some tests have been conducted to validate the software control. In particular, the operation of the control buttons has been tested.

Tests on the control buttons aim at proving that if the controller or the motor control are switched off, no reference signal is received by the motor drive. The following conditions have been tested considering a sine wave motor target toque:

- Experiment Clock off, Drive off, Motor control off

- Experiment Clock off, Drive on, Motor control off

- Experiment Clock on, Drive on, Motor control off

- Experiment Clock on, Drive on, Motor control on

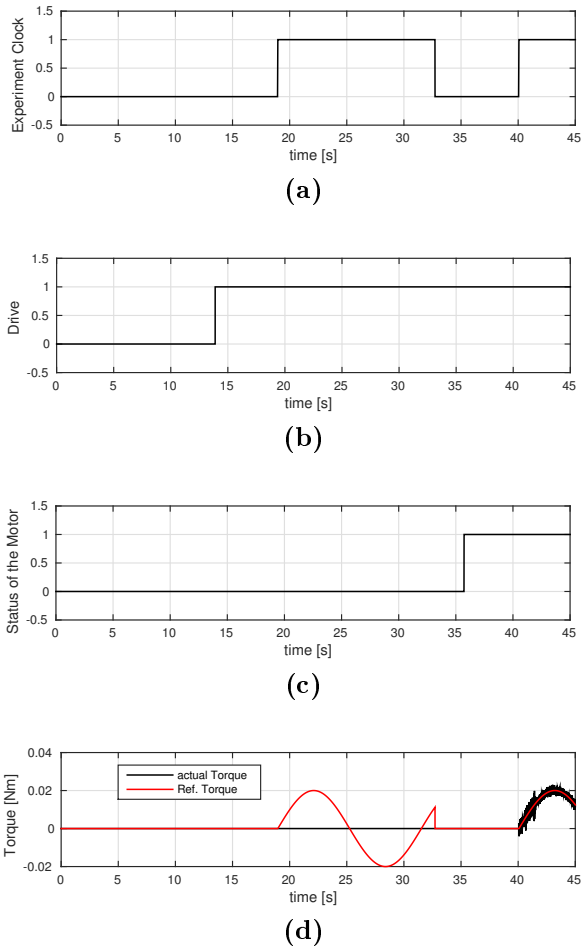

Figure 4.8: From top to bottom: *a)* experiment clock time (0=off, 1 = on), *b)* status of the drive(0 = off, 1 = on state, *c)* motor control state (0 = operation disabled, 1 = operation enabled), d) actual torque measured by the encoder compared with the motor reference torque.

The unit and zero value identifies the on and off conditions of all the variables considered respectively. Results of figure 4.8show that:

1. A non-zero reference torque is executed only if the experiment is active (Fig. 4.8a, d). Normally there is another constraint to this: an event trigger generated in the Simulink block "Controller" of the control model after the falling of the subject is detected.
2. The motor operation can be enabled (Fig. 4.8c) only if the drive is switched on (Fig. 4.8b).

3. The motor does not generate torque when the motor block status is disabled, regardless of the generated reference torque.
4. The motor provides a torque when it is switched on (i.e. status of the motor is 1) and the experiment clock is active (Fig. 4.8a, c,d).
5. Oscillations in the measured torque are due to electrical noise in the encoder.

4.6 Experimental investigation of the balance device

4.6.1 Objectives

The contribution of the flywheel inertial actuator in helping people to keep balance has been evaluated trough experiments on healthy subjects in perturbed standing. During experiments subjects were asked to wear the device and to stand on a treadmill with their feet together, while their equilibrium was perturbed by sudden and horizontal forces exerted at the pelvis by mean of a pelvis perturbator.

The main goal of the experiments was to asses if the balance device could improve the balance keeping response of humans and thus, if it could be effectually used as a rehabilitation robotic device for recovery of patients or eventually included into exoskeletons for controlling their lateral balance. Therefore, the balance performance of subjects while they were wearing the balance device has been compared with their natural response to perturbed standing (i.e. when they did not wear the device).

All the experiments were carried on with the permission from Medisch Ethische Toetsingscommissie (METC) Twente.

4.6.2 Study design

The human balance response to lateral perturbing actions has been be investigated. During these experiments, the subjects were asked to stand on a treadmill with feet together while sudden and horizontal forces were exerted at their pelvis to perturb their equilibrium (Fig. 4.9). Perturbations were applied through the pelvis perturbator, a system developed at the University of Twente that can provide a wide

range of perturbations by directly controlling the forces on the pelvis. Subjects were also told to cross their arms to the chest to avoid any arm balancing effect.

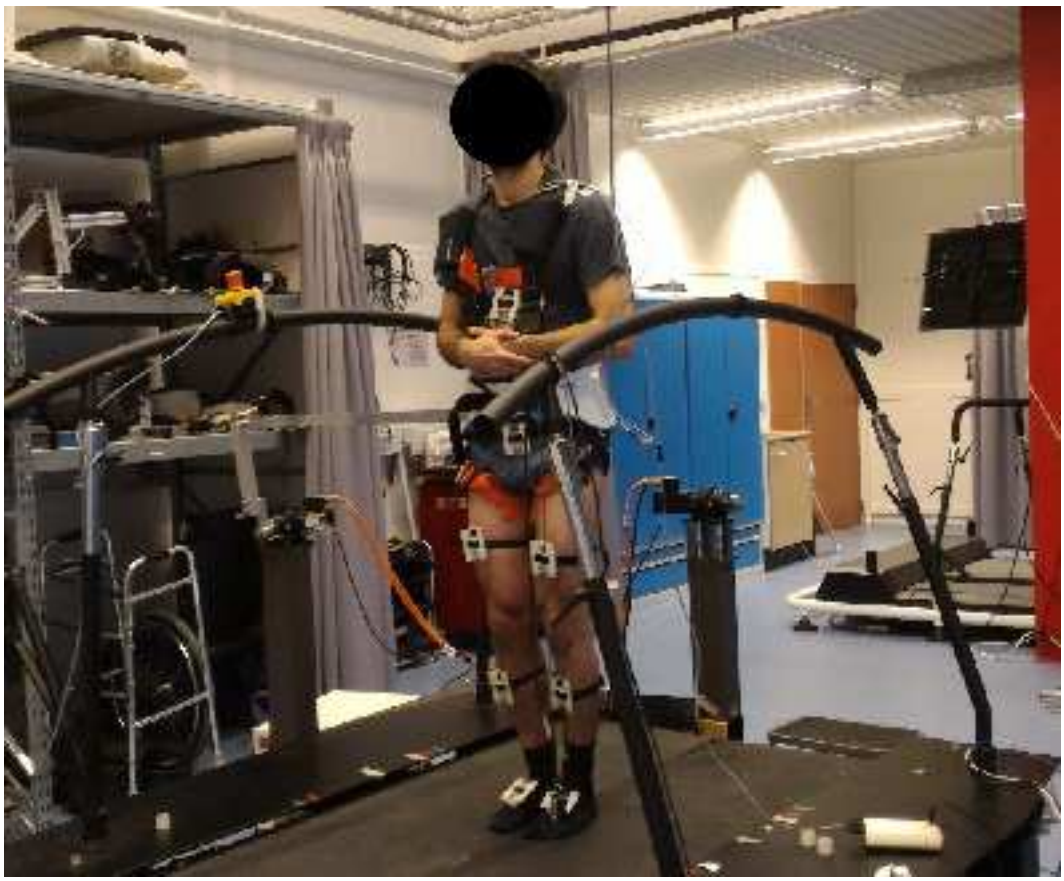

Figure 4.9: Experimental setup to assess the how the flywheel inertial actuator affects human balance. During experiments subjects were instructed to stand with bare feet on a treadmill including force plates, keeping their arms close to the chest to avoid any balancing effect. The subjects were attached to the pelvis perturbator system using a pelvis belt, and to a safety harness to prevent them from falling down if they were not able to keep balance by themselves.

The balance of the subjects was challenged not to make them fall, but to make them react to perturbations with ankle and hip strategies, or in the worst cases by making a step. However, even if the magnitude of perturbations provided was similar to the one of disturbances that could occur in daily life, subjects worn a safety harness for the entire duration of the experiments in order to prevent them from falling down if they were not able to keep balance by themselves. Furthermore, the safety harness is also a reliable measure to safely face unexpected malfunctioning of the system.

The study consisted of four sessions of the same main experiment. Each session had

similar structure and setup, but also some altered conditions. In order to assess how the balance supportive device could affect human balance performance, the balance response of subjects to lateral perturbations has been investigated both while they were wearing the balance device, and while they were not. Furthermore, in order to assess the effect of the mass of the device on human posture and balance response, two more sessions of the main experiment were distinguished. Subjects performed experiments wearing the balance device while it was operating and while it was turned off. The operation of the device was tested with two different controller. The first one considers both the error on sway angle and velocity of the human trunk, the second one only the error on the sway velocity as in [24].

Subjects' standing was perturbed through pushes and pulls of three different magnitudes randomly applied with a mean time of 10 s in between. The magnitude of the perturbations scaled on the body weight of the participants. Their value was 0.1, 0.08 and 0.06 times the body weight.

Healthy subjects were asked to participate in all the additional sessions in order to collect and compare data from the same subject in the different conditions. A single session lasts approximately 2 to 2.5 hours (depending on how much rest a subject desires to take). A duration estimation is shown below in table 4.5.

	Explanation and preparation	Measurement	Cleaning up
Healthy Subject	45	45	15

Table 4.5: Duration estimation of the experiment per subject (in minutes).

4.6.3 Study population

Data were collected on 10 healthy young adults (5 females, 5 males) which participated as volunteers at the experiments. They were recruited from students and staff of the University of Twente by posting flyers. Subjects were asked to participate at all the sessions of the experiment in order to collect and compare data from the same subjects. The number of subjects to involve in the study has been chosen on the basis of what has been done in previous studies investigating assisting balance

devices. A sample size of 10 subjects is most common in both perturbed standing and walking [24].

Subjects eligible to participate in this study met all of the following criteria:

- between 18 and 30 years of age
- body weight $<$ 100 kg
- given written informed consent

Subjects were excluded from the study if they met one or more of the following criteria.

- have current lower extremity problems or deficiencies (e.g. knee problems, disabilities in walking)
- have (a history of) neurological or balance related disorders
- are using medication that can affect balance control
- are pregnant, or have a chance of being pregnant
- have chronic joint pain
- have orthopedic problems
- have (a history of) cardiac conditions that interfere with physical load .

4.6.4 Investigational and non-investigational instruments

Pelvis Perturbator

The pelvis perturbator is a setup developed at the University of Twente that can apply a wide range of perturbations by directly controlling the forces on the pelvis. It consists of two torque controlled motors (Moog, Nieuw-Vennep, The Netherlands) that are placed adjacent to a dual-belt instrumented treadmill, such that the motors are located to the right and behind of the subject respectively. The motors are connected to a hip brace (Universal hip abduction system, Distrac, Belgium) worn by the subject. In this study the motor to the right of the subject is connected to the brace with a cable, while the motor to the right is disconnected (Fig. 4.9). Each motor contains a torque sensor for measuring the torque on the motor axis. When the motors are turned on but no external force is applied to the subject, the interaction force between motors and the subject is regulated to be minimal

(zero impedance mode). A custom made computer algorithm in Matlab Simulink (Mathworks, Natick, USA) is used to generate control signals for the motors, and record torque and position data from them.The risks for subjects while connected to the pevis perturbator are small. Altough perturbations could not lead to a fall, a safety harness will prevent injury when falling.

Dual belt instrumented treadmill

The dual-belt instrumented Y-Mill (Forcelink, Culemborg, The Netherlands) is a custom made treadmill consisting of two belts. This way it is possible to have both legs walk at a different speed, during investigations on human walking. The treadmill furthermore contains a force plate beneath each belt. These was used to obtain 3 DoF ground reaction forces and moments. The treadmill has a CE-IIB certificate (Fig. 4.9).

VisualEyez motion capture system

The VisualEyez VZ4000-II motion capture system (Phoenix Technologies, Vancouver, B.C. Canada) was used to capture the subject's movements. 3 stationary cameras were used to record the position of multiple light emitting diodes (LEDs). Wireless battery powered LEDs incorporated in small plastic frames in clusters of 3, were attached to different part of the human body using soft elastic straps. Marker frames (9) were positioned on the chest, on the pelvis, on the each upper leg, lower leg and foot. A cluster of LEDs was also attached to the balance device to measure its movement relatively to the human body.

XSENS IMU

Inertial Measurement Unit is a self-contained system that measures linear and angular motion usually with a triad of gyroscopes and triad of accelerometers. An IMU can either be gimballed or strap down, outputting the integrating quantities of angular velocity and acceleration in the sensor/body frame. In literature, they are commonly referred to as the rate-integrating gyroscopes and accelerometers. It was used to track human body movements and to detect falls. During experiments they were attached to subjects chest through skin friendly tape..

4.6.5 Study parameters

Many different methods exist today for assessing postural stability. The most commonly measurement used to evaluate human sway consider the deviation of the sway

angle. It can be easily measured through inertial measurement units or through data collected by motion capture systems.

Using the equipment described in section 4.6.4, data on body kinematics and ground reaction forces were collected. In particular, the main parameters considered in this study to evaluate human balance performance in perturbed standing are :

- sway angle of the human body
- ground reaction forces of the stance legs
- number of lift feet

4.6.6 Study procedures

The total experimental procedure can be separated into 4 phases: general preparation, subject preparation , probe measurements and perturbations measurements.

1. *General preparation*

   - The subject inclusion and exclusion criteria are re-evaluated

   - The researcher explains the content of the study and the experiment

   - If the subject complies, the subject is given the opportunity to read and fill out the permission form

   - If the subject has given written informed consent, the researcher completes the form by signing it

   - The subject is asked to change clothes (shorts, t-shirt, barefooted)

   - The subject's body height, leg length (distance malleolus lateralis – trochanter major) and body weight is measured

2. *Subject preparation*

   - The size of the universal hip brace is adjusted such that it tightly fits the subject's pelvis.

   - The size of the balance device backpack is adjusted such that it tightly fits the subject's trunk.

   - The IMU is positioned on the trunk of the subject.

3. *Probe measurements*

   Probe measurements aim to define the location of some anatomical points of the human body relatively to the cluster of LEDs, whose position is measured during experiments. It consists of the following phases:

   - The subject is asked to stand on the dual belt instrumented treadmill and put on the safety harness, connected to the ceiling.

   - Up to 26 probe measurements of 8 seconds each must be done with the Visualeyez.

   - During a probe measurement the experimenter points toward a location on the subject's body using a LED based stylus.
   - Using the probe measurements, these locations can be reconstructed for all subsequent measurement in which only the 9 marker frames are measured.
   - Probe locations are the following:

     Feet : caput metatarsale 1 and 5, calcaneus

     Lower legs : malleolus medialis and lateralis, tuberositas tibiae, caput fibulae

     Upper legs : epicondylus medialis and lateralis, trochanter major

     Pelvis : spina iliaca anterior superior, spina iliaca posterior superior

     Thorax : incisura jugularis, proc. xyphoideus, C7 and T8 vertebra

   - A 10 second static trial must be captured with the Visualeyez to obtain reference joint angles. In the static trial the subject will be asked to stand still for 10 seconds, with knees and hip extended, feet at shoulder width, toes pointing forward.

4. *Perturbation measurements*

   The balance response of healthy subjects standing on a treadmill while they receive perturbations is measured. The procedure is the same for all of the sessions of the main experiment, with the exception of the phases involving the balance device. Purturbation measurements includes:

   - The subject is asked to stand on a treadmill with his feet at a location indicated on the floor (toes in forward direction).

- The subjects is put on the universal safety harness

- The subjects is connected to a hip brace

- The subjects is put on the balance assistive device (only in experiment sessions 2, 3 and 4)

- The handrails of the dual-belt treadmill can provide support when taking this leaning position

- The subject is instructed to stand in a comfortable position keeping knees and hip straight, to cross his arms to the chest to avoid any arm balancing effect and to prevent a fall in case of fall onset .

- The subject is be allowed to step to keep balance, but he is told to postpone step initiation as long as possible.

- The balance device is activated (only in experiment session 3 and 4).

- Perturbations are provided trough the pelvis perturbator.

- Subjects can rest at any time

4.6.7 Safety reporting

All experiments are non-invasive procedures involving disturbances similar to those that could occur in daily life. An experiment required approximately 45 minutes of active participation for healthy subjects and was not expected to put extensive load on the subjects. All subjects could take rests during the experiment and participate on their own pace. Risks leading to injury of the subject were low, given the safety precautions. The study did not lead to any direct benefits for the subject, but may lead to the development of technologies to support human balance control. This knowledge might be applied in both clinical and robotics fields of research.

5 Results

5.1 Performance estimation of the flywheel based actuators

In order to evaluate which are the potential benefits or the drawbacks of the flywheel based actuators for wearable robots, their performance have been estimated through the model provided in section 3.2.3. The energetic and power requirements of all the actuators have been calculated following an inverse dynamic approach, that is to say starting from the load characteristics (knee angle and torque vs time) given as input data to the model.

Three main performance indexes have been taken into consideration for comparison: the energy consumption (per gait), the peak values of electric power and motor torque. Both the electric energy and power have been calculated at the motor electrodes. This means that the power losses in the electronics and in the batteries have not been considered in our calculations. These are significant quantities for the development of lightweight and portable wearable robots because they affect the size and the weight of the actuator, as well as the operating range of the device.

The investigation of the flywheel based actuators has started with the evaluation of the operation of the *rotating F-IVT* in one specific walking condition, for which it has been optimally designed. In this case, calculations have been done under the assumption that the motor mostly works with the maximum efficiency. This means that it has been selected in order to always provide its nominal power. Two different power demanding walking regimes have been examined, i.e. level ground walking and running. A traditional stiff actuation scheme has been also considered for comparison.

However, estimation of the performance of the F-IVT actuator when it works under its nominal condition gives a limited sight of its potential. Portable lower-limb

wearable robots are required to support the wearer in his daily activity, thus their actuators do not usually work under the best condition. In this view, the flywheel based actuators have been further investigated by predicting their performances when they do not work under the condition for which they were optimally designed, like different walking speeds and stairs climbing. The energy and power requirements of F-IVT actuators, i.e. *rotating F-IVT* and *linear F-IVT,* have been compared with those of two very efficient actuators already used in biomechatronics devices, the SEA and the C-SEA, in order to evaluate if they could be a competitive actuator for artificial knee joints of wearable robots, or not.

In the end, the possibility of assisting human walking by only taking advantage of the efficient energetics of knee joints without resorting to any additional source of energy, has been considered. The amount of energy that the self-powered F-IVT can deliver to knee joint in level ground walking in a range of speeds has been calculated.

5.1.1 F-IVT in optimal designed conditions

In this section results published in [2] are provided. The performance of the *rotating F-IVT* actuator has been compared to a traditional system, named *Fixed Ratio Drive* (FR-D), where the joint speed is regulated by controlling the motor speed. The aim of this section is to give a proof of the working principle of the actuator and of its potential benefits. Therefore the F-IVT has been optimally sized for the walking condition examined. This means either that the motor mostly works at its nominal working point, and that the IVT ratio range has been selected in order to minimize power losses in the transmission device. Two different locomotion conditions have been examined: level ground walking at 1.1 m/s and running. GCA data taken from [16] have been given as input data to our model to estimate the power requirements of the two actuators compared.

The nominal values of the components of the system are listed in Table 5.1 for both F-IVT and FR-D configurations, considering a body mass of 75 kg. The sizing of all the components pursued the principle of minimizing their weight and of maximizing their efficiency, resulting in a high-speed motor paired with a large gear reduction. In fact high speed motors are usually adopted is this kind of applications because of their very small mass. The low value of τ_{HD} resulted both from the high speed of the motor and from the load requirements.

	LEVEL GROUND WALKING		RUNNING	
	rotating F-IVT	FR-D	rotating F-IVT	FR-D
NOMINAL SPEED [RPM]	3406	2911	8657	8283
NOMINAL TORQUE [NM]	0.008	0.811	0.045	2.58
RADIUS [M]	0.07	-	0.07	-
WEIGTH [KG]	0.2	-	0.2	-
τ_{IVT}^{max}	0.8	-	1	-
τ_{IVT}^{min}	-1	-	-0.85	-
τ_{HD}	1/50	1/50	1/80	1/80
NOMINAL TORQUE [NM]	25	25	63	63

Table 5.1: Nominal values of the components of the actuation system of the exoskeleton in the two configurations considered in this work (F-IVT and FR-D). The design is proposed for two operating conditions: level ground walking and running.

Level ground walking at the speed of 1.1 m/s requires an overall negative amount of energy at the knee, about equal to -0.21 J/kg. For this reason, in ideal working condition no external positive power source would be needed, i.e. the electric machine should work as a generator recovering energy to be stored in the batteries. Unfortunately, transmissions often work far away from the condition of unit efficiency. In the knee joint, transmission devices are forced to work under variable speed and torque, even with changes of power flow direction. As a consequence, the instant working efficiency varies very much in particular when passing from direct to reverse mode. Furthermore, the reverse mode is not always possible, i.e. in particular working conditions, the IVT and the HD could result to have negative efficiency, which means they are non-reversible. I refer to this condition naming it "irreversible motion". In this case (Fig. 3.3) both P_F, P_M and P_K are delivered to the transmission and are dissipated as heat losses. This situation can involve the HD, the IVT or both simultaneously, depending on the actual values of speed and torque. We considered all the possible directions of power flows in the actuation system, providing for each of them detailed efficiency models for all the elements of the transmission: the efficiency of the IVT and the HD in direct and reverse mode was estimated as function of the speed ratio, the torque and the speed.

In general, the effect of the power loss on the energy balance of the system cannot

be neglected. Indeed, it results that in real working conditions, as a consequence of the power loss in the powertrain components (Fig. 5.2), the motor is asked to deliver a positive amount of power (Fig. 5.3). It can be noticed in Fig. 5.2 that, as a consequence of the strongly variable angular speed and torque, the efficiency of the IVT and of the HD is far from being constant and sometimes it is even equal to zero or negative (only positive efficiency points are shown in Fig. 5.2). Negative efficiency points (non-reversible motion) are achieved for the 15% and 20% of the cycle for the IVT and the HD respectively. In these intervals, even if the power at the output shaft of the transmission is negative, the energy is not transferred from the knee to the flywheel because the transmission devices do not permit the power flow inversion and additional power is requested to the motor/flywheel block to keep the system in motion.

Figure 5.3 shows the time histories of P_F, P_M and P_K in level ground walking . It can be noticed that the electric machine works as a motor providing a nearly constant amount of power, while the flywheel follows the trend of the power requested by the knee joint. Despite the variable power demand of the load, the motor works almost at fixed point, close to the nominal working condition and maximum efficiency value (Fig. 5.2).

The achievement is due to the flywheel, which plays the role of energy storage device, and the micro IVT, the ratio of which has to change as shown in figure 5.1ato perform the energy transfer properly. An ideal control of the IVT was also assumed i.e. it is assumed that the IVT gives exactly the required speed ratio at each instant of the gait cycle. Figure 5.1b shows that the motor/flywheel speed varies between 300-360 rad/s, that is always by far greater than zero even when the angular speed of the knee joint is zero thanks to the neutral gear condition of the IVT.

The advantages that can be achieved are clearer if the F-IVT is compared with a FR-D system, where the electric machine is asked to fulfill the power requirement of the knee joint adapting torque and speed. Under these variable operating conditions, the efficiency of electric machine is usually lower than the maximum value (Fig. 5.4). The F-IVT permits to reduce the electric energy required per cycle, from 0.34 J/kg of the FR-D to 0.05 J/kg of the F-IVT, achieving a -85.3% of energy consumption. Also the peak of electric power demanded to the motor is reduced from 0.61 W/kg with FR-D to 0.05W/kg of the F-IVT. (Fig. 5.5a), resulting in -91.8% of peak electric power requested. Thus the F-IVT system results to be very

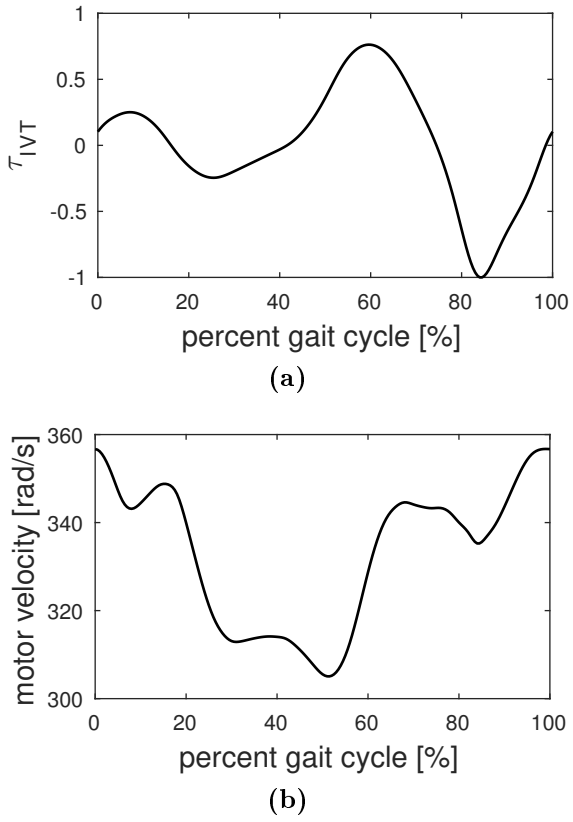

Figure 5.1: IVT ratio (a) and the motor/flywheel speed (b) in level ground walking .

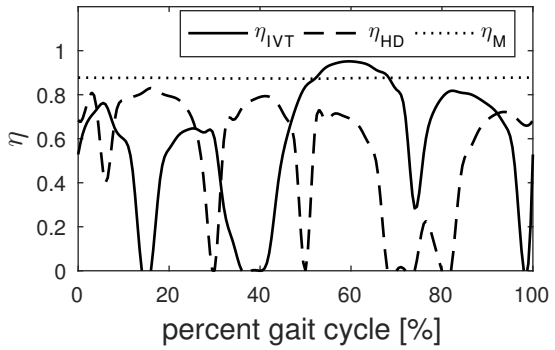

Figure 5.2: Efficiency of the motor, of the IVT and of the HD unit of F-IVT in level ground walking at 1.1 m/s.

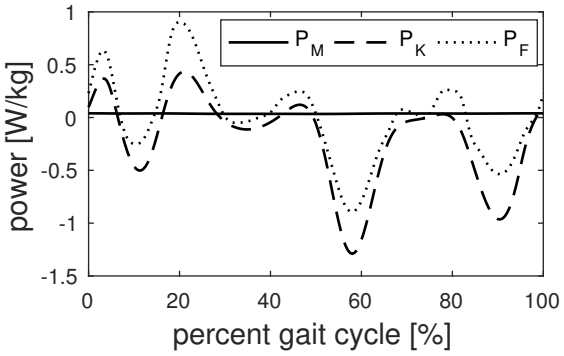

Figure 5.3: Power requirements of the knee joint, the flywheel and the electric machine in the F-IVT. The assumed operating condition is level ground walking at 1.1 m/s. Power loss in all the components of the actuator is simulated in detail.

efficient permitting to reduce both the energy and peak power requirements of the motor, which lead to downsize the electric machine. We roughly estimated that such reduction in size of the motor of F-IVT with respect to the motor of FR-D, makes both the actuators almost equal in weight.

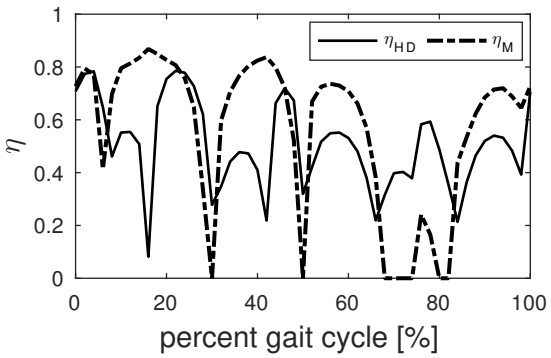

Figure 5.4: Efficiency of the motor and of the HD unit of FR-D in level ground walking at 1.1 m/s.

As done for level ground walking, the energy and power requirements of the F-IVT actuator was predicted in running, by changing the input data (Fig. 5.6). The knee joint requires a more negative value of energy in running (-0.96 J/kg) than in level ground walking. This means that a greater amount of energy could be recovered and that running would be potentially more efficient than walking. The higher values of speed and power (Fig. 5.6) of the knee joint, requires a different design of the transmission devices. In particular a bigger HD gear is needed because of the higher output torque involved. This penalizes the HD efficiency over all the gait cycle and in particular when low torques are required, reducing the potential efficiency of the

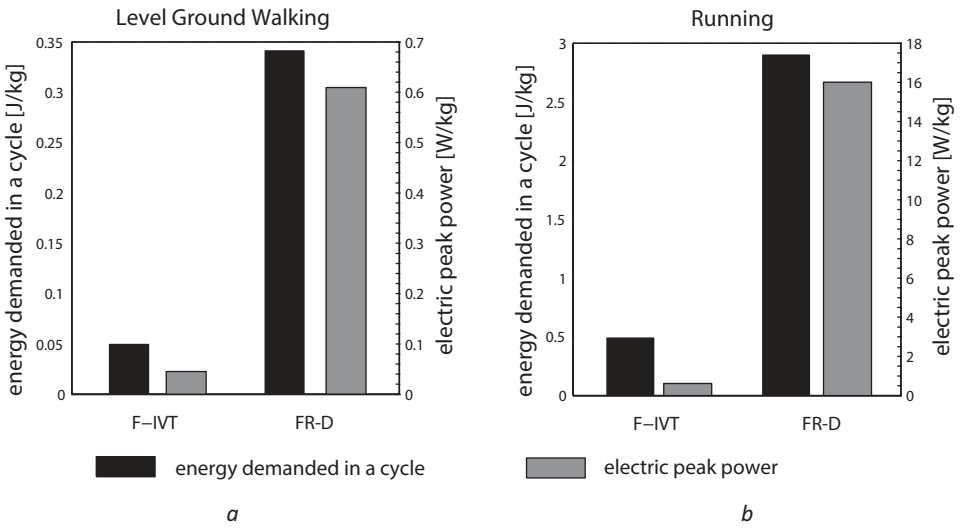

Figure 5.5: Electric energy and peak power requirements in level ground walking (a) and running (b) with F-IVT and FR-D actuators.

system.

Like in level ground walking, even if the energy required by the knee joint is negative, because of the power losses in the transmission, the motor is asked to provide a nearly constant amount of positive power, whereas the flywheel follows the trend of the power requirements of the knee joint. Simulations show that the F-IVT actuator outperforms the FR-D system (Fig. 5.5) also in running. In fact, F-IVT actuator allows heavy motor downsizing, since the peak of electric power is reduced by 96.2 % respect to FR-D system. Furthermore the electric energy consumption is reduced by 83.1 %. It can be noticed that the energy economy achieved in walking is almost equal to the one obtained in running. These results could be counterintuitive, since in running the magnitude of the negative peaks of power is much larger than in walking, giving the chance to recover more energy. Unfortunately, the average HD efficiency is lower because of the larger average speed.

5.1.2 F-IVT in daily life conditions

The potential benefits of the flywheel based actuators have been further investigated by predicting their performance when they do not work under the condition for which they have been optimally designed. Actuators of lower limb joints are expected to support the subject in his daily activities, which often requires different amount of power. In this study the energy and power consumption of the flywheel based

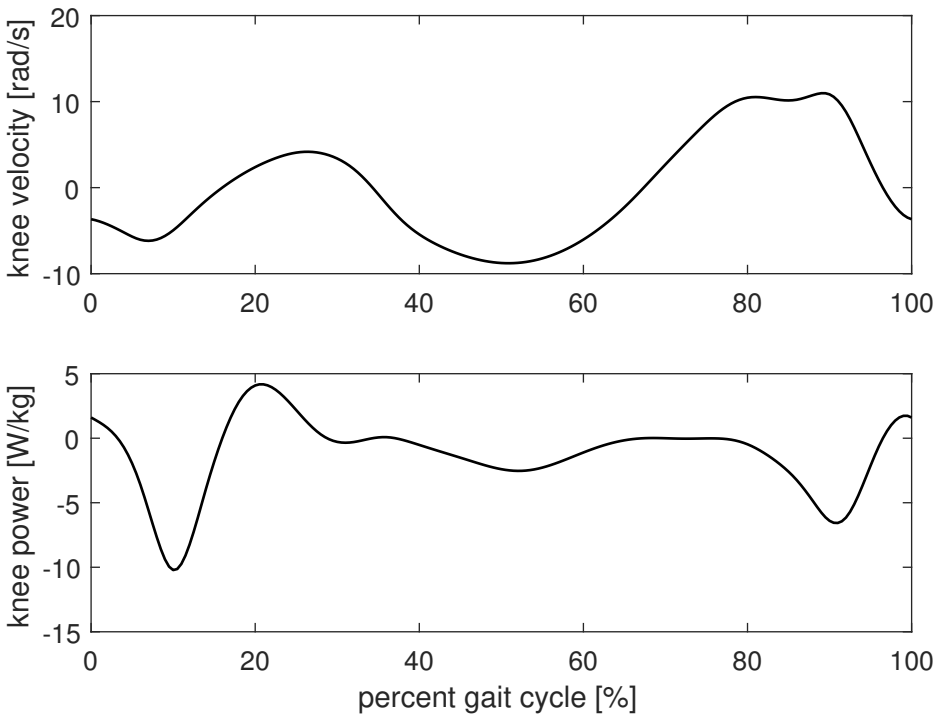

Figure 5.6: Speed and power requirements of the knee joint in a cycle of running [3].

actuators has been estimated in the following conditions: level ground walking in a range of speeds (0.5, 1.1, 1.6, 2.1 m/s) and stairs climbing of different inclinations (24, 30 and 42°). The flywheel based actuators, the *rotating F-IVT* and the *linear F-IVT*, have been compared with two other high performance actuators, the SEA and the C-SEA, which were largely investigated in the literature.

The electric power and energy consumption of the actuators compared has been estimated following a model based approach in back dynamics. We used the model described in section 3.2.3 to estimate the performance of the flywheel based actuators, and models available in literature for the SEA and C-SEA 2.3. Representative weight-normalized gait cycle data from[16, 106] have been given as input data to the models considering a 75 kg person. The *rotating F-IVT* and the *linear F-IVT* have been sized according to the procedure explained in Section 3.2.4to maximize the efficiency at the most frequent working condition (Table 5.2) ensuring that the actuator is capable of operating correctly in any other working condition examined. In order to have a fair comparison, also the SEA and C-SEA have been sized to ensure knee powering in the selected tasks (Table 1).

In order to give an evaluation of the performance of the actuators, their energy

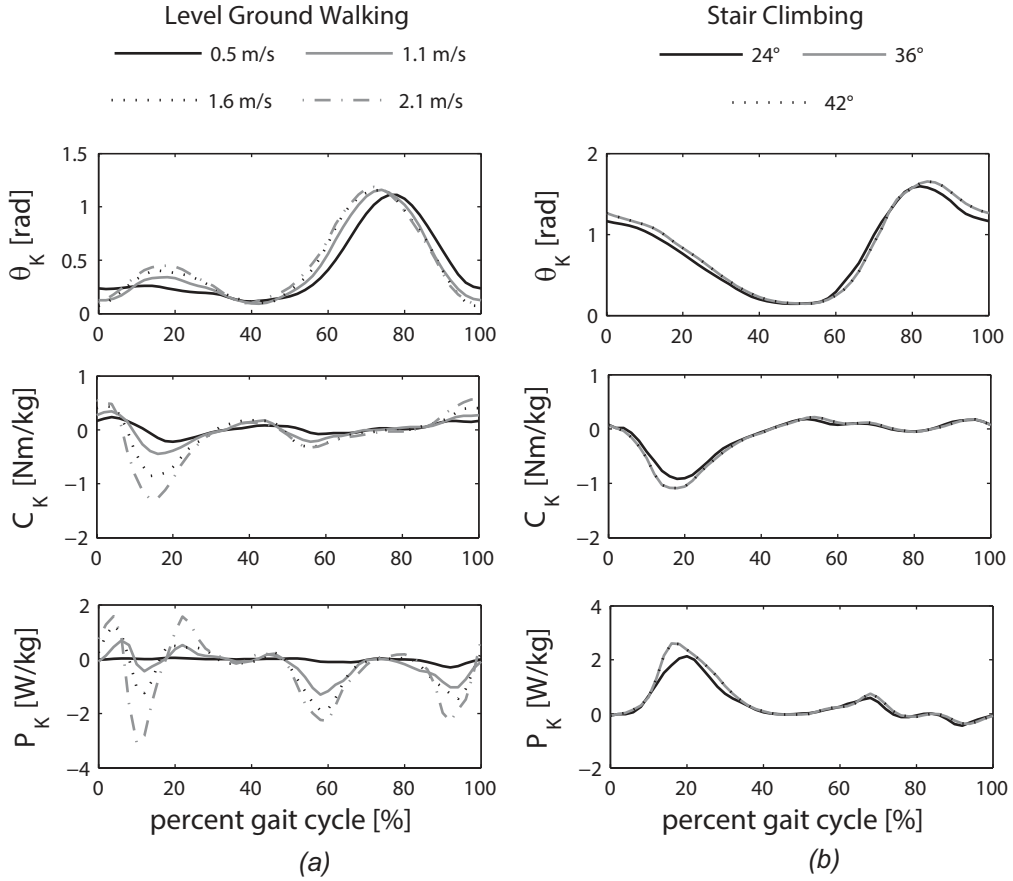

Figure 5.7: Clinical Gait Cycle data of knee joint (angle ϑ_K, torque C_K and power P_K) in level ground walking at different speeds (a) and at stair climbing at different inclination (b)[16, 106] .

consumption and the peak of the electric power demanded to the motor have been estimated. Such quantities can be considered as indexes of the challenging development of lightweight and portable wearable robots with an operating range adequate to daily activities. Furthermore, an estimation of the energy recovery capabilities of the actuator has been done by calculating the energy stored and released by the storage device in a cycle.

The electric energy demanded by the motor was calculated through Eq. 3.13 for all the cited actuators. In this study, for all devices we neglect the possibility to recover electric energy (i.e. $\eta_{gen} = 0$): data available in the literature of bio-mechatronic devices[110, 105] are not yet clear enough on this topic to allow us to make calculations of electric re-generation straightforwardly. Indeed, although mathematical model of the brushless motor (Eq. 3.113.10) predicts very large values of the efficiency of the electric motor in the 2nd and 4th quadrant, experimental measurements are only in qualitative agreement with the model, since the measured values of efficiency are in the range 18-30% [110]. This assumption explains the null energy consumption of the linear F-IVT and of the SEA at the slowest walking speed (Fig. 5.8).

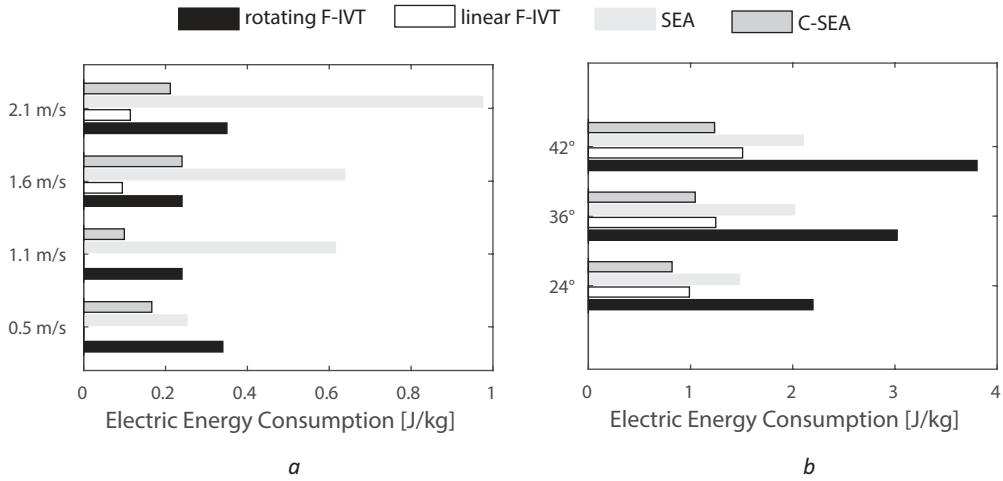

Figure 5.8: Energy demanded at the motor electrodes of the rotating F-IVT, of the linear F-IVT, of the SEA and of the C-SEA in level ground walking at different speed (a)s and stair climbing at different inclinations (b).

Figure 5.8 shows the values of energy consumption of all the actuators considered. From calculations, it results that the SEA has the greatest energy consumption almost at all the walking speeds, while the rotating F-IVT is the the most energy demanding actuator in stairs climbing. The C-SEA has better energy performance

		rotating F-ITV	**linear F-IVT**	**SEA**	**C-SEA**
	model	EC-max 40 p.n. 283871	EC-max 30 p.n. 272764	EC 60 p.n. 167131	EC 45 p.n. 136209
Brushless DC Motor	$P_{Nom}[W]$	120	60	400	250
	$C_{fr}[mNm]$	5.2	0.03	0.8	0.77
	$J_M[g\,cm^2]$	101	21.9	831	209
	$M_M\,[g]$	720	300	2400	1100
	$k_{emf}\,[\frac{V}{rad/s}]$	0.0628	0.0359	0.147	0.0739
	$k_t[\frac{mNm}{A}]$	62.8	35.9	147	73.9
	$R\,[\Omega]$	2.02	2.48	1.03	1.01
	$\nu\,[\frac{Nm}{rad/s}]$	$8.66\,10^{-6}$	$4.3\,10^{-6}$	$1.4\,10^{-4}$	$2.7\,10^{-5}$
	$i_c[A]$	-	-	-	0.25
	$v_c[V]$	-	-	-	24
Flywheel	$J_V[g\,cm^2]$	$5\,10^3$	$5\,10^3$	-	-
IVT	τ_{IVT}	[-1.35, 1.21]	[-1.04, 1.17]	-	-
Gear Train	τ_{FR}	1/50	$3.18\,10^{-4}\,\frac{m/s}{rad/s}$	1/80	1/143
	η_{FR}	by model	0.97	by model	0.9
Spring	$K\,[Nm/rad]$	-	-	375.14	330
Mechanism	$l_1\,[cm]$	-	15	-	15
	$l_3\,[cm]$	-	30	-	30
	$l_4\,[cm]$	-	5	-	5
	$\psi\,[^\circ]$	-	36	-	36

Table 5.2: Model parameters of the actuators compared in this study:rotating F-IVT, linear F-IVT, SEA and C-SEA. The motor damping parameters and the coulomb friction torque are not provided by data-sheet, but they were estimated following the guide lines given by Maxon.

than the SEA thanks to the greater efficiency of the transmission devices. It is also more efficient than the rotating F-IVT at all the locomotion condition considered.

The linear architecture of the F-IVT improves the efficiency of the flywheel based actuators. If the linear and the rotating F-IVT are compared, it can be noticed that the the energetic consumption of the F-IVT is highly reduced at all the walking speeds and stair inclinations (mean value of the reduction: 72%). By comparing the linear F-IVT with the C-SEA, two cases must be distinguished: in walking, the linear F-IVT outperforms the C-SEA, in particular at very low walking speeds; in stairs climbing, the C-SEA has better energy saving performance if compared with the linear F-IVT, even though the energy consumption is very similar. It is important to notice that the results of figure 5.8 do not include the power losses in the electric modules between the motor and the batteries. These power losses may alter the final comparison of the energy consumption of all the actuators because they have different impact in each of them [11]. Indeed, the electronic modulus and the batteries are expected to work very differently in the F-IVT and in the C-SEA: the working conditions are almost stationary in the F-IVT, and very changeable in the C-SEA. This can advantage the F-IVT further but we cannot discuss this point herein.

Another important index to evaluate an actuator for artificial leg joints is the electric peak power, which affects the size of the motor and consequently the size and the weight of the whole actuator. In figure 5.9 the electric peak power provided by the motor of all the actuators compared is normalized to the knee peak power at all the locomotion regimes explored. The results shown in figure 5.9 highlights the benefits of both the flywheel and the IVT in cutting down the power demanded to the motor of the F-IVT. They reduce the irregularity of the working point of the motor, which must provide an almost constant amount of power, nearer to the mean value of the power request than to the peak, giving the chance to design properly the whole actuator such the motor works very efficiently. On the contrary, the working points of the motors of the SEA and of the C-SEA are very changeable and both the motors must supply the peak of power demanded by the knee. This is clearly shown in figure 5.10 where the instant value of motor power is shown as a function of time for all the devices under analysis and in two walking regimes, for instance walking at 2.1 m/s (Fig. 5.10a) and stairs climbing at inclination of 30° (Fig. 5.10b). Similar results have been obtained in all other walking regimes.

For this reason, the electric peak power of the flywheel based actuators is by far lower than the C-SEA both in level ground walking and stair climbing. Thanks to the greater efficiency of the powertrain, the linear F-IVT is also characterized by lower peaks of electric power than the rotating F-IVT, permitting to select motor with a halved nominal power (Table 5.2).

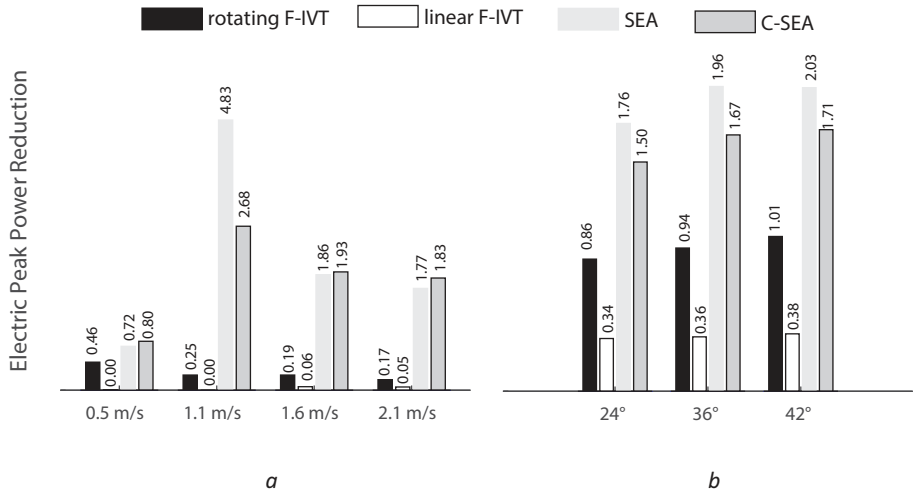

Figure 5.9: Peak values of the electric power provided by the motor, normalized to the peak of the power demanded by the knee joint. Results are shown for the linear F-IVT, the rotating F-IVT and the C-SEA in level ground walking at different speeds(a) and stair climbing at different inclinations (b).

Besides the peak of electric power supplied by the motor, also the peak value of the torque significantly affects the size of the motor. The size and the weight of a motor increase by increasing the nominal torque [21, 20, 17]. In figure 5.11 the peak value of the motor torque of all the actuators is normalized to the peak value of the knee torque at all the conditions examined. It can be noticed that values of the SEA and C-SEA are always greater than the others, which take advantage from the stabilizing effect of the flywheel.

Figures 5.9 5.11 prove that the the flywheel based actuators can entail a significant downsizing of the motor as it can also be noticed comparing the masses of the motor (M_M) of the linear F-IVT, rotating F-IVT, SEA and C-SEA which were selected in this study (Table 5.2). Since all the actuators considered in this study involve a mechanical energy storage device with regenerative potential usage (the flywheel and the spring, respectively), it is interesting to compare the energy actually re-cycled in both devices. Data shown in Table 5.3 prove that the flywheel is able to re-cycle much more energy (about three times) than the spring in all walking

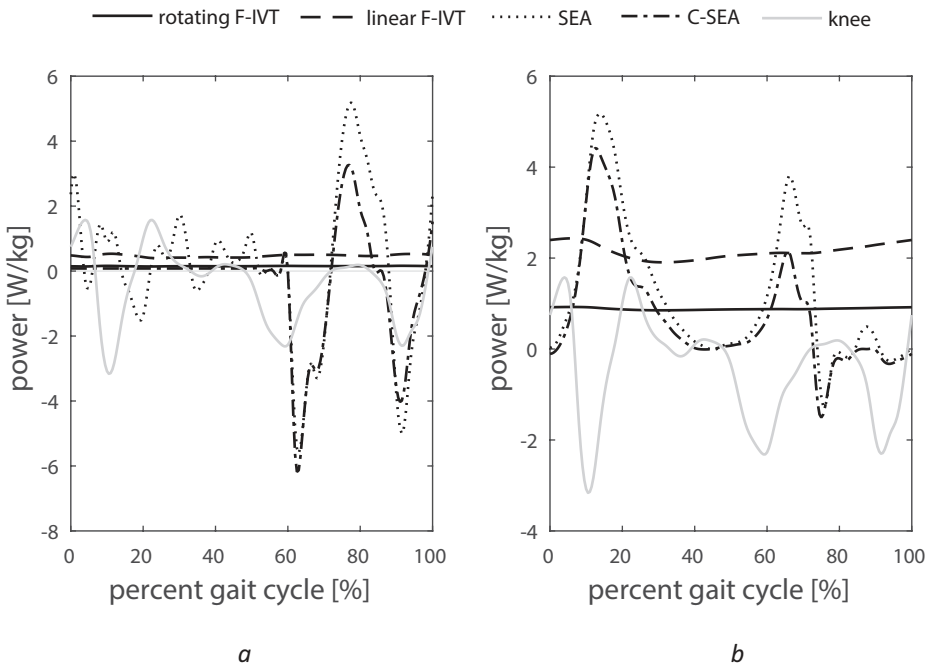

Figure 5.10: Instant power requirements of the knee joint and of the electric motor of the actuators compared (F-IVT, SEA, C-SEA) in level ground walking at 2.1 m/s (a) and in stairs climbing at inclination of 30° (b).

regimes, in particular in the case of linear F-IVT. It follows that the benefits given by the spring in terms of energy recovery in the C-SEA are much less then the ones given by the flywheel in the F-IVT, meaning that in the C-SEA most of the reusable energy should be recovered electrically.

5.1.3 Self-powered F-IVT

The energetic capacity of the self-powered F-IVT actuator has been evaluated by estimating how much energy it delivers to knee joint in level ground walking in a range of speeds. The mathematical model provided in the previous section has been used for calculations considering normalized knee gait cycle analysis data [111] (Fig. 5.7).

Table 3.3 lists the size of each device included into the self-powered F-IVT actuator. In this paper, the self-powered F-IVT has been designed with reference to a 75 kg healthy subject. While the highest load demand has constrained the selection of the BS from data-sheet, a specific operating condition of the device has been selected in order to optimize the design of the actuator, specifically relating to the IVT

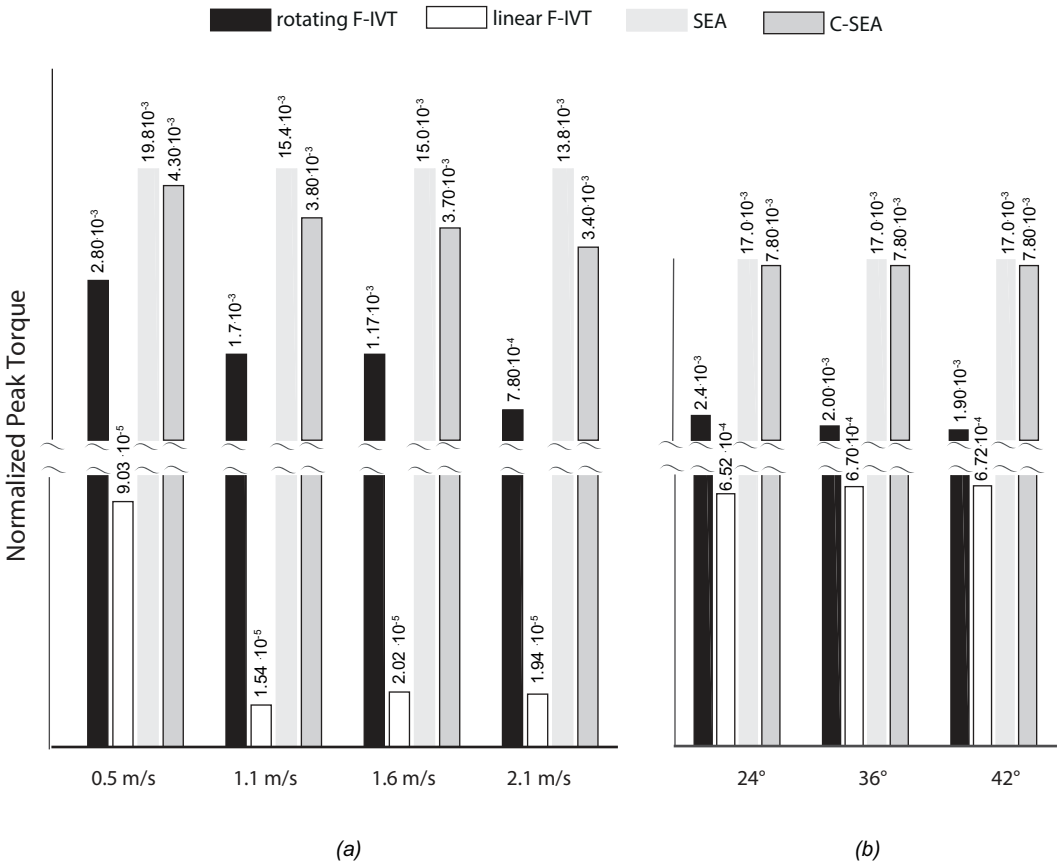

Figure 5.11: Peak values of the motor torque provided by the motors of the linear F-IVT, of the rotating F-IVT and of the C-SEA in level ground walking at different speeds and stair climbing at different inclinations. Peak torque values are normalized to the peak value of the knee torque.

AMOUNT OF ENERGY STORED AND RELEASED BY THE STORAGE DEVICE [J/KG]

	0.5 m|s	*1.1 m|s*	*1.6 m|s*	*2.1 m|s*	*24°*	*30°*	*42°*
rotating F-IVT	0.04	0.13	0.24	0.32	0.08	0.01	0.01
linear F-IVT	0.09	0.16	0.26	0.32	0.16	0.19	0.14
SEA	0.01	0.03	0.09	0.18	0.00	0.00	0.00
C-SEA	0.02	0.06	0.09	0.14	0.00	0.00	0.00

Table 5.3: Amount of energy re-cycled by the storage device of the three actuators compared in this work: rotating F-IVT, linear F-IVT, SEA and C-SEA.

efficiency. This aspect mainly affects the design of the BS joint to the knee (i.e. the mechanism) and the selection of the IVT ratio range.

According to [89], the IVT speed ratio profile has to fully exploit the IVT ratio range in order to minimize power losses in the IVT (fig. 3.3). The size and the geometry of the mechanism, which determine τ_{MECH} and thus the IVT ratio profile, have been found through an optimization procedure aimed at maximizing η_{IVT} under the assumption of an infinite flywheel inertia. In this paper, the IVT ratio range and the mechanism have been selected with reference to walking at natural speed.

A comparative analysis of the effect of the flywheel inertia and speed on the global performance of the system has lead to the selection of the flywheel. Figure 5.12 shows the estimated value of the K index for a self-powered F-IVT whose flywheel inertia changes in a range coming from 10^{-5} to 10^{-3}kgm^2. It reveals that after a positive peak, K does not change significantly by increasing the flywheel inertia. Additionally, the trend of K in figure 5.12, proves that the lower irregularity of the flywheel speed, got equally for high values of J_F or of ω_F, negatively affects the efficiency of the IVT. However, lower motion irregularity involves high speed variation of τ_{IVT}. Therefore, a flywheel inertia of $5 \cdot 10^{-4}$kgm^2 has been considered a good compromise among size, performance and motion irregularity.

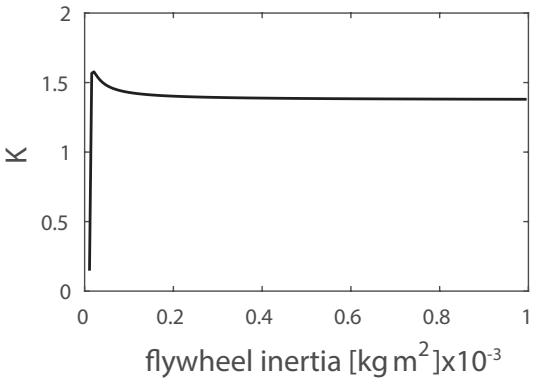

Figure 5.12: Estimated values of K index as a function of the flywheel inertia in a range changes in a range coming from 10^{-5} to $10^{-3} kg \cdot m^2$

Figure 5.13 is a proof of concept of the operating principle of the actuator. In figure 5.13a the instant trend of the flywheel speed is compared with the knee power requirement in a gait cycle of natural level ground walking. It can be noticed that the rate of change of the (nearly constant) flywheel speed is opposite to the sign of the instant knee power requirement: when P_K is negative, energy moves from the knee

to the flywheel whose speed increases, conversely when P_K is positive the flywheel delivers energy to the joint and ω_F decreases. This general operation of the actuator makes an exception in some phases of the gait cycle because of the power losses in the transmission devices, and in particular in the IVT. These happen when, under the reverse operation mode of the device, the amount of power losses into the IVT makes the motion not back drivable (i.e. irreversible motion condition) and, even if P_K is negative, both the flywheel and the knee deliver power to the transmission gear to keep the system in motion. As a consequence of that under these phases of non-reversible motion, which are characterized by negative IVT efficiency points (Fig.5.14), ω_F decreseas when the P_K is negative (Fig.5.13 b, c).

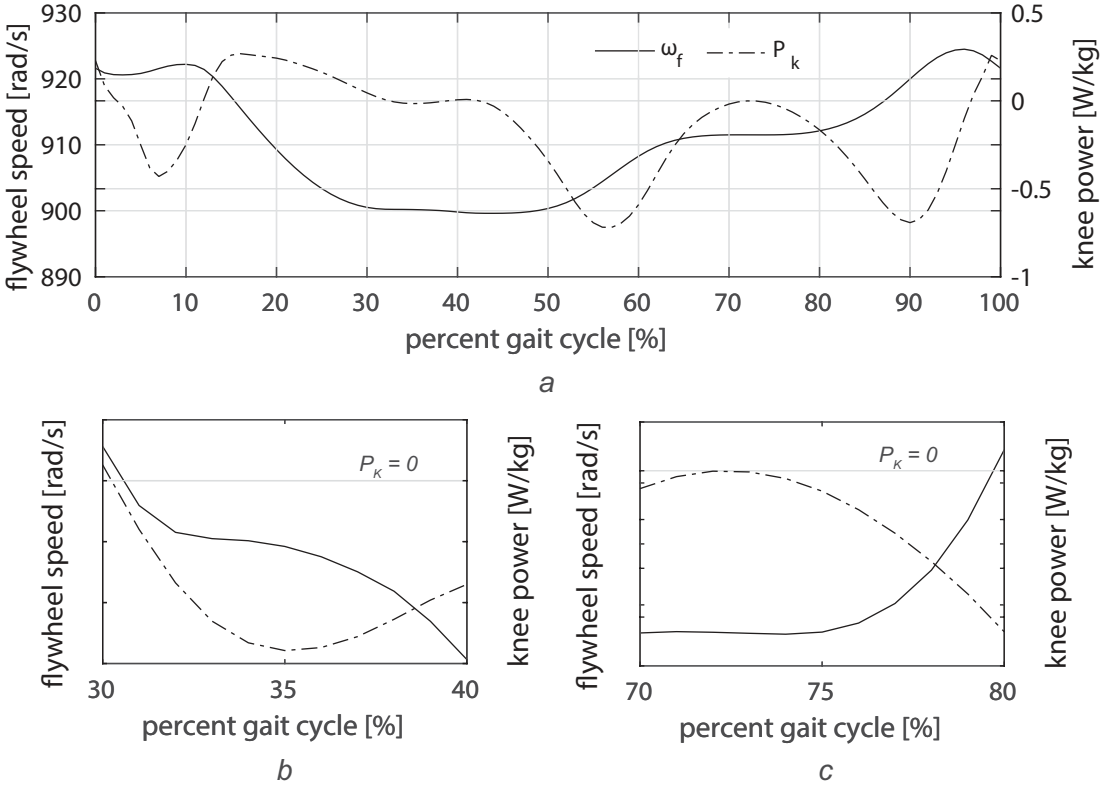

Figure 5.13: a) Instant flywheel speed profile (ω_F) compared with the instant knee power requirement (P_K) in a gait cycle of natural level ground walking. In b) and c) the trend of ω_F and P_K is shown in two intervals of the gait cycle in which the motion is non-reversible (30-40%, 70-80%).

In order to evaluate the effectiveness of the self-powered F-IVT, K index has been calculated at all the walking regimes considered and its values are shown in figure 5.15. Despite the very low average value of the efficiency of the transmission (Fig.

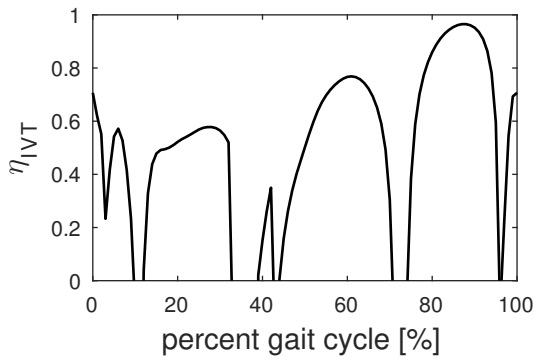

Figure 5.14: IVT efficiency (η_{IVT}) in a gait cycle of natural walking. The IVT efficiency points are very changeable according to the operating condition of the transmission device. They are negative under the non-reversible motion condition. Only positive efficiency points are shown in this figure.

5.14), it can be noticed that K is always greater than one, meaning that the instant profile of the power provided by the self-powered actuator (P_{out}) coincides with the knee power requirement (P_K) when both are negative (i.e. in reverse operating mode), while P_K is greater than P_K when they are positive (Fig. 5.16). Therefore, the self-powered F-IVT actuator is able to recover enough power from the passive dynamic of knee joint in walking to deliver even more than the knee power request in the active phases of the gait cycle, giving also the chance to face unexpected obstacles or situations which could require more torque.

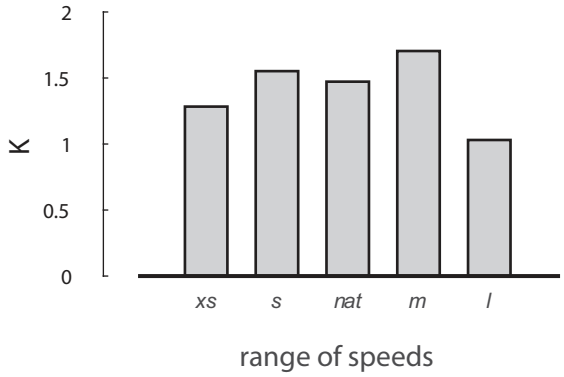

Figure 5.15: Value of K index in real operating condition of the self-powered F-IVT at different walking speeds (xs - extra slow; s - slow; nat - natural; m - medium; l - large).

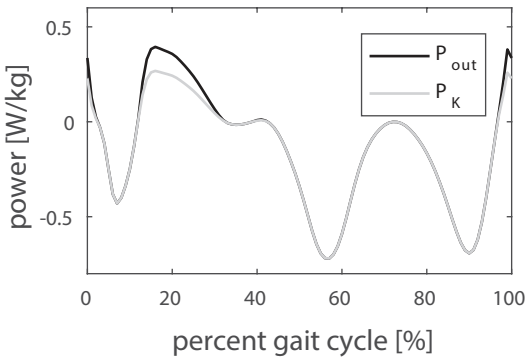

Figure 5.16: Instant profile of the power provided by the self-powered actuator (P_{out}) compared with the knee power requirement (P_K) in a gait cycle of natural walking. Both profiles coincide when they are negative (i.e. in reverse operating mode), while P_{out} is greater than P_{out} when they are positive.

5.2 Balance performance estimation of the flywheel inertial actuator

The flywheel inertial actuator was experimentally tested to estimate how it affects balance keeping performance of people in perturbed standing. All the experiments were carried on with the permission from Medisch Ethische Toetsingscommissie (METC) Twente. Ten healthy subject in the age 23-30 years participated in the study. The participants in the study were asked to stand still on a treadmill including force plates, with bare feet, in upright position. The subjects were attached to the pelvis perturbator system using a pelvis belt. The pelvis perturbator applied lateral perturbations of three different magnitudes at the pelvis in both directions. For each subject and for each direction, the magnitude of the force applied was scaled on the human body mass using the following weight 0.1, 0.08, 0.06. According to the value of the weight, the magnitude of the perturbations can be distinguished in maximum, medium and minimum. The subject received sixty perturbations in each session of the experiment every 10 seconds. The order of the perturbations, i.e. weight used to cause the perturbation, was randomly selected. The subjects were instructed to keep their arms close to the chest to avoid any balancing effect, and to try to maintain balance without stepping in order to consider the number of foot lifts as an index of their balance performance.

Each experiments consisted of four different sessions whose details follow below:

1. Trial I, *Baseline*: subjects do not wear the device
2. Trial II, *Off*: subjects wear the device but it is turned off
3. Trial III, *On*: subjects wear the device that operates with *Controller 1*. *Controller 1* activates the balance device on the basis of the sway angle and velocity.
4. Trial IV, *On2*: subjects wear the device that operates with *Controller 2*. *Controller 2* activates the balance device on the basis of the sway velocity.

5.2.1 Proof of the operating principle of the balance device

In this section the instant trends of some quantities measured during trial 3 and 4 are provided in order to explain how the control of the balance device works and which is its effect on the human sway. Figures 5.175.18 show the instant trend of some quantities measured during trials III and IV, in which the device operates with two different controllers. In trial III (i.e. *On*) , the operation of the device is controlled on the basis of the values of the sway angle and velocity and thus threshold values have been considered for both of them (*Controller 1*). In trial IV (i.e. *On2*) , the operation of the device is controlled only on the basis of the sway velocity (*Controller 2*). All the quantities represented in figures 5.175.18 are normalized to the maximum values they got in the time span considered. Therefore the value of all the quantities can change between -1 and 1.

Figure 5.17refers to *Controller 1* and 5.18 to *Controller 2*. Figures reveals that both the amplitude of the sway angle and the magnitude of the sway velocity increases in the same direction after the perturbation is applied. In the experimental trial selected (Fig. 5.17), *Controller 1* activates the balance device when the threshold value on the sway velocity is overcome ($t \simeq 0.3$sec). The motor provides a corrective torque proportional to the error on the angle, defined as the difference between the actual sway angle and the velocity threshold value, that quickly reduces the sway velocity. In the mean while, the amplitude of the sway angle decreases and this makes the balance device still operate even if the sway velocity is lower than the threshold value ($t \simeq 0.4$sec) until both the measured sway angle and velocity are lower than the threshold values ($t \simeq 0.5$sec). After this phase, the subject still experiences sway whose amplitude requires the intervention of the balance device that provides again torque ($0.7 \leq t \leq 0.9$sec). When the corrective torque of the

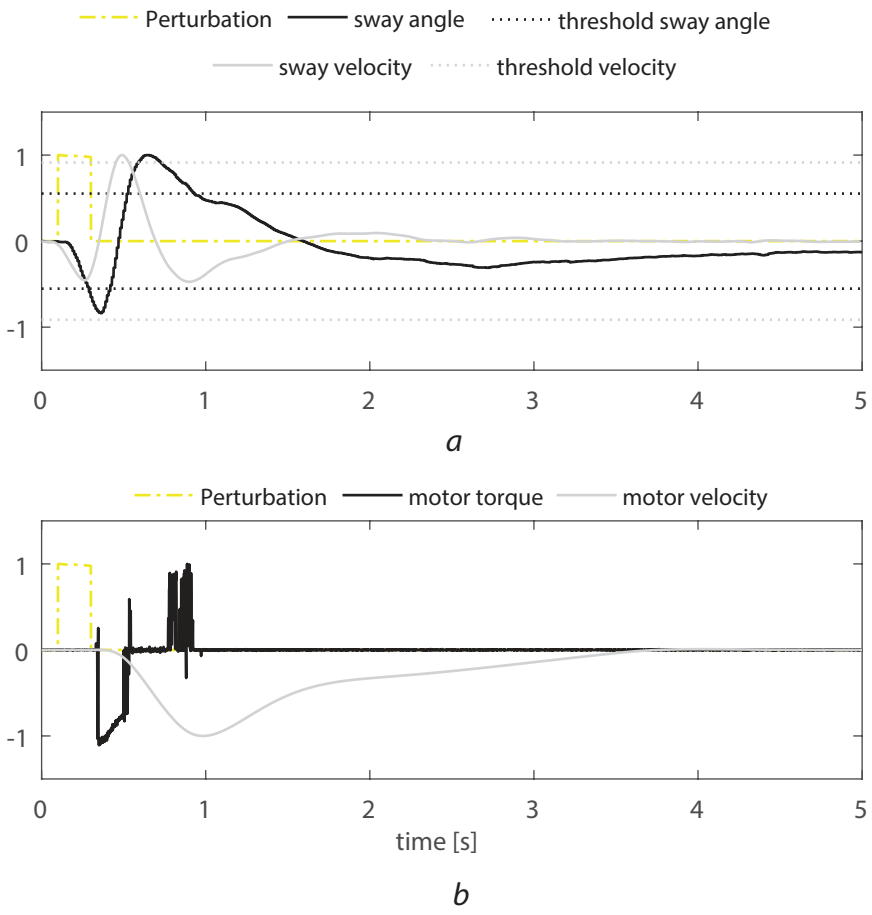

Figure 5.17: Instant trend of some quantities measured during experiment trial III, when the device operates with controller 1. Figure *a* shows the sway angle and the sway velocity after a perturbation. The threshold values of the angle and velocity which define the starting of the operation of the device are also shown. Figure *b* shows the torque provided by the motor and the velocity of the flywheel after the perturbation considered. All the quantities represented in the picture have been normalized to their maximum value in the trial.

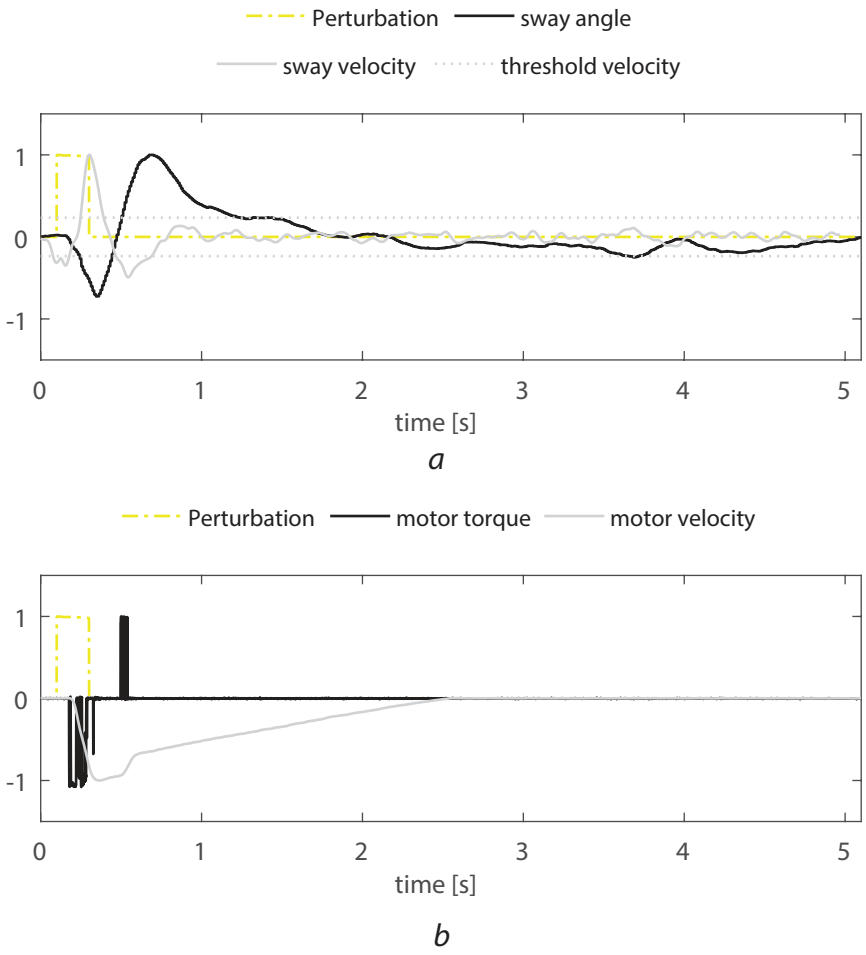

Figure 5.18: Instant trend of some quantities measured during experiment trial IV, when the device operates with controller 2. Figure *a* shows the sway angle and the sway velocity after a perturbation. The threshold value of the sway velocity which defines the starting of the operation of the device are also shown. Figure *b* shows the torque provided by the motor and the velocity of the flywheel after the perturbation considered. All the quantities represented in the picture have been normalized to their maximum value in the trial.

balance device is not needed anymore ($t \simeq 0.5$sec, $t \simeq 0.9$sec,), the flywheel is slowly decelerated in order to minimize the effect of the inertial torque that in this case would disrupt body balance. When *Controller 1* detects the loss of balance of the subject, the motor provides the maximum torque and then its value decreases because of the constrains on the safe operating area of the motor.

Controller 2 operates similarly to *Controller 1*, with the difference that it detects the subject loss of balance only on the basis of the sway velocity (Fig. 5.18). The motor starts around $t \simeq 0.2$ sec by providing almost the maximum motor torque. After the balance device applies torque on the human body, the sway velocity decreases and oscillates around its threshold value. This explains the trend of the motor torque from $t \simeq 0.2$sec to $t \simeq 0.35$sec. After the operation of the balance device the sway velocity decreases and changes its direction. Around $t \simeq 0.5$sec, when the sway velocity is higher than the threshold value and it has the same direction of the sway angle, the controller activates again the balance device. In this time span, the motor is fast decelerated to provide the corrective torque, because its velocity is still non null. Then the motor is slowly speeded down and it stops at $t \simeq 2.5$sec.

5.2.2 Analysis of the human balance performance

Data collected during experiments have been analyzed to assess human balance performance. Some of these data are collected in figure 5.19, which shows the values of some measured quantities in a generic session of the experiment.

Figure 5.19 clearly shows that once the subject receives a perturbation (i.e. he\she is pushed or pulled by the pelvis perturbator) it starts to oscillate in the M/L plane experiencing larger body sway than in quiet standing. Indeed, the sway angle gets peaks values just at the perturbations (5.19 b). The COP excursion has the same trend that changes similarly according to the perturbations applied (5.19c). The magnitude of the vertical ground reaction forces also changes at the perturbed instants. The perturbation usually involves a weight shift in human body. Depending on the direction of the perturbation, the subject unloads one foot and loads the other. In particular, when the perturbation is positive and the subject is pushed toward the left, the ground reaction force on the right foot decreases and the one on the left foot increases. The contrary happens when the subject is pulled toward the right side. Sometimes, it also happens that the subject needs to lift one or both of

his feet to keep balance. In this condition the ground reaction force of the lift foot is null.

These considerations motivated to assess the balance performance of subjects by considering the following parameters:

- maximum amplitude of the oscillation of the subject's body in the frontal plane after a perturbation is applied;
- number of lifts foot after a perturbation is applied.

In the data analysis, the effect of the first two perturbations has not been considered for the experimental session 2 to 4 (*Off, On, On2*). The first four perturbation has not been considered for the session 1 (*Baseline*) to minimize start up effects.

5.2.2.1 Maximum amplitude of the oscillation of the subject body in the frontal plane after a perturbation

The amplitude of the sway angle ($\Delta\vartheta$) at each perturbation provided (i.e. peak to peak value) has been calculated for each subject in each session of the experiment (i.e. trial I to IV). For each subject and trial, the maximum sway amplitude ($\Delta\vartheta_{PEAK}$) at each magnitude of the perturbation applied has been computed. Then, the average value of $\Delta\vartheta_{PEAK}$ of all the subjects and its standard deviation has been got for each trial (5.20). Data from the non-stepping trials were used in the following analysis, so perturbations that caused a step have not been considered in the calculation. Results shown in figure 5.20 have been obtained.

Figure 5.20 shows that the device decreases the amplitude of the maximum sway of the human trunk of the 24% with *Controller 1* (trial *On*) and of the 28% with the *Controller 2* (trial *On2*). However, if $\Delta\vartheta_{PEAK}$ of trial I (*Baseline*) is compared with that of trial II (*Off*), it can be noticed that the peak of the sway angle decreases already of about the 16% when the device is worn but it does not operate. The balance device increases the total mass of the perturbed system (i.e. human body plus balance device) and the effect of perturbations is lower if it is compared with that of trial II (i.e. Baseline). The effect of both the controllers on human sway can be assessed by comparing the trial in which the device is switched off (i.e., Trial II, *Off*) and the trials in which the device operates with *Controller 1* (i.e. trial III, *On*) and *Controller 2* (i.e. trial IV, *On2*). *Controllers 1* and *2* further improves the balance performance of the subject in perturbed standing by reducing of the 10%

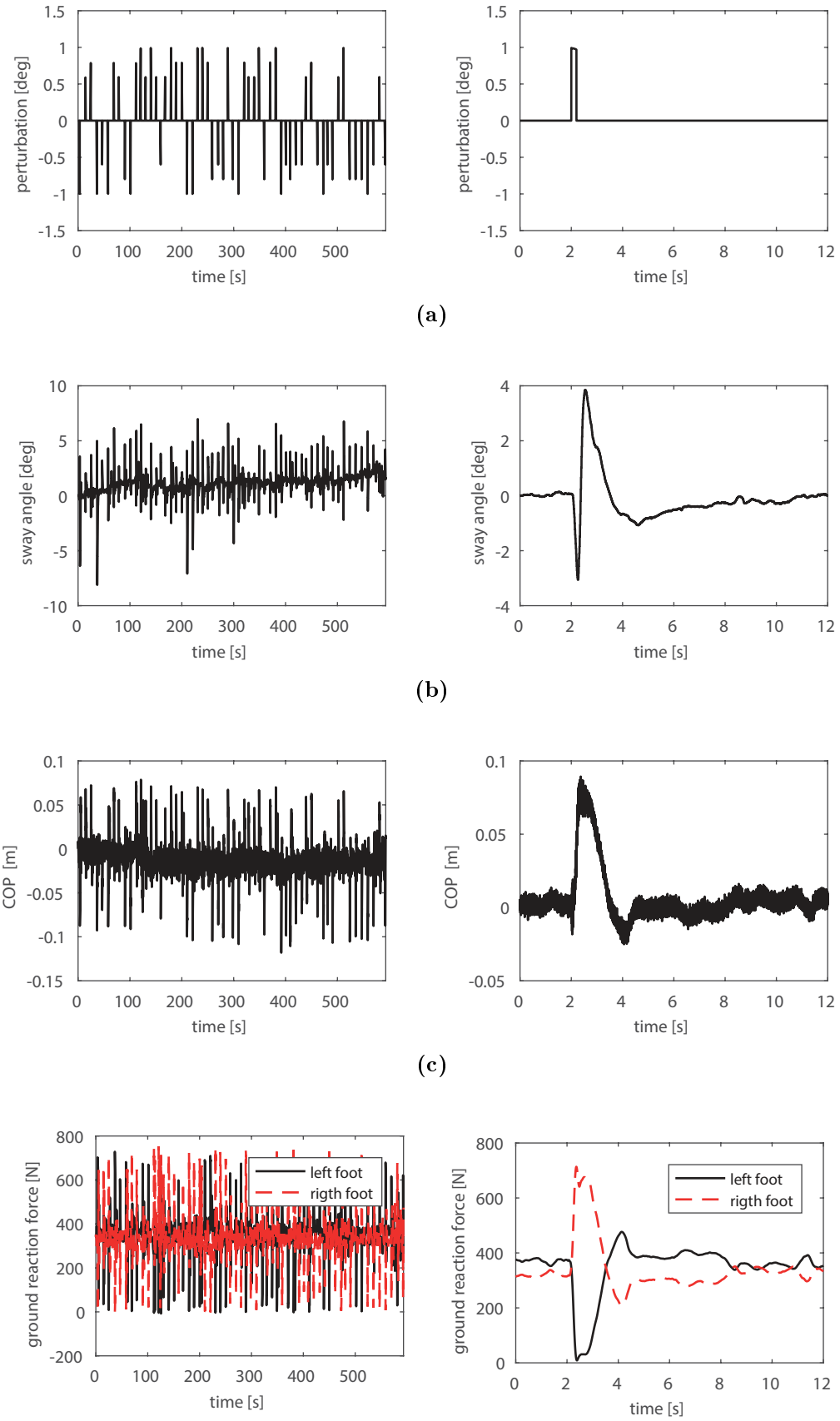

Figure 5.19: Instant trend of some quantities measured during one session of the experiment: a) perturbations applied whose value is normalized to the maximum perturbation applied; b) sway angle of human trunk; c) COP displacements in M\L direction; d) vertical components of the ground reaction forces of the right and left foot. For each quantity the trend during the whole trial is given on the left, and a zoom out of them in the very close range of a maximum perturbation on the right.

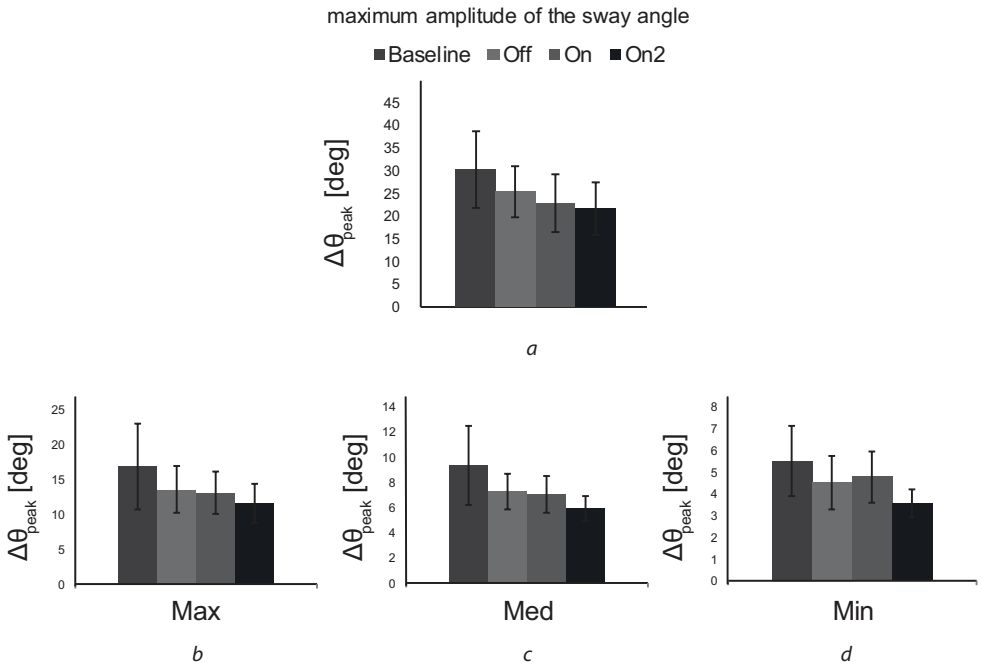

Figure 5.20: Avarege value of the maximim sway angle in te four sessions of the experiments with reference to the total number of perturbation applied (a), to the number of the maximum perturbation applied (b), to the number of the medium perturbation applied (c) and to the number of the minimum perturbation applied (d).

and 15% the maximum amplitude of the sway angle respectively. In table 5.4the percentage change of $\Delta\vartheta_{PEAK}$ in trials II-III-IV and III-IV relatively to trial I and trial II is shown. *Controller 2* performs better than *Controller 1* and that it is advantageous especially at the medium and minimum magnitudes of perturbations, when it reduces the amplitude of the sway angle of the 18% and 21% respectively.

	PERCENTAGE VARIATION OF THE SWAY ANGLE RELATIVELY TO				
	TRIAL I: BASELINE			TRIAL II: OFF	
	TRIALS			TRIALS	
MAGNITUDE OF THE PERTURBATIONS	II	III	IV	III	IV
TOT	-16%	-24%	-28%	-10%	-15%
MAX	-19%	-22%	-31%	-4%	-14%
MED	-22%	-24%	-36%	-3%	-18%
MIN	-18%	-13%	-35%	6%	-21%

Table 5.4: Percentage variations of the maximum amplitude of the sway angle relatively to the trial *Baseline*, when subjects do not wear the device, and the trial *Off* when subject wear the device but it do not operate.

5.2.2.2 Number of foot lifts after a perturbation

The percentage of perturbations that caused a foot lift has been evaluated for each subject and trial. It has been calculated as the ratio between the number of the foot lifts and the total number of perturbations applied. The percentage of perturbations has also been distinguished on the basis of the magnitude of perturbations applied, in order to analyze how the balance performance of the subject changes with reference to the disruptive force applied. Therefore the percentage of foot lifts caused by the maximum, medium and minimum perturbations have been calculated. The average value of the percentage of foot lifts to the total number of perturbation applied and to the three magnitudes of perturbations applied (i.e. max, med. min.) are provided in figure 5.21 for each trial.

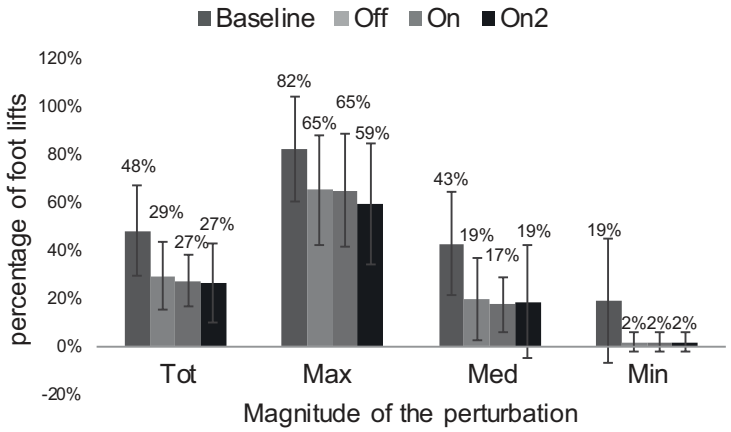

Figure 5.21: Average value of the number of foot lifts in the four sessions of the experiments with reference to the total number of perturbation applied (Tot), to the number of the maximum perturbation applied (Max), to the number of the medium perturbation applied (Med) and to the number of the minimum perturbation applied (Min). The error bars show the values of the standard deviations of data.

Results shown in figure 5.21 reveal that the percentage of foot lifts after a perturbation decreases if subjects wear the balance device, even if it is turned off. As already discussed for the trunk sway, the higher total mass of the subject wearing the device significantly reduces the number of foot lifts because the effect of the perturbation is lower. In trial II-III-IV subjects wear the device and receive perturbations of the same magnitude, that generate comparable effects on the total weight of the system "human body plus device". Therefore, data collected during these sessions can be fairly compared to assess the effect of both the controllers on human balance performance. This comparison proves that *Controllers 1* and *2* reduce additionally the number of steps respect to the performance measured in trial *Off*. They reduce the foot lifts of the 6% and 9% respectively (Table 5.5). Furthermore, results show that *Controller 1* is more effective in reducing the number of step at the medium perturbations, while *Controller 2* is more effective at the maximum perturbations (Table 5.5).

	PERCENTAGE VARIATION OF THE SWAY ANGLE RELATIVELY TO				
	TRIAL I: BASELINE			TRIAL II: OFF	
	TRIALS			TRIALS	
MAGNITUDE OF THE PERTURBATIONS	II	III	IV	III	IV
TOT	-40%	-43%	-45%	-6%	-9%
MAX	-20%	-21%	-28%	0%	-9%
MED	-55%	-60%	-57%	-11%	-5%
MIN	-91%	-91%	-91%	-5%	-5%

Table 5.5: Percentage variations of the maximum amplitude of the sway angle relatively to the trial *Baseline*, when subjects do not wear the device, and the trial *Off* when subject wear the device but it do not operate.

6 Conclusions and Discussions

Even though research on wearable robots developed a lot in the last decades, their portability still challenges their development and widespread among users. Effectiveness of wearable robots depends on their portability, which is conceived as the capability of these robots to be worn and carried around by users who need to be supported in a large variety of operational scenarios and for an extended length of time in daily life. Comfortable and ergonomic mechanical structures, as well as efficient and convenient actuation systems contribute to the progress of portable and free-standing robotic devices.

Actuation of these devices must fulfill often opposing requirements which are hard to conciliate at the same time. They must be powerful enough for providing the high peaks of torque and power demanded in a gait cycle of locomotion tasks, they should have low energy consumption in order to increase the operating range of the device and finally they must be as small and lightweight as possible in order to decrease the metabolic expenditure and facilitate portability. As a consequence of the difficult conciliation of weight and performance requirements of the actuation, most currently developed wearable robots for lower limbs are heavy and they can provide limited torques and power, restricting the effectiveness of these devices, especially in case of patient assistance.

Reducing the energy and power consumption of the source of power is a valuable way for reducing the weight and size of the actuator and for permitting a long-lasting usage of the device, with consequent advantages in terms of portability. A lot of research effort is focused on the design of innovative and efficient actuators capable of exploiting the passive dynamic of human walking by storing and releasing energy according to phases of the gait cycle, to reduce the energy requirement of the motor [6, 7, 8, 9, 10, 11, 12, 13, 14, 15, 16, 19]. Energy recovery is a commonly accepted solution to pursue this goal, but it does not always entail effective motor downsizing, which can be achieved if both the motor power and torque requirements

are reduced. It is indeed well known that the size of an actuator is related to the value of its rated torque. Actuators including springs to store energy, reduce the peaks of electric power and the energy consumption, but they transfer the same torque at the motor shaft [21, 20].

More than the joint power augmentation, also the balance challenges the development of portable wearable robots. Most of wearable robots have been not primarily designed to assist balance and users have to count on conventional assistive technologies, such as canes or crutches, to prevent the risk of falling. However, these external assistive devices are hold in the hands and this is not convenient for people with limited strength in upper limbs. Furthermore, they can interfere with balance in some situations and they reduce the effectiveness of wearable robots in comparison to wheel chairs. Multi degree of freedom actuated joints would improve gait stability, despite the increase of the weight and of the control complexity. Robotic assistive technologies, such as moment exchange actuators, have the potential of providing balance assistance to the wearer in his daily life actions and consistently with human balance control. They detect the subject's loss of balance and provide corrective actions to avoid or delay the risk of falling. Balance assistive devices can either be included in powered wearable robots or be worn separately by subjects suffering balance disorders to control and improve their balance.

This thesis gives a contribution to the development of portable wearable robots in terms of energetic efficiency and safety. The current actuation technologies for joint power augmentation and balance assistance have been investigated with the aim of finding novel solutions that could improve the portability of wearable robots for human locomotion assistance and human strength augmentation. This thesis presents two actuators focused on enhancing joint strength and on balance compensation respectively. The fist actuator, named F-IVT, transfers power to the knee to enhance the strength of the joint, the second one is a flywheel inertia actuator for assisting human balance.

6.1 Flywheel based actuators for knee power augmentation

In this thesis we propose an innovative and more efficient actuation system (named F-IVT actuator) to power knee joints of exoskeletons. F-IVT is an actuator adapt-

able to any walking regime and its effectiveness comes from an advantageous exploitation of inherent characteristics of human locomotion.

F-IVT is made up of an electric motor, a flywheel, an Infinitely Variable Transmission (IVT) and a fixed ratio drive (FR). The IVT allows to properly move the energy between the flywheel and the load: when the knee joint demands negative (positive) power, energy is driven to (from) the flywheel through a proper variation of the speed ratio of the IVT. The flywheel works as a mechanical storage system. The rate of change of the energy stored in the flywheel follows instantly the requirements of the joint. In this way the flywheel reduces the motion irregularity of the motor shaft and the motor works almost at fixed operating point. With a proper design of the motor, the working point corresponds to almost maximum efficiency, thus reducing the electric energy consumption.

The performance of the F-IVT actuator has been compared to a traditional system, named Fixed Ratio Drive (FR-D), where the speed is regulated by controlling the motor speed. Two conditions have been analyzed: level ground walking and running. Both the actuators have been optimally designed for the specific walking conditions. The results show that the peak of electric power and the electric energy required in a gait cycle are reduced respectively of the 91.8% and 85.3% in level ground walking, and of the 96.2% and 83.1% in running with the F-IVT system, with great advantages in terms of reduction of motor size and improvement of the operating range. We proved that the F-IVT architecture permits to undersize the electric motor, which in F-IVT delivers an almost constant power value roughly equal to the mean power requested and by far less than the peak power. Moreover, the electric motor can be sized for working at a nearly fixed point at the greatest efficiency values, with a resulting potential saving of electric energy consumption. The motor undersizing would be a great advantage in this kind of application because it facilitates the portability of the device, also enlarging its operating range. However, these results give a limited sight on the F-IVT potential because the performance are therein estimated in the nominal working condition, i.e. the one taken as a reference to optimally design the F-IVT components. Indeed, the portable lower-limb wearable robots are required to support the wearer in his daily activity, thus their actuators do not usually work under the nominal condition.

We have further investigated the F-IVT by predicting its performance when it does not work under the condition for which it was optimally designed, like different

walking speeds and stairs climbing. The energy and power requirements of the rotating F-IVT and of the linear F-IVT have been estimated through a model based approach and compared with those of two very efficient actuators already used in biomechatronics devices, the SEA and the C-SEA, in order to evaluate if it could be a competitive actuator for artificial knee joints of wearable robots. We have estimated the motor performance of the different actuators in powering an artificial knee joint under different locomotion regimes very recurring in daily life: level ground walking at different speeds and stairs climbing at different inclinations. Detailed efficiency models of all the devices have been used to obtain realistic estimations of the motor consumption following an inverse dynamic approach. Two main performance indexes have been taken in consideration for comparison: the energy consumption (per gait) and the peak of electric power, both calculated at motor electrodes. As a result of the simulations, it was found that the motors of the linear F-IVT and of the C-SEA have the lowest energy consumption in level ground walking and stairs climbing respectively. Thus they would permit a larger operating range of the device. However, it is important to specify that in this work the energy requirement of the motor has been calculated at the motor electrodes, not at batteries. There are at least two reasons why the effective energy requirement of the actuators, i.e. the energy demanded by the battery, may be different with respect to the motor energy requirement, in particular in SEA and C-SEA. First, the working point of the motor is quickly and repeatedly variable, and this may affect the actual efficiency of the electronic devices between the batteries and the motor, and the batteries themselves. Second, the electrical power generated by the motor could be smaller than the estimated, as the very low experimental values of the regeneration efficiency achieved in practice [110] would demonstrate. Unfortunately, these issues are still debated, and no precise data are available in the literature.

Furthermore, this study proves that the F-IVT permits to achieve a drastic reduction of the peak power and of the peak torque at all the conditions examined. In fact, the flywheel and the IVT stabilize the working point of the motor, which always provides a nearly constant amount of power that is very lower than the peak power request. This achievement is very important in view of the possibility to downsize the electric motor, which would also mean reducing the size and the weight of the actuator, with advantages in terms of portability. Moreover, the motor of the F-IVT always works very efficiently, even when it does not work under the condition for which it is optimized, and this may be true for the power electronics and the batteries. Of

course, even if the motor mass is the most critical one, in order to make the F-IVT more lightweight than the other devices developed for the same purpose, the mass loss due mainly to the reduced motor size should overcome the additional masses of the micro-IVT and the flywheel. We have also roughly estimated that the motor downsizing achieved through the flywheel based actuators is such that they and the other actuation systems considered have almost equal weight. Moreover the mass of the F-IVT could be further reduced through the design of proper transmission devices properly developed for such biomechanical applications.

This thesis also explores the idea of a self-powered actuator for artificial knee joint of wearable robots. The novel actuator, named self-powered F-IVT, uses only the energy recovered during the passive phases of a gait cycle to power the knee joint in level ground walking. As in the powered F-IVT, the role of the IVT is crucial to control the energy exchanges between the flywheel and the knee joint: when the knee absorbs power ($P_K < 0$), τ_{IVT} has to change in order to move energy from the knee to the flywheel where it is stored, conversely when the knee demands positive power ($P_K \geq 0$), energy has to be delivered to the joint. The efficacy of the F-IVT has been evaluated in level ground walking in a range of speed. The model based estimation of the amount of power deliverable by the self-powered F-IVT reveals that the energy recoverable in a gait cycle of walking is enough to fulfill the total knee power requirement and also more, despite the low average efficiency of the transmission. This means that the actuator would also permit to face unpredictable increases of the knee load, as obstacles or waste of power. This is a promising result in the view of developing lightweight actuators for artificial leg joints in the field of wearable robots. Indeed, the lack of the motor, of the battery and of all the electronics related to them, would significantly decrease the weight and the size of the actuator, improving the portability of such devices.

The results presented in this thesis reveal that flywheel based technologies are promising actuation technologies that could improve portability of wearable robots by significantly downsizing the motor and reducing the energy consumption of the actuator, that means enlarging its operating range. However, this thesis contains the results of a preliminary assessment of the actuator and experimental investigations are needed. The comparative analysis of the actuators done in this thesis were firstly aimed at assessing which are the potential benefits and the drawbacks of the flywheel based actuators, in order to evaluate if they could be or not competitive actuators for artificial knee joints of wearable robots. Then, the results of the

compared analysis are also usefully supporting the development of a prototype of the F-IVT, leading to the selection of the most efficient solutions to include in the actuator. For example, results of this thesis shown that the linear F-IVT is more advantageous that the rotating F-IVT in terms of energetic efficiency.

These promising results stimulate us to work on the design and development of compact, light and efficient IVT drives that can actually be used for active exoskeletons. The commercially available IVTs cannot be used for leg joints actuators because they are designed for higher power demanding applications. Indeed, IVTs are currently largely used in the automobile field and in wind power systems, but they have never been included in biomechatronic devices.

Future investigations will also aim to define an efficient control strategy of the actuator and to investigate the interaction of the actuator with the human subject, such as the evaluation of the effect of gyroscopic torques due to the rotating flywheel on walking.

6.2 Flywheel inertial actuator for human balance assistance

A flywheel inertial reactionless actuator for human balance assistance is also presented in this thesis. It is a wearable moment exchange device including a reaction wheel that assists people in keeping balance in the M\L direction. It counterbalances balance disturbance actions in the frontal plane through the inertial torque generated by accelerating and decelerating a flywheel around the falling direction.The working principle of the actuator emulates the contribution of arms in changing the angular momentum of the trunk to restore balance. The control of the device has been designed in order to make it work in parallel with humans. The device is started when the falling condition is detected and stopped once the steady posture is attained again. When the balancing intervention of the device is required, the flywheel is speeded up in the direction that make its inertial torque opposite to the gravitational perturbing action. The flywheel is then slowly stopped to minimize any additional disturbance effect.

The flywheel inertial actuator imparts a free moment to a body without the need of contacting it with a frame. It is included into a backpack to connect the device

to the user's upper body. It is easy to be worn and it is also a valuable assistive technology to be used independently from exoskeletons and orthoses. People with balance impairments who do not wear active orthoses, could use it in their rehabilitation sessions or to receive everyday life assistance. In order to promote the natural recovery of the patient, the control of the flywheel inertia actuator has been developed so that it acts consistently with human intent and provides assistance only when it is needed.

The device developed weights around 6 kg and it can apply a maximum torque of about 10 Nm on human body. The value of the peak torque of balance assistive device we developed is higher than that of the device presented in [24], that also includes a heavier flywheel.

The contribution of the flywheel inertial actuator in helping people to keep balance has been evaluated trough experiments on healthy subjects in perturbed standing. During experiments subjects were asked to wear the device and to stand on a treadmill with their feet together, while their equilibrium was perturbed by sudden and horizontal forces exerted at the pelvis by mean of a pelvis perturbator. Perturbations of three different magnitudes, whose value was scaled according to the subject's body weight, were applied.

The final goal of this research activity was to evaluate how the balance performance of a subject changes by wearing the supportive device. To this aim, the effectiveness of the device have been be evaluated by comparing the balance keeping performance of subjects when they wear and when they do not wear the inertial flywheel actuator. Each experiment consisted of four different trials: in trial I (*Baseline*) subjects did not wear the device, in trial I (*Off*) subjects worn the device but it was turned off, in trial III (*On*) and in trial IV (*On2*) subjects worn the device that operated with *Controller 1* and with *Controller 2* respectively. *Controller 1* activates the balance device on the basis of the sway angle and velocity, instead *Controller 2* activates the balance device on the basis of the sway velocity.

The human balance performance has been assessed through the following parameters: the peak values of the trunk sway after a perturbation and the number of foot lifts after a perturbation . Data collected during experiments have been analyzed on the basis of the magnitude of perturbations applied and of the different experiment sessions. The comparison of trial II-III-IV, when subjects wore the device, and trial I when subjects did not, reveals that the balance device improves the balance

performance even if it is turned off due to the increase the total mass of the perturbed system (i.e. human body plus balance device) that reduces the effect of the perturbation. Interesting considerations on the effectiveness of the controller come from the comparison of trial II and trials III-IV. In trial II subject wore the device that was kept turned off, on the contrary in trials III-IV subjects wore the device which was activated by two different controllers. The comparison reveals that both the trunk sway and the number of foot lifts decreases when the device operates. Better performance are achieved through *Controller 2*, which detects subject's loss of balance on the basis of the sway velocity. It determines a stronger reduction of both the sway peaks (15%) and of the number of foot lifts (9%), especially at the medium and maximum magnitudes of perturbations.

One of the limits of this study is that the balancing effect of the flywheel cannot be separated by the human balance strategy. Even if they wore the device, subjects reacted to perturbations with their natural postural mechanisms during experiments. This would also explain the low value of the percentage change of some trials. A preliminary estimation of the contribution of human strategies during experiments could be evaluated by estimating the torque exerted at the ankle. This would allow to asses human effort and to quantify subject's participation during the trials. Another aspect to consider is that both the learning effect and the fatiguing effect could have been affected results. Further experimental investigations could support the evaluation of these effects.

This thesis collects only some preliminary results of this study. The effect of some parameters useful to asses human balance has been estimated, but more parameters could give a wider overview of the effect of the flywheel inertial actuator on human balance (e.g. torque exerted at the ankle). For this reason no statistical test has been done at this stage of the study. However, a reliable discussion of the results needs also statistical considerations of the data collected and analyzed. Therefore, next stages of the study will surely include both the analysis of additional parameters and the statistical analysis of the results.

Data analysis also included the operation of the balance device. The instant trend of some measured motor quantities reveals that the motor provides torque after the controller detects the subject's loss of balance and for a very short length of time. What usually happens is that once the motor provides torque, it brings the dynamics of human body in the region in which no balance intervention is required.

This sometimes generates an intermittent behavior of the motor, and sometimes it just slows down the balance recovery of the system. The controller could be improved in order to make the motor providing a maximum torque for a longer time span in order to quicken the balance recovery. This would mean either implementing a feed-forward control algorithm that activates the motor once the loss of balance is detected and stop it when the subject get the upright stable position, or reducing the threshold value which limit the region in which the subject experiences natural sway.

Acknowledgments

(english version below)

Eccomi qui al compiersi di un'intensa esperienza iniziata pressappoco tre anni fa. Un percorso di studio, di lavoro e di vita che nonostante alcune indubbie difficoltà, ha concesso tante piccole soddisfazioni. È stato un percorso costellato da incontri, da presenze significanti e significative che consciamente o inconsciamente hanno reso migliore e più piacevole quest'esperienza. Ed è per questa ragione che voglio soffermarmi un attimo per dedicare a ciascuna di queste persone un pensiero sincero, con cui spero di esprimere loro tutta la mia gratitudine.

Il primo grazie non può che andare ai miei due tutor di dottorato, il prof. Giacomo Mantriota e il prof. Francesco Bottiglione, per il rilevante contributo all'attività di ricerca.

Al prof. Mantriota va tutta la mia riconoscenza per la fiducia che ha riposto in me all'inizio di questa avventura e che non ha mai mancato di confermare. Stimo moltissimo la sua professionalità, la sua lungimiranza e la sua dedizione all'attività scientifica, che lo rendono per me una figura esemplare da cui imparare molto.

Un infinito grazie va a Francesco per essere sempre stato un valido e importante riferimento. Innumerevoli sono stati i suoi consigli e suggerimenti rivelatisi utili ai fini di molti risultati raccolti in questa tesi. Parimenti importanti sono state la sua solita disponibilità ad ascoltare ogni problema (a volte anche paranoia), e la frequente condivisione di idee, opinioni e speculazioni scientifiche varie. In molte di quelle chiacchierate ho ritrovato e rafforzato la motivazione che difficoltà e preoccupazioni hanno fatto a volte vacillare.

Un significativo contributo a questa tesi proviene anche dal dipartimento di Ingegneria Biomeccanica dell'Università di Twente, ove ho lavorato per oltre un anno

trovando stimoli nuovi e interessanti per il mio lavoro. Un sentito grazie va al prof. Herman van der Kooij per avermi prontamente accolta nel suo laboratorio fornendomi ogni mezzo utile allo svolgimento dell'attività. È stato per me un onore poter lavorare con lui e con tutto il suo gruppo di ricerca. In particolare, desidero ringraziare Lianne e Janine per la loro sempre gentile ed efficace disponibilità, e Amber, Edwin, Mark, Wouter, Victor, Gijs, Nicolai, Simone, Annerike, Heidi, Martijn, Kyrian e Quint per la piacevole e fattiva collaborazione.

Oltre al lavoro, da cui ho fortunatamente ricevuto positivi e propositivi stimoli, non posso che riconoscere la valenza dell'unico incondizionato sostegno della mia vita, la mia famiglia. Un groviglio di affetto, attenzioni, emozioni, normalità e scompigli, che mi ha sempre permesso di vivere avvolta da un senso di totale benessere e serenità! In tutto questo, impagabili e inestimabili sono loro, mamma e papà, l'infinita dolcezza e la premurosa razionalità. Grazie per il costante impegno e per il continuo prodigarsi per noi figli, per avermi sempre incoraggiata a inseguire le mie scelte, per custodire sempre il giusto consiglio o la cercata consolazione che, sebbene talvolta di parte, aiuta sempre!

E grazie anche ai miei splendidi fratelli. Claudia, colonna portante della mia vita, sorella e amica complice, la cui infinita forza e coinvolgente entusiasmo stupiscono sempre! E il grande piccolo di casa, Pierangelo, con la sua allegria e saggia leggerezza del non prendere mai nulla troppo sul serio.

Quanto mai fondamentale è anche tutto ciò che loro, gli amici di ogni dove, vicini e ormai un po' lontani, sono sempre in grado di regalarti. Tra tutti certamente gli "scalini" trionfano! Grazie ragazzi per essere da sempre una presenza pregevole e importante in cui la mente trova il suo svago e il cuore la sua dimora: Chiara, Stella, Claudia, Antonello, Antonio, Salvatore, Vincenzo, Francesca, Alberto, Alessia, Ciro, Mimmo, Giuseppe, Francesco, Fabio.

Grazie anche a Luisa e Arianna, due donne meravigliose in grado di rendere sempre speciale la solita "chiacchierata tra amiche".

Un affettuoso e nostalgico pensiero va anche alla famiglia di Enschede (Kostas, Sergios, Camilo, Mae, Eamon, Andrea, Federico, Luigi, Luca, Federica, Guido, Francesco, Michela, Ernesto, Nick, Bob e tutti gli altri), per l'accoglienza immediata, per l'avermi fatto sentire subito a casa e per la condivisione di tutti gli attimi

che un anno può regalare. Un grazie particolare a Nicole e Giorgio per quella singolare, fraterna e complice amicizia che inorgoglisce.

E infine, uno speciale grazie al mio tester più tenace, Marco! Non dimenticherò mai le interminabili e talvolta dolorose ore in laboratorio! È stato un aiuto preziosissimo, ma ancor di più lo è l'inaspettata vertigine che sei.

So, here I am at the end of an intense and in-depth experience started about three years ago. It has been an educational, working and life path that, despite some difficulties, permitted several small and pleasant accomplishments. I met several persons along this path, and some of them have consciously or unconsciously improved it by making it even more enjoyable. Therefore, I really care to dedicate an honest thought to each of them to express all my thankfulness.

Firstly, I would like to thank my PhD tutors, prof. Giacomo Mantriota and prof. Francesco Bottiglione, for their relevant contribution to the research carried on.

I am grateful to prof. Mantriota for placing his trust and confidence in my abilities at the beginning of the PhD, and for having always confirmed it. I esteem him for his professionality, his good capability to look forward and his great dedication to science. I should learn a lot from him.

A big thanks to Francesco, who has always been a sort of mentor for me. He has always been there for me, for listening to my concerns, for providing me with valuable advices. Many of his suggestions were useful for some of the results collected in this thesis. Furthermore, I have always appreciated the time we spent sharing ideas, opinions and scientific thoughts. To be honest, this has often helped me to reinforce my motivation, that was sometimes made uncertain by some concerns and difficulties.

A great contribution to this thesis comes from the Department of Biomechanical Engineering of the University of Twente, where I worked for more than one year. There, I found new and interesting stimuli for my work. I thank prof. Herman van der Kooij for having promptly welcome me in his lab and for providing me with all I needed to carry on my activity. It has been an honour for me working with him and his research group. I would also like to thank Lianne and Jeanine for their usual kindness and for having always been there for me, and Amber, Edwin, Mark, Wouter, Victor, Gijs, Nicolai, Simone, Annerike, Heidi, Martijn, Kyrian e Quint for the pleasant and active cooperation.

Beyond the work side, from which I received positive and constructive stimuli, there is another important part of my life that had a strong influence on what I did. I am talking about my family, the only unconditional and absolute support of my life. I would define it as a nest of love, cares, emotions, normality and mess, that has

always ensured my peacefulness and well-being. What my parents did and still do, as well as what they are, is invaluable for me. I should thank them for their love, for every opportunity they have given me, for having encouraged me to realize my own potential, for holding always the right advice or the needed consolation.

Then, there are my sister and brother. Claudia, pillar of strength for me, sister and dear friend, whose unlimited strength and enthusiasm always astonish me! And then, the great little man of the family, Pierangelo, with his happiness and wise levity of never take things too seriously.

There is one more thing, there are friends from everywhere with their exceptional capacity to gift emotions and nice moments. Among them, there is people from the "scalini"! Thank you guys for being always a precious and important presence in which the mind finds his recreation and the heart his home: Chiara, Stella, Claudia, Antonello, Antonio, Salvatore, Vincenzo, Francesca, Alberto, Alessia, Ciro, Mimmo, Giuseppe, Francesco, Fabio.

Thank also to Luisa and Arianna, two wonderful women that can always make special any usual chat among friends.

A lovely and nostalgic thought is for people I met in Enschede (Kostas, Sergios, Camilo, Mae, Andrea, Federico, Luigi, Luca, Eamon, Federica, Guido, Francesco, Michela, Ernesto, Nick, Bob and all the others), for their welcome, for having made me feel soon at home and for all the things we shared in more than one year spent together. In particular, my mind goes to Giorgio and Nicole, to our exceptional, close and emphatic friendship that makes me feel proud.

In the end, a special thanks to the most resistant and long-lasting test I have ever had, Marco! I will never forget the many and sometimes painful hours spent in the lab. His help was so needed and precious, but even more precious is the unforeseen and exciting vertigo he is.

Bibliography

[1] Bing Chen, Hao Ma, Lai-Yin Qin, Fei Gao, Kai-Ming Chan, Sheung-Wai Law, Ling Qin, and Wei-Hsin Liao. Recent developments and challenges of lower extremity exoskeletons. *Journal of Orthopaedic Translation*, 5:26 – 37, 2016. Special Issue: Orthopaedic Biomaterials and Devices.

[2] R. Aló, F. Bottiglione, and G. Mantriota. An innovative design of artificial knee joint actuator with energy recovery capabilities. *ASME. Journal of Mechanisms Robotics*, 8, 2015.

[3] A. M. Dollar and H. Herr. Lower extremity exoskeletons and active orthoses: Challenges and state-of-the-art. *IEEE Transactions on Robotics*, 24(1):144–158, Feb 2008.

[4] Tingfang Yan, Marco Cempini, Calogero Maria Oddo, and Nicola Vitiello. Review of assistive strategies in powered lower-limb orthoses and exoskeletons. *Robotics and Autonomous Systems*, 64:120 – 136, 2015.

[5] José Luis Pons. *Wearable Robots: Biomechatronic Exoskeletons*. John Wiley & Sons Ltd Chichester UK, 2008.

[6] Pierre Cherelle, Glenn Mathijssen, Qining Wang, Bram Vanderborght, and Dirk Lefeber. Advances in propulsive bionic feet and their actuation principles. *Advances in Mechanical Engineering*, 6, 2014.

[7] G. Carpino, D. Accoto, F. Sergi, N. L. Tagliamonte, and E. Guglielmelli. A novel compact torsional spring for series elastic actuators for assistive wearable robots. *Journal of Mechanical Design*, 134, 2012.

[8] B. J. Bergelin and P. A. Voglewede. Design of an active ankle-foot prosthesis utilizing a four-bar mechanism. 134, 2012.

[9] L. Mooney and H. Herr. Continuously-variable series-elastic actuator. In *Rehabilitation Robotics (ICORR), 2013 IEEE International Conference on*, pages 1–6, June 2013.

[10] D. F. B. Haeufle, M. D. Taylor, S. Schmitt, and H. Geyer. A clutched parallel elastic actuator concept: Towards energy efficient powered legs in prosthetics and robotics. In *2012 4th IEEE RAS EMBS International Conference on Biomedical Robotics and Biomechatronics (BioRob)*, pages 1614–1619, June 2012.

[11] Elliott J. Rouse, Luke M. Mooney, and Hugh M. Herr. Clutchable series-elastic actuator: Implications for prosthetic knee design. *The International Journal of Robotics Research*, 33(13):1611–1625, 2014.

[12] J. E. Pratt, B. T. Krupp, C. J. Morse, and S. H. Collins. The roboknee: an exoskeleton for enhancing strength and endurance during walking. In *Robotics and Automation, 2004. Proceedings. ICRA '04. 2004 IEEE International Conference on*, volume 3, pages 2430–2435 Vol.3, April 2004.

[13] Daniel Paluska and Hugh Herr. The effect of series elasticity on actuator power and work output: Implications for robotic and prosthetic joint design. *Robotics and Autonomous Systems*, 54(8):667 – 673, 2006. Morphology, Control and Passive Dynamics.

[14] Bram Vanderborght, Ronald Van Ham, Dirk Lefeber, Thomas G. Sugar, and Kevin W. Hollander. Comparison of mechanical design and energy consumption of adaptable, passive-compliant actuators. *The International Journal of Robotics Research*, 28(1):90–103, 2009.

[15] G. A. Pratt and M. M. Williamson. Series elastic actuators. In *Intelligent Robots and Systems 95. 'Human Robot Interaction and Cooperative Robots', Proceedings. 1995 IEEE/RSJ International Conference on*, volume 1, pages 399–406 vol.1, Aug 1995.

[16] Martin Grimmer, Mahdy Eslamy, and AndrÃ© Seyfarth. Energetic and peak power advantages of series elastic actuators in an actuated prosthetic leg for walking and running. *Actuators*, 3(1):1, 2014.

[17] G. Mathijssen, D. Lefeber, and B. Vanderborght. Variable recruitment of parallel elastic elements: Series x2013;parallel elastic actuators (spea) with dephased mutilated gears. *IEEE/ASME Transactions on Mechatronics*, 20(2):594–602, April 2015.

[18] Rafael R. Torrealba and Samuel B. Udelman. Design of cam shape for maxi-

mum stiffness variability on a novel compliant actuator using differential evolution. *Mechanism and Machine Theory*, 95:114 – 124, 2016.

[19] Giorgio Grioli, Sebastian Wolf, Manolo Garabini, Manuel Catalano, Etienne Burdet, Darwin Caldwell, Raffaella Carloni, Werner Friedl, Markus Grebenstein, Matteo Laffranchi, Dirk Lefeber, Stefano Stramigioli, Nikos Tsagarakis, Michael van Damme, Bram Vanderborght, Alin Albu-Schaeffer, and Antonio Bicchi. Variable stiffness actuators: The user's point of view. *The International Journal of Robotics Research*, 34(6):727–743, 2015.

[20] G. Mathijssen, B. Brackx, M. Van Damme, D. Lefeber, and B. Vanderborght. Series-parallel elastic actuation (spea) with intermittent mechanism for reduced motor torque and increased efficiency. In *2013 IEEE/RSJ International Conference on Intelligent Robots and Systems*, pages 5841–5846, Nov 2013.

[21] Glenn Mathijssen, Pierre Cherelle, Dirk Lefeber, and Bram Vanderborght. Concept of a series-parallel elastic actuator for a powered transtibial prosthesis. *Actuators*, 2(3):59, 2013.

[22] Y. Takahashi, H. Takahashi, K. Sakamoto, and S. Ogawa. Human balance measurement and human posture assist robot design. In *SICE Annual, 1999. 38th Annual Conference Proceedings of the*, pages 983–988, Aug 1999.

[23] Hian Kai Kwa, Jerryll H. Noorden, Matthew Missel, Travis Craig, Jerry E. Pratt, and Peter D. Neuhaus. Development of the ihmc mobility assist exoskeleton. In *Proceedings of the 2009 IEEE International Conference on Robotics and Automation*, ICRA'09, pages 1349–1355, Piscataway, NJ, USA, 2009. IEEE Press.

[24] Hitoshi Konosu Masashi Yamashita Shingo Shimoda Fady Alnajjar Hidenori Kimura Tytus Wojtara, Makoto Sasaki. Artificial balancer â supporting device for postural reflex. *Gait Posturel*, 35(2):316–321, 2011.

[25] D. Li and H. Vallery. Gyroscopic assistance for human balance. In *2012 12th IEEE International Workshop on Advanced Motion Control (AMC)*, pages 1–6, March 2012.

[26] Jimmy Chiu and Ambarish Goswami. Design of a wearable scissored-pair control moment gyroscope (sp-cmg) for human balance assist. In *ASME 2014 International Design Engineering Technical Conferences and Computers and*

Information in Engineering Conference, volume 5A: 38th Mechanisms and Robotics Conference.

[27] R. Matsuzaki and Y. Fujimoto. Walking assist device using control moment gyroscopes. In *Industrial Electronics Society, IECON 2013 - 39th Annual Conference of the IEEE*, pages 6581–6586, Nov 2013.

[28] Lance L. Cai, Andy J. Fong, Chad K. Otoshi, Yongqiang Liang, Joel W. Burdick, Roland R. Roy, and V. Reggie Edgerton. Implications of assist-as-needed robotic step training after a complete spinal cord injury on intrinsic strategies of motor learning. *Journal of Neuroscience*, 26(41):10564–10568, 2006.

[29] A. Esquenazi, M. Talaty, A. Packel, and M. Saulino. The rewalk powered exoskeleton to restore ambulatory function to individuals with thoracic-level motor-complete spinal cord injury. *American Journal of Physical Medicine and Rehabilitation*, 91(11):911–921, 2012. cited By 109.

[30] G. Colombo, M. Joerg, R. Schreier, and V. Dietz. Treadmill training of paraplegic patients using a robotic orthosis. *Journal of rehabilitation research and development*, 37(6):693–700, 2000.

[31] J. F. Veneman, R. Ekkelenkamp, R. Kruidhof, F. C.T. van der Helm, and H. van der Kooij. A series elastic- and bowden-cable-based actuation system for use as torque actuator in exoskeleton-type robots. *The International Journal of Robotics Research*, 25(3):261–281, 2006.

[32] H. Kazerooni, Ryan Steger, and Lihua Huang. Hybrid control of the berkeley lower extremity exoskeleton (bleex). *The International Journal of Robotics Research*, 25(5-6):561–573, 2006.

[33] http://epomedicine.com/clinical-medicine/physical-examination-gait/.

[34] Robert J. Peterka. *Model-Based Interpretations of Experimental Data Related to the Control of Balance During Stance and Gait in Humans*, pages 245–270. Springer New York, New York, NY, 2016.

[35] Akin O. Kapti and M. Sait Yucenur. Design and control of an active artificial knee joint. *Mechanism and Machine Theory*, 41(12):1477 – 1485, 2006.

[36] Modeling and optimal control of an energy-storing prosthetic knee. *ASME Journal of Biomechanical Engineering*, 2012.

[37] C. J. Walsh, D. Paluska, K. Pasch, W. Grand, A. Valiente, and H. Herr. Development of a lightweight, underactuated exoskeleton for load-carrying augmentation. In *Proceedings 2006 IEEE International Conference on Robotics and Automation, 2006. ICRA 2006.*, pages 3485–3491, May 2006.

[38] Hiroaki Kawamoto and Yoshiyuki Sankai. Power assist system hal-3 for gait disorder person. In *Proceedings of the 8th International Conference on Computers Helping People with Special Needs*, ICCHP '02, pages 196–203, London, UK, UK, 2002. Springer-Verlag.

[39] Adam Zoss and H. Kazerooni. Design of an electrically actuated lower extremity exoskeleton. *Advanced Robotics*, 20(9):967–988, 2006.

[40] D. F. B. Haeufle, M. D. Taylor, S. Schmitt, and H. Geyer. A clutched parallel elastic actuator concept: Towards energy efficient powered legs in prosthetics and robotics. In *2012 4th IEEE RAS EMBS International Conference on Biomedical Robotics and Biomechatronics (BioRob)*, pages 1614–1619, June 2012.

[41] Vincenzo Luciano, Emilio Sardini, and Mauro Serpelloni. *An Electromechanical Generator Implanted in Human Total Knee Prosthesis*, pages 25–30. Springer New York, New York, NY, 2014.

[42] J. M. Donelan, Q. Li, V. Naing, J. A. Hoffer, D. J. Weber, and A. D. Kuo. Biomechanical energy harvesting: Generating electricity during walking with minimal user effort. *Science*, 319(5864):807–810, 2008.

[43] B.J. Bergelin, J.O. Mattos, J.G. Wells, and P.A. Voglewede. Concept through preliminary bench testing of a powered lower limb prosthetic device. *Journal of Mechanisms and Robotics*, 2(4), 2010. cited By 13.

[44] J. Borra's and A.M. Dollar. Actuation torque reduction in parallel robots using joint compliance. *Journal of Mechanisms and Robotics*, 6(2), 2014. cited By 5.

[45] M. Hutter, C. David Remy, M.A. Hoepflinger, and R. Siegwart. High compliant series elastic actuation for the robotic leg scarleth. pages 507–514, 2012. cited By 1.

[46] C. Lagoda, A.C. Schouten, A.H.A. Stienen, E.E.G. Hekman, and H. Van Der Kooij. Design of an electric series elastic actuated joint for robotic gait rehabilitation training. pages 21–26, 2010. cited By 31.

[47] F. Sergi, D. Accoto, G. Carpino, N.L. Tagliamonte, and E. Guglielmelli. Design and characterization of a compact rotary series elastic actuator for knee assistance during overground walking. pages 1931–1936, 2012. cited By 29.

[48] K. Bharadwaj, T.G. Sugar, J.B. Koeneman, and E.J. Koeneman. Design of a robotic gait trainer using spring over muscle actuators for ankle stroke rehabilitation. *Journal of Biomechanical Engineering*, 127(6):1009–1013, 2005. cited By 39.

[49] D. Accoto, G. Carpino, F. Sergi, N.L. Tagliamonte, L. Zollo, and E. Guglielmelli. Design and characterization of a novel high-power series elastic actuator for a lower limb robotic orthosis. *International Journal of Advanced Robotic Systems*, 10, 2013. cited By 11.

[50] K.W. Hollander, R. Ilg, T.G. Sugar, and D. Herring. An efficient robotic tendon for gait assistance. *Journal of Biomechanical Engineering*, 128(5):788–791, 2006. cited By 76.

[51] Uwe Mettin, Pedro X. La Hera, Leonid B. Freidovich, and Anton S. Shiriaev. Parallel elastic actuators as control tool for preplanned trajectories of underactuated mechanical systems. *The International Journal of Robotics Research*, 2009.

[52] S. Wang, W. van Dijk, and H. van der Kooij. Spring uses in exoskeleton actuation design. In *2011 IEEE International Conference on Rehabilitation Robotics*, pages 1–6, June 2011.

[53] M. Scheint, M. Sobotka, and M. Buss. Optimized parallel joint springs in dynamic motion: Comparison of simulation and experiment. In *Biomedical Robotics and Biomechatronics (BioRob), 2010 3rd IEEE RAS and EMBS International Conference on*, pages 485–490, Sept 2010.

[54] S. Shirata, A. Konno, and M. Uchiyama. Design and evaluation of a gravity compensation mechanism for a humanoid robot. In *2007 IEEE/RSJ International Conference on Intelligent Robots and Systems*, pages 3635–3640, Oct 2007.

[55] S. K. Au, H. Herr, J. Weber, and E. C. Martinez-Villalpando. Powered ankle-foot prosthesis for the improvement of amputee ambulation. In *2007 29th Annual International Conference of the IEEE Engineering in Medicine and Biology Society*, pages 3020–3026, Aug 2007.

[56] S. Wolf and G. Hirzinger. A new variable stiffness design: Matching requirements of the next robot generation. In *Robotics and Automation, 2008. ICRA 2008. IEEE International Conference on*, pages 1741–1746, May 2008.

[57] Ronald Van Ham, Bram Vanderborght, MichaÃ«l Van Damme, BjÃ¶rn Verrelst, and Dirk Lefeber. Maccepa, the mechanically adjustable compliance and controllable equilibrium position actuator: Design and implementation in a biped robot. *Robotics and Autonomous Systems*, 55(10):761 – 768, 2007.

[58] R. Schiavi, G. Grioli, S. Sen, and A. Bicchi. Vsa-ii: a novel prototype of variable stiffness actuator for safe and performing robots interacting with humans. In *Robotics and Automation, 2008. ICRA 2008. IEEE International Conference on*, pages 2171–2176, May 2008.

[59] M. G. Catalano, G. Grioli, M. Garabini, F. Bonomo, M. Mancini, N. Tsagarakis, and A. Bicchi. Vsa-cubebot: A modular variable stiffness platform for multiple degrees of freedom robots. In *Robotics and Automation (ICRA), 2011 IEEE International Conference on*, pages 5090–5095, May 2011.

[60] C.E. English and D. Russell. Mechanics and stiffness limitations of a variable stiffness actuator for use in prosthetic limbs. *Mechanism and Machine Theory*, 34(1):7 – 25, 1999.

[61] L. C. Visser, R. Carloni, and S. Stramigioli. Energy-efficient variable stiffness actuators. *IEEE Transactions on Robotics*, 27(5):865–875, Oct 2011.

[62] B. S. Kim and J. B. Song. Design and control of a variable stiffness actuator based on adjustable moment arm. *IEEE Transactions on Robotics*, 28(5):1145–1151, Oct 2012.

[63] N. G. Tsagarakis, I. Sardellitti, and D. G. Caldwell. A new variable stiffness actuator (compact-vsa): Design and modelling. In *2011 IEEE/RSJ International Conference on Intelligent Robots and Systems*, pages 378–383, Sept 2011.

[64] M. Fumagalli, E. Barrett, S. Stramigioli, and R. Carloni. The mvsa-ut: A miniaturized differential mechanism for a continuous rotational variable stiffness actuator. In *2012 4th IEEE RAS EMBS International Conference on Biomedical Robotics and Biomechatronics (BioRob)*, pages 1943–1948, June 2012.

[65] S. S. Groothuis, G. Rusticelli, A. Zucchelli, S. Stramigioli, and R. Carloni. The vsaut-ii: A novel rotational variable stiffness actuator. In *Robotics and Automation (ICRA), 2012 IEEE International Conference on*, pages 3355–3360, May 2012.

[66] D. Shin, X. Yeh, and O. Khatib. Variable radius pulley design methodology for pneumatic artificial muscle-based antagonistic actuation systems. In *2011 IEEE/RSJ International Conference on Intelligent Robots and Systems*, pages 1830–1835, Sept 2011.

[67] Bram Vanderborght, Nikos G. Tsagarakis, Ronald Van Ham, Ivar Thorson, and Darwin G. Caldwell. Maccepa 2.0: compliant actuator used for energy efficient hopping robot chobino1d. *Autonomous Robots*, 31(1):55, 2011.

[68] S. Stramigioli, G. van Oort, and E. Dertien. A concept for a new energy efficient actuator. In *2008 IEEE/ASME International Conference on Advanced Intelligent Mechatronics*, pages 671–675, July 2008.

[69] C. Everarts, B. Dehez, and R. Ronsse. Variable stiffness actuator applied to an active ankle prosthesis: Principle, energy-efficiency, and control. In *2012 IEEE/RSJ International Conference on Intelligent Robots and Systems*, pages 323–328, Oct 2012.

[70] J. Schuy, P. Beckerle, J. Wojtusch, S. Rinderknecht, and O. von Stryk. Conception and evaluation of a novel variable torsion stiffness for biomechanical applications. In *2012 4th IEEE RAS EMBS International Conference on Biomedical Robotics and Biomechatronics (BioRob)*, pages 713–718, June 2012.

[71] Julian Hamm, Arthur G. Money, Anita Atwal, and Ioannis Paraskevopoulos. Fall prevention intervention technologies: A conceptual framework and survey of the state of the art. *Journal of Biomedical Informatics*, 59:319 – 345, 2016.

[72] Sara M. Bradley. Falls in older adults. *Mount Sinai Journal of Medicine: A Journal of Translational and Personalized Medicine*, 78(4):590–595, 2011.

[73] M. Gajamohan, M. Merz, I. Thommen, and R. D'Andrea. The cubli: A cube that can jump up and balance. In *2012 IEEE/RSJ International Conference on Intelligent Robots and Systems*, pages 3722–3727, Oct 2012.

[74] S.C. Spry and A.R. Girard. Gyroscopic stabilisation of unstable vehi-

cles: Configurations, dynamics, and control. *Vehicle System Dynamics*, 46(SUPPL.1):247–260, 2008. cited By 5.

[75] Y. Ou and Y. Xu. Stabilization and line tracking of the gyroscopically stabilized robot. volume 2, pages 1753–1758, 2002. cited By 6.

[76] Y. Ou and Y. Xu. Gyroscopically stabilized robot: Balance and tracking. *International Journal of Advanced Robotic Systems*, 1(1):23–32, 2004. cited By 7.

[77] S.M. Lee and S.-W. Rhee. Experiments of singularity avoidance steering control laws for redundant single-gimbal control moment gyros. pages 175–178, 2007. cited By 2.

[78] K.A. Ford and C.D. Hall. Flexible spacecraft reorientations using gimbaled momentum wheels. volume 97 PART 2, pages 1895–1913, 1997. cited By 26.

[79] H. Schaub, S.R. Vadali, and J.L. Junkins. Feedback control law for variable speed control moment gyros. volume 99, pages 581–600, 1998. cited By 6.

[80] B. R. Andrievsky. Global stabilization of the unstable reaction-wheel pendulum. *Automation and Remote Control*, 72(9):1981, 2011.

[81] Jordan Meyer, Nathan Delson, and Raymond A. de Callafon. Design, modeling and stabilization of a moment exchange based inverted pendulum. *IFAC Proceedings Volumes*, 42(10):462 – 467, 2009.

[82] F. Bottiglione and G. Mantriota. Effect of the ratio spread of cvu in automotive kinetic energy recovery systems. *Journal of Mechanical Design*, 135(6), 2013.

[83] M. Bazyn, J. Carter, C.B. Lohr, C. Malone, L.T. McDaniel, and P.D. Poxton. Continuously and/or infinitely variable transmissions and methods therefor, November 20 2012. US Patent 8,313,405.

[84] L.G. Brown, G.A.M. Brown, and B.A. Brown. Locked contact infinitely variable transmission, April 16 2013. US Patent 8,419,589.

[85] C.J. Greenwood, A.D. De Freitas, and R.A. Oliver. Drive mechanism for infinitely variable transmission, July 8 2014. US Patent 8,771,133.

[86] K. Kazerounian and Z. Furu-Szekely. Parallel disk continuously variable transmission (pdcvt). *Mechanism and Machine Theory*, 41(5):537–566, 2006. cited By 3.

[87] J. Carter, C. Lohr, B. Pohl, and D.J. Dawe. Infinitely variable transmissions, continuously variable transmissions, methods, assemblies, subassemblies, and components therefor, January 7 2010. WO Patent App. PCT/US2008/053,951.

[88] D. Magyari. Infinitely variable transmission, April 27 2010. US Patent 7,704,184.

[89] F. Bottiglione and G. Mantriota. Reversibility of power-split transmissions. *ASME. Journal of Mechanical Design*, 133(8), 2011.

[90] L Mangialardi and G Mantriota. Power flows and efficiency in infinitely variable transmissions. *Mechanism and Machine Theory*, 34(7):973 – 994, 1999.

[91] G Carbone, L Mangialardi, and G Mantriota. A comparison of the performances of full and half toroidal traction drives. *Mechanism and Machine Theory*, 39(9):921 – 942, 2004.

[92] G. Mantriota. Performances of a parallel infinitely variable transmissions with a type ii power flow. *Mechanism and Machine Theory*, 37(6):555–578, 2002. cited By 35.

[93] G. Mantriota. Performances of a series infinitely variable transmission with type i power flow. *Mechanism and Machine Theory*, 37(6):579–597, 2002. cited By 33.

[94] G. Mantriota and E. Pennestrí. Theoretical and experimental efficiency analysis of multi-degrees-of-freedom epicyclic gear trains. *Multibody System Dynamics*, 9(4):389–408, 2003. cited By 19.

[95] G. Carbone, L. Mangialardi, and G. Mantriota. Influence of clearance between plates in metal pushing v-belt dynamics. *Journal of Mechanical Design, Transactions of the ASME*, 124(3):543–557, 2002. cited By 19.

[96] G. Carbone, L. Mangialardi, and G. Mantriota. Fuel consumption of a mid class vehicle with infinitely variable transmission. *SAE Technical Papers*, 2001. cited By 25.

[97] Mantriota G. De Pinto, S. A simple model for compound split transmissions. *Proceedings of the Institution of Mechanical Engineers, Part D: Journal of Automobile Engineering*, 228(5):549–564, 2014. cited By 6.

[98] F. Bottiglione, S. De Pinto, and G. Mantriota. Infinitely variable transmissions in neutral gear: Torque ratio and power re-circulation. *Mechanism and Machine Theory*, 74:285 – 298, 2014.

[99] L. Mangialardi and G. Mantriota. Dynamic behaviour of wind power systems equipped with automatically regulated continuously variable transmission. *Renewable Energy*, 7(2):185–203, 1996. cited By 26.

[100] G. Mantriota. Fuel consumption of a vehicle with power split cvt system. *International Journal of Vehicle Design*, 37(4):327–342, 2005. cited By 23.

[101] G Mantriota. Case study: Infinitely variable transmissions with automatic regulation. *Proceedings of the Institution of Mechanical Engineers, Part D: Journal of Automobile Engineering*, 215(12):1267–1280, 2001.

[102] L. Mangialardi and G. Mantriota. Continuously variable transmissions with torque-sensing regulators in waterpumping windmills. *Renewable Energy*, 4(7):807 – 823, 1994.

[103] Francesco Bottiglione, Leonardo De Novellis, Luigi Mangialardi, and Giacomo Mantriota. Mechanical hybrid kers based on toroidal traction drives: An example of smart tribological design to improve terrestrial vehicle performance. *Advances in Tribology*, 2013.

[104] I. Schafer, P. Bourlier, F. Hantschack, E.W. Roberts, S.D. Lewis, D.J. Forster, and C. John. Space lubrication and performance of harmonic drive gears. Number 591, pages 65–72, 2005. cited By 8.

[105] M. R. Tucker and K. B. Fite. Mechanical damping with electrical regeneration for a powered transfemoral prosthesis. In *2010 IEEE/ASME International Conference on Advanced Intelligent Mechatronics*, pages 13–18, July 2010.

[106] Robert Riener, Marco Rabuffetti, and Carlo Frigo. Stair ascent and descent at different inclinations. *Gait Posture*, 15(1):32 – 44, 2002.

[107] J. Meuleman, W. Terpstra, J. Meuleman, E. H. F. van Asseldonk, and H. van der Kooij. Effect of added inertia on the pelvis on gait. In *2011 IEEE International Conference on Rehabilitation Robotics*, pages 1–6, June 2011.

[108] Yongjie Han, Zhengyi Ren, and Yongxiang Tong. General design method of flywheel rotor for energy storage system. *Energy Procedia*, 16:359 – 364, 2012.

[109] J. H. Gully, S. B. Pratap, R. N. Headifen, C. Marinos, W. Dick, and B. Goodel. Investigation of an alternator charged pulse forming network with flywheel energy storage. *IEEE Transactions on Magnetics*, 29(1):969–974, Jan 1993.

[110] R. Rarick, H. Richter, A. Van Den Bogert, D. Simon, H. Warner, and T. Barto. Optimal design of a transfemoral prosthesis with energy storage and regeneration. pages 4108–4113, 2014. cited By 1.

[111] Gabriele Bovi, Marco Rabuffetti, Paolo Mazzoleni, and Maurizio Ferrarin. A multiple-task gait analysis approach: Kinematic, kinetic and {EMG} reference data for healthy young and adult subjects. *Gait & Posture*, 33(1):6 – 13, 2011.